2021

Electrospun Biomaterial-Induced Neutrophil Extracellular Traps: Characterization and Regulation for Biomaterial-Guided Tissue Regeneration

Allison Fetz

ELECTROSPUN BIOMATERIAL-INDUCED NEUTROPHIL EXTRACELLULAR TRAPS: CHARACTERIZATION AND REGULATION FOR BIOMATERIAL-GUIDED TISSUE REGENERATION

by

Allison Elizabeth Fetz

A Dissertation

Submitted in Partial Fulfillment of the

Requirements for the Degree of

Doctor of Philosophy

Major: Biomedical Engineering

The University of Memphis

May 2021

DEDICATION

This dissertation is dedicated to my parents, Gary and Susan Fetz, for their constant love, support, and encouragement. They nurtured my creative and inquisitive nature at a young age, instilling in me a passion for education that developed into a love of lifetime learning through biomedical research.

ACKNOWLEDGEMENTS

Completing this dissertation would not have been possible without the support of my committee. First, I would like to acknowledge my mentor and research advisor, Dr. Gary Bowlin, for his wisdom and guidance throughout my graduate education. Since I started working in his laboratory as an undergraduate student, Dr. Bowlin has been a consistent source of inspiration and encouragement, pushing me to reach my full potential as a student and as a researcher. I would also like to acknowledge committee members, Drs. Marie van der Merwe, Marko Radic, and Richard Smith, for their scientific expertise and wealth of knowledge. They were invaluable for experimental design, data analysis, and manuscript preparation. Because of my committee and their dedication to my training, I am a more well-rounded researcher. I am forever grateful for their time and effort.

Additionally, I would like to acknowledge my fellow students and lab mates – past and present – for their constant encouragement throughout this process. Ben Minden-Birkenmaier, Gretchen Selders, Hunter King, Isaac Rodriguez, Jenny Jarvis, Kasyap Cherukuri, and Will Cain were especially important as good classmates but even better friends. Whether troubleshooting experiments or talking about life outside of research, they made graduate school enjoyable, and I am grateful for their comradery.

I would also like to acknowledge my parents, Gary and Susan Fetz, my brother, Patrick Fetz, and my fiancé, Peter Palazola. I could not have done this without their love and support. They have encouraged me through the toughest times in my graduate education, and it has been reassuring to know I can consult any of them for advice, a laugh, and a hug when needed. I am especially grateful for Peter's support of my career

aspirations and timing his proposal so that planning a wedding and writing my dissertation would both be enjoyable processes.

Finally, I would like to acknowledge my six-month-old standard poodle, Beale, who as I am writing this is licking my laptop. Her goofy puppy behavior has been a great source of stress relief, and our lunchtime walks give me the mental break I need after a morning of writing or data analysis. Beale has brought life – and lots of grass and dirt – into our home, and her companionship has made working from home much more enjoyable the last couple of months.

PREFACE

The purpose of this work is to begin understanding the role of neutrophils and the release of neutrophil extracellular traps (NETs) in the potential for electrospun biomaterial-guided tissue regeneration. Although they comprise 40-80% of the white blood cells in circulation, neutrophil participation in the response to biomaterials in tissue engineering applications has long been neglected in favor of macrophages. However, a growing body of literature suggests that neutrophils have the potential to precondition the tissue environment and drive tissue healing. Moreover, the dysregulated release of NETs propagates thrombosis and fibrosis, two responses that are particularly detrimental to biomaterial-guided tissue regeneration. Therefore, this work was undertaken to delve into the release of NETs on electrospun biomaterials, evaluate their impact on the potential for tissue healing, and elucidate mechanisms and methods of regulating biomaterial-induced NET release.

Several chapters and portions of chapters within this dissertation have been previously published or are under review in peer-reviewed journals. Chapter 1 contains excerpts that were published in a book chapter entitled “Electrospun Tissue Regeneration Biomaterials for Immunomodulation” in *Immunomodulatory Biomaterials* (2021) as well as excerpts from the review “Neutrophils in Biomaterial-Guided Tissue Regeneration: Matrix Reprogramming for Angiogenesis” in *Tissue Engineering: Part B* (2020). Chapter 2 is under review as an article entitled “Neutrophil Extracellular Traps in Inflammation and the Preconditioning of Biomaterials for Tissue Engineering” in *Tissue Engineering: Part B* (2021). Chapter 3 is published as “Electrospun Template Architecture and Composition Regulate Neutrophil NETosis *In Vitro* and *In Vivo*” in *Tissue Engineering:*

Part A (2017). Chapter 4 is published as "Surface Area to Volume Ratio of Electrospun Polydioxanone Templates Regulates the Adsorption of Soluble Proteins from Human Serum" in *Bioengineering* (2019). Chapter 5 is under review as an article entitled "Human Neutrophil FcγRIIIb Regulates Neutrophil Extracellular Trap (NET) Release in Response to Electrospun Biomaterials" in *Acta Biomaterialia* (2021). Chapter 6 is published as "Localized Delivery of Cl-amidine From Electrospun Polydioxanone Templates to Regulate Acute Neutrophil NETosis: A Preliminary Evaluation of the PAD4 Inhibitor for Tissue Engineering" in *Frontiers in Pharmacology* (2018). Chapter 7 is under review as an article entitled "Electrospun Polydioxanone Biomaterials Loaded with Chloroquine Modulate Template-Induced NET Release and the Inflammatory Response from Human Neutrophils" in *Frontiers in Bioengineering and Biotechnology* (2021). Last, portions of Chapter 9 are published as "Neutrophils in Biomaterial-Guided Tissue Regeneration: Matrix Reprogramming for Angiogenesis" in *Tissue Engineering: Part B* (2020).

The work in this dissertation was supported by the University of Memphis First Generation Ph.D. Fellowship, Herff College of Engineering Fellowship, and the Steve Slack Fellowship. Additionally, this work was supported by the National Science Foundation Graduate Research Fellowship Program under Grant No. 1451514. Research reported in this dissertation was also supported by the National Institute of Biomedical Imaging and Bioengineering of the National Institutes of Health under Award No. R15EB022345. This content is solely the responsibility of the authors and does not necessarily represent the official views of the National Institute of Health.

ABSTRACT

The neutrophil has long been acknowledged as an abundant responder to an implanted biomaterial, but its importance as a dynamic effector cell has only recently been realized. The neutrophil response is especially important for *in situ* tissue regeneration where acellular biomaterials must be populated by endogenous cells and guide the growth of new tissues. More specifically, the release of neutrophil extracellular traps (NETs), or extracellular chromatin structures decorated with toxic nuclear and granular components, can cause collateral tissue damage, uncontrolled inflammation, and fibrosis, thereby preventing functional tissue regeneration. Therefore, the purpose of this work was to investigate the role of neutrophils and their release of NETs in the potential for electrospun biomaterial-guided *in situ* tissue regeneration. We evaluate the hypothesis that NETs are released in response to electrospun biomaterials, governed by biomaterial design features, and further postulate that the release of NETs is intimately related to biomaterial surface-adsorbed proteins and outside-in signaling, which can be regulated by the local delivery of pharmacological additives. Using *in vitro* assays with primary human neutrophils and *in vivo* subcutaneous implant models, we found that both electrospun fiber size and composition regulate the *in vitro* and *in vivo* release of NETs. Additionally, we show that the up-regulation of NETs on an implanted biomaterial nucleates tissue fibrosis, demonstrating that NET release is a significant, physiological preconditioning event in guided tissue regeneration. Moreover, through the characterization and quantification of protein adsorption on the biomaterial surfaces, we found that IgG, ligation of fragment crystallizable domain receptor IIIb, and signaling through transforming growth factor beta-activated kinase 1 is involved in electrospun

biomaterial-induced NET release. Finally, using drugs that inhibit two different molecular pathway targets, we showed that biomaterial-induced NETs can be regulated through the local delivery of active drugs *in vitro* and *in vivo,* improving tissue integration and promoting a pro-healing neutrophil phenotype. Together, the findings of this dissertation illustrate that the release of NETs is a significant preconditioning event on an electrospun biomaterial. Therefore, designing immunomodulatory biomaterials to regulate NET release and the neutrophil response may enhance *in situ* tissue regeneration and the clinical application of electrospun biomaterials.

TABLE OF CONTENTS

LIST OF TABLES

LIST OF FIGURES

ABBREVIATIONS

Abbreviation	Corresponding Term	Page
NETs	Neutrophil extracellular traps	1
ECM	Extracellular matrix	2
SAVR	Surface area to volume ratio	2
SEM	Scanning electron micrograph	3
PDO	Polydioxanone	3
DAMPs	Damage associated molecular patterns	4
IL-8	Interleukin 8	4
LTB4	Leukotriene B_4	4
ROS	Reactive oxygen species	5
DNA	Deoxyribonucleic acid	9
PAD4	Peptidyl arginine deiminase 4	10
MMP	Matrix metalloproteinase	10
MMP-8	Matrix metalloproteinase 8	10
MMP-9	Matrix metalloproteinase 9	10
NE	Neutrophil Elastase	10
MPO	Myeloperoxidase	10
NGAL	Neutrophil gelatinase associated lipocalin	10
HMGB1	High mobility group box 1	11
TLR4	Toll-like receptor 4	12
RAGE	Receptor for advanced glycation end products	12
GM-CSF	Granulocyte-macrophage colony-stimulating factor	14

3D	Three dimensional	15
DAPI	4,6-diamidino-2-phenylindole	15
NOX2	NADPH oxidase 2	16
NF-κB	Nuclear factor kappa B	16
PMA	Phorbol-12-mysirate 13-acetate	16
PKC	Protein kinase C	16
LPS	Lipopolysaccharide	17
JNK	c-Jun N-terminal kinase	17
IL-1β	Interleukin 1 beta	17
TNF-α	Tumor necrosis factor alpha	17
TAK1	Transforming growth factor beta activated kinase 1	17
PSGL-1	P-selectin glycoprotein ligand 1	17
CXCR2	CXC chemokine receptor 2	17
IL-1R1	Interleukin 1 receptor type 1	17
TNFR	Tumor necrosis factor receptor	17
TSG-6	Tumor necrosis factor stimulated gene 6	21
JAK	Janus kinase	22
Mac-1	Macrophage-1 antigen	22
FcγRIIa	Fragment crystallizable gamma receptor IIa	22
FcγRIIIb	Fragment crystallizable gamma receptor IIIb	22
ICs	Immune complexes	22
FcγRs	Fragment crystallizable gamma receptors	23
MSU	Monosodium urate	24

TANs	Tumor-associated neutrophils	34
TIMP	Tissue inhibitor of metalloproteinase	34
COL	Collagen type I	35
HFP	1,1,3,3,3 hexafluoro-2-propanol	35
SD	Small diameter	35
LD	Large diameter	35
v/v	Volume per volume	35
PC	PDO and COL blend	36
HBSS	Hank's balanced salt solution	37
HEPES	2-[4-(2-hydroxyethyl)piperazin-1-yl]ethanesulfonic acid	37
EDC	1-ethyl-3-(3-dimethyl-aminopropyl)carbodiimide hydrochloride	37
CO_2	Carbon dioxide	37
SG	SYTOX Green	38
DI	Deionized	38
B:G ratio	Blue to green ratio	38
CitH3	Citrullinated histone H3	39
PBS	Phosphate buffered saline	39
PVDF	Polyvinylidene fluoride	39
IR	Infrared	40
H&E	Hematoxylin and eosin	41
ANOVA	Analysis of variance	42
TCP	Tissue culture plastic	51

TLRs	Toll-like receptors	53
SDS	Sodium dodecyl sulfate	61
TLR7	Toll-like receptor 7	78
TLRR8	Toll-like receptor 8	78
CD11b	Cluster of differentiation 11b	83
CD18	Cluster of differentiation 18	83
FcγRI	Fragment crystallizable gamma receptor I	83
CD64	Cluster of differentiation 64	83
DMSO	Dimethylsulfoxide	85
ELISA	Enzyme-linked immunosorbent assay	88
GPI	Glycosylphosphatidylinositol	99
ERK	Extracellular signal-regulated kinase	99
TGF-β	Transforming growth factor β	127
VEGF-A	Vascular endothelial growth factor A	136
HGF	Hepatocyte growth factor	136
FDA	Food and Drug Administration	136
MLOD	Minimum level of detection	145
MMP-2	Matrix metalloproteinase 2	163
MMP-3	Matrix metalloproteinase 3	163

CHAPTER 1

INTRODUCTION

Introduction

The neutrophil has long been acknowledged as an abundant responder to an implanted biomaterial, but its importance as a dynamic effector cell that preconditions the tissue environment has only recently been realized. Neutrophil preconditioning of the biomaterial environment is especially important for *in situ* tissue regeneration where acellular biomaterials must be populated by endogenous cells and guide the growth of new tissues. Therefore, the purpose of this work is to investigate the role of neutrophils and their release of NETs in the potential for electrospun biomaterial-guided *in situ* tissue regeneration. We evaluate the hypothesis that NETs are released in response to electrospun biomaterials, governed by biomaterial design features, and further postulate that the release of NETs is intimately related to biomaterial surface-adsorbed proteins and outside-in signaling, which can be regulated by the local delivery of pharmacological additives. A greater understanding of biomaterial-neutrophil interactions and NET release will enhance the design of immunomodulatory electrospun biomaterials that regulate acute neutrophil interactions and guide functional *in situ* tissue regeneration. This chapter discusses electrospun biomaterials for *in situ* tissue engineering and summarizes the immune response to biomaterials with an emphasis on the neutrophil response.

Electrospun Biomaterials for *In Situ* Tissue Engineering

The goal of *in situ* tissue engineering is to design biomaterials that use the body as a bioreactor to stimulate the regenerative capacity of autologous cells, tissues, and organs. Rather than creating viable tissues *in vitro,* which is associated with costly

technical and regulatory hurdles, the goal is to engineer an acellular biomaterial that induces endogenous tissue regeneration [1]. Thus, the biomaterial should provide some biomimetic properties to instruct the interacting and infiltrating cells to drive the regeneration of tissue while the biomaterial is resorbed. In many cases, the biomaterial attempts to recapitulate the fibrous architecture of the ECM [2]. While multiple fabrication techniques exist, electrospinning and the resultant electrospun biomaterials are increasingly popular for creating ECM-mimicking biomaterials for guided tissue regeneration.

Electrospinning is a relatively simple method of producing continuous nano- to micro-sized fibers that are collected into a non-woven substrate (Figure 1) [3]. During the electrospinning process, a potential difference is established between a polymer solution and a collector, which drives the formation and collection of fibers. As such, the typical system is easy to build and scale-up, making it a cost-effective method for producing fibrous biomaterials at mass quantities. In addition, electrospinning is an appealing fabrication technique because of its vast versatility for *in situ* tissue engineering. Electrospun biomaterials can be made from natural polymers, synthetic polymers, or blends of polymers, and the fiber size can be controlled to mimic the scale, composition, and morphology of the natural ECM in the target tissue [4]. The high SAVR of the fibers and pore interconnectivity between the fibers are desirable for guiding cell attachment and migration while allowing for nutrient and oxygen diffusion and waste removal. Furthermore, the fibers can function as a foundation for innumerous application-specific modifications to the biomaterial and can be customized by incorporating, adsorbing, or chemically linking additives, such as proteins, small molecules, or drugs, to the

biomaterial [5]. Given the cost-effectiveness and versatility of the technique, electrospun biomaterials have the potential for a far-reaching clinical impact in tissue engineering for treating congenital abnormalities, trauma, or disease.

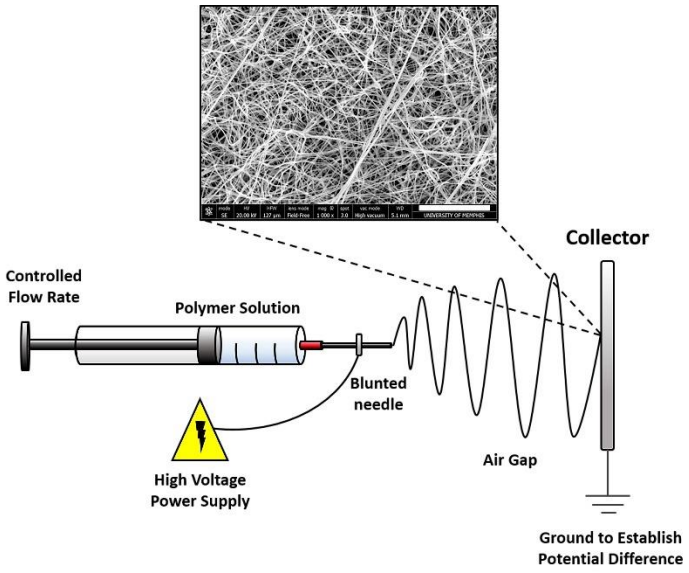

Figure 1. Schematic of the electrospinning process and a SEM of an electrospun biomaterial made from PDO. In the example micrograph, the non-woven fibers mimic the random orientation of some ECM fibers, and average fiber size is approximately 400 nm (scale bar = 30 μm).

The Immune Response to Biomaterials

The need for *in situ* tissue engineering and electrospun biomaterials exists because mammals tend to heal injured tissue imperfectly with a loss of function, resulting in fibrosis and scarring, rather than regenerating the tissue. This imperfect healing is believed to be the result of the immune system. Lower vertebrates and human fetuses, which have limited immunity, have complete regenerative capacity while higher vertebrates and adult humans with well-developed immunity have impaired regeneration, suggesting an inverse relationship between immunity and regeneration [6]. Historically, interpretation of this inverse relationship suggested a need to block the immune system for efficient tissue regeneration, but we now know that inflammation and immunity can

have profoundly positive impacts on tissue regeneration when regulated [7]. Most importantly, the regulation requires a coordinated response between immune cells to facilitate progression from the acute inflammatory response towards resolution in order to mitigate fibrosis. Thus, the most promising avenue for promoting functional regeneration is engaging the immune system and modulating it down the pathway of resolution, repair, and rebuilding, beginning with the neutrophil.

The implantation of a biomaterial (Figure 2) results in tissue damage, which triggers acute inflammation and an innate immune response, characterized by neutrophil recruitment [8]. Signals such DAMPs, IL-8, and LTB4 are released from the ECM and necrotic cells to recruit neutrophils from the circulation (Figure 2A) [9-11]. These signals establish a chemotactic gradient that can be immobilized in the ECM to direct neutrophil migration. Aided by the increase in vascular permeability from the acute inflammatory response, there is a rapid amplification of phenotypically plastic neutrophils in the local microenvironment, referred to as neutrophil swarming (Figure 2B) [12]. Within 25-40 minutes, neutrophils undergo extravasation from the vasculature and swarm infected or sterile wounds before clustering around the site of tissue damage. LTB4, released from endothelial cells after exposure to DAMPs, is also secreted by neutrophils to mediate swarming in a feed-forward manner [12, 13]. Furthermore, vascular damage resulting from the surgical insult will lead to pooled blood, containing neutrophils, around the biomaterial. As a result, biomaterial implantation establishes a dynamic and complex microenvironment that is acutely infiltrated by neutrophils, eager to interact with and respond to the biomaterial.

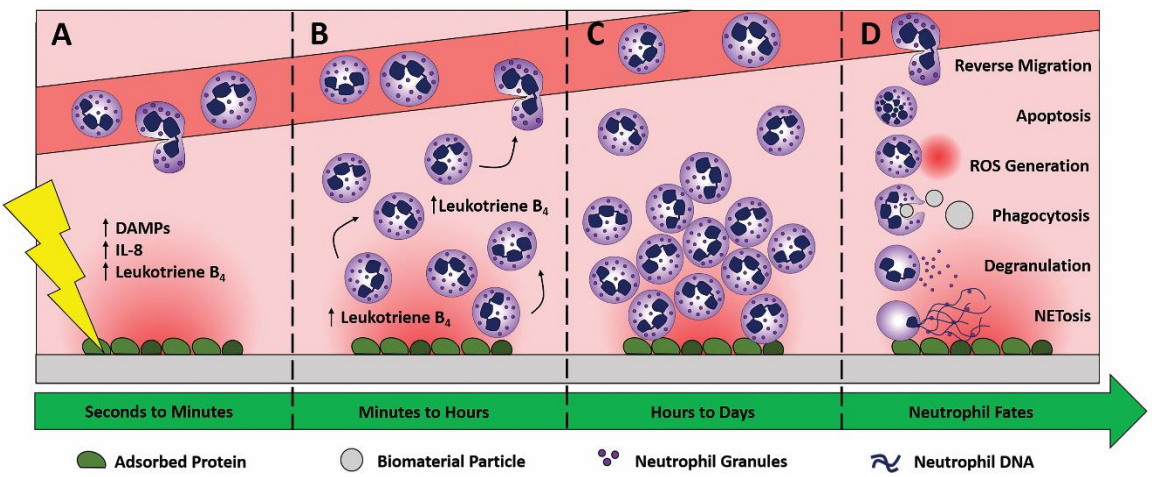

Figure 2. Implantation of a biomaterial triggers an innate immune response and neutrophil recruitment. (A) Injury up-regulates DAMPs, IL-8, and LTB4 to recruit neutrophils from circulation. (B) Neutrophils are recruited to a biomaterial-induced injury through LTB4 secretion in a feed-forward manner. (C) Swarming neutrophils interact with the biomaterial directly or indirectly through surface adsorbed proteins. (D) Neutrophils respond to the biomaterial and modulate the microenvironment through the production of ROS, phagocytosis, degranulation, and the release of NETs. Additionally, neutrophils can undergo apoptosis or reverse migrate back into circulation.

The swarming and clustering neutrophils either interact with the biomaterial directly through binding sites on the material surface or indirectly through binding sites on surface-adsorbed proteins (Figure 2C). Natural polymer biomaterials, made from collagens, gelatin, and fibrinogen, are derived from the ECM and are inherently bioactive. They contain binding sites for integrins, which can induce outside-in signaling within neutrophils resulting in a multitude of effects [14]. In addition, synthetic materials present binding sites on their surface through the adsorption of blood plasma proteins [15]. Surface-adsorbed proteins may contain binding sites in their native conformation or may reveal cryptic binding sites through conformational alterations due to adsorption [16]. Direct or indirect interactions with the biomaterial results in a dynamic interplay between the material, the neutrophils, and the response.

The biomaterial-interacting neutrophils can respond through several effector functions to modulate the inflammatory state of the tissue (Figure 2D). Tools in their arsenal of responses include the production of ROS, the ability to clear pathogens and debris through phagocytosis, the exocytosis of granules through degranulation, and the capacity to release NETs. Importantly, these processes determine the outcome after biomaterial implantation by regulating the extent of inflammation and the rate of resolution [17].

Final resolution of the innate immune response and removal of neutrophils from the injury site are essential for biomaterial-guided *in situ* tissue regeneration. In the classical wound healing response, neutrophil recruitment peaks within the first 48 hours and declines rapidly over the next several days while macrophages infiltrate the inflammatory site. This rapid response and subsequent decline suggest an important pre-conditioning function for neutrophils in the acute inflammatory phase. However, some studies have shown that neutrophils can persist for several days and weeks in the presence of inflammatory signals that decrease the levels of pro-apoptotic proteins [18-20]. For example, neutrophils have been found in the peritoneal cavity two weeks after the implantation of alginate microcapsules, indicating their pro-longed participation in the chronic response to a biomaterial [21]. Removal of neutrophils can occur through efferocytosis, where apoptotic neutrophils are cleared by macrophages, or can occur through reverse migration, where neutrophils return to the vasculature during resolution [22, 23]. The efferocytosis of apoptotic neutrophils by macrophages is an anti-inflammatory process that is essential for wound healing, implicating this as an important clearance mechanism to resolve inflammation [24, 25]. Ultimately, the biomaterial must be designed to

direct the neutrophils to a restorative phenotype that promotes resolution of inflammation followed by tissue regeneration.

Conclusion

Electrospun biomaterials hold great therapeutic potential for stimulating *in situ* tissue regeneration and improving the quality of life for many patient populations. Although macrophages have long been considered the maestros of tissue regeneration, neutrophil recruitment precedes the arrival of macrophages, suggesting that macrophage effector functions lie downstream from neutrophil effector functions. Therefore, while macrophages are undoubtedly needed for *in situ* tissue regeneration, our understanding and ability to design immunomodulatory biomaterials may be inherently limited by our lack of understanding of the neutrophil's preconditioning response.

The following work characterizes the release of NETs on electrospun biomaterials, evaluates its impact on tissue regeneration, and investigates its regulatory mechanisms. Of the neutrophil effector functions, the release of NETs was selected as the primary focus of this work for two reasons. First, there was a significant gap in the literature evaluating NET release in response to biomaterials, despite increasing evidence from other inflammatory environments that NETs are present. Second, NETs have been linked to thrombosis and fibrosis, two outcomes that are particularly detrimental to biomaterial-guided *in situ* tissue regeneration. Ultimately, our results indicate that electrospun biomaterial-induced NET release can be controlled through biomaterial design and that it shapes the regenerative microenvironment and potential for functional tissue regeneration and healing.

CHAPTER 2

LITERATURE REVIEW

Introduction

An injury to a tissue or organ initiates a tissue repair program that is initially characterized by inflammation and the local recruitment and accumulation of immune cells at the wounded site [26]. Independent of injury location, neutrophils are rapidly recruited to the damaged area and dominate the acute response. The early and robust recruitment of neutrophils is essential for preventing pathogen dissemination when barriers such as the skin or mucosa are damaged because their multiple effector functions efficiently kill bacteria. These effector functions include the production of ROS, the release of granules, the phagocytosis of invaders, and the extrusion of NETs [17]. NETs, which are extracellular structures composed of decondensed chromatin and various nuclear and granular components, were initially characterized in the context of host defense as a mechanism to locally concentrate the noxious anti-microbial cargo of the neutrophil and kill trapped pathogens [27]. However, it is now well established that the recruitment of neutrophils and the release of NETs occurs both in the context of infection and in response to sterile injuries [28, 29], such as the implantation of a biomaterial or tissue-engineered construct [21, 30, 31]. Moreover, dysregulated neutrophil recruitment and NET release can cause collateral tissue damage and uncontrolled inflammation, which are particularly detrimental to biomaterial-guided tissue regeneration and repair. This review discusses our knowledge of NETs and their role in inflammatory pathologies, including cancer, thrombosis, and fibrosis, and the resolution of inflammation. In addition, we discuss what is known about NETs in the response to biomaterials and highlight future

considerations for immunomodulatory biomaterial design to control the neutrophil response and enhance tissue repair and regeneration.

The Biology of NETs

The Composition and Morphology of NETs

NETs are extracellular structures composed of a physical network of DNA nanofibers that are decorated by bound proteins derived from several compartments within the neutrophil. Although an initial description included only 25 proteins [32], more recent proteomic analyses have identified nearly 700 proteins within NETs with the vast majority implicated in autoimmunity and inflammatory disorders [33]. Additionally, most investigations into the protein cargo of NETs indicate that the proteomic profiles change slightly depending on the stimuli and whether neutrophils are used from healthy donors or a disease state [33-36]. Therefore, while some differences likely exist when NETs are released in response to biomaterials, the most abundant proteins in NETs substantially overlap independent of disease state or stimulus, suggesting their relevance in biomaterial-induced NET release. Here we present a non-exhaustive list of the most important NET components to consider for tissue repair and regeneration (Table 1) and recommend that interested readers reference the proteomic studies for a complete list of NET components [32-34, 36-38].

Table 1. NET-bound protein cargo and their significance in tissue engineering.

Protein	**Significance in Tissue Engineering**
Cytoskeletal	
β-actin [32-35, 38]	DAMP that activates some immune cells [39] Physiologic inhibitor of DNase [40, 41]
Vimentin [33, 34, 36, 38]	Pro-inflammatory stimulus susceptible to citrullination [42]

Table 1 (Continued). NET-bound protein cargo and their significance in tissue engineering.

Protein	Significance in Tissue Engineering
Cytoskeletal	
Vimentin [33, 34, 36, 38]	Stabilize activated platelets complexed with plasminogen activator inhibitor 1 [43] Exacerbate epithelial damage [44]
Cytosolic	
PAD4 [36]	Citrullinates proteins leading to inflammatory responses [34]
S100-A8 Protein [32-34, 38]	DAMP that activates some immune cells and endothelial cells [45] Pro-inflammatory stimulus that triggers neutrophil chemotaxis and adhesion [46]
S100-A9 Protein [32-34, 38]	DAMP that activates some immune cells and endothelial cells [45] Pro-inflammatory stimulus that triggers neutrophil chemotaxis and adhesion [46]
S100-A12 Protein [32, 33, 38]	DAMP that activates some immune cells and endothelial cells [45] Pro-inflammatory stimulus that triggers neutrophil chemotaxis and adhesion [46]
Granular	
Cathepsin G [32, 33, 36, 38]	Activates MMPs [47] Promotes platelet activation and aggregation [48]
MMP-8 [34, 36]	Degrades ECM components [49]
MMP-9 [33, 34, 36, 38]	Degrades ECM components [49]
MPO [32, 33, 35, 38]	Generates ROS [50]
NE [33, 34, 36, 38]	NE-DNA complexes inactivate plasminogen [51] Degrades all ECM components [52] Activates MMPs [53]
NGAL [33, 34, 36]	Stabilizes MMP-9 to enhance activity [54]
Nuclear	
Histone 2A [32-34, 36, 38]	DAMP that activates pro-inflammatory responses from immune cells [55]
Histone 2B [32-35, 38]	DAMP that activates pro-inflammatory responses from immune cells [55]

Table 1 (Continued). NET-bound protein cargo and their significance in tissue engineering.

Protein	Significance in Tissue Engineering
Nuclear	
Histone 3 [32-34, 36, 38]	DAMP that activates pro-inflammatory responses from immune cells [55]
Histone 4 [32-35, 38]	DAMP that activates pro-inflammatory responses from immune cells [55]
HMGB1 [33, 36]	Induce NET release and pro-inflammatory responses [28]
Non-Neutrophilic	
Tissue Factor	Promotes thrombin generation [56] Contributes to thrombosis through thrombin generation [29, 57]

The composition of NET-derived proteins can be grouped into four major categories: cytoskeletal proteins, cytosolic proteins, nuclear proteins, and granular proteins. Of the cytoskeletal proteins found in NETs, actin and vimentin are significant in tissue healing. Actin is an evolutionarily conserved DAMP recognized by some immune cells [39] that acts as a physiologic inhibitor of DNase [40, 41], which can degrade NETs. Therefore, the presence of actin in NETs can contribute to immune activation and the resistance of NETs to degradation, leading to aberrant NET accumulation and collateral tissue damage [35]. Similarly, vimentin, which can be secreted by activated neutrophils [58] and macrophages [59], can promote pro-inflammatory responses and is susceptible to citrullination, an enzymatic modification intimately tied to neutrophil-driven autoimmune disorders and NET release [42]. Moreover, it can stabilize activated platelets complexed with plasminogen activator inhibitor 1 and exacerbate epithelial damage [43, 44], hindering tissue healing.

Of the array of cytosolic proteins found in NETs, the S100 proteins and PAD4 can have a significant impact on tissue healing for biomaterial applications. The S100 proteins, a set of calcium-binding proteins, have a broad range of functions in

inflammation and immune homeostasis [60]. When they are released into the extracellular space, S100 proteins function as DAMPs to activate immune cells and endothelial cells [45]. S100A8 and S100A9, together known as calprotectin [61], and S100A12 are abundantly expressed in neutrophils and bind to TLR4 and RAGE to initiate pro-inflammatory responses implicated in chronic neutrophil-driven inflammation [46, 62]. Likewise, PAD4 is an enzyme that citrullinates histones to facilitate chromatin unraveling during NET release [63] but also citrullinates other extracellular proteins, contributing to autoantibody generation in inflammatory pathologies [34, 64]. Therefore, while an inflammatory response is necessary for tissue healing, the highly localized expression of S100 proteins and PAD4 on NETs can lead to overactivation of an inflammatory response and drive chronic responses rather than resolution.

Majority of the NET protein cargo are granular proteins with diverse enzymatic activity [33]. The two granular proteins commonly associated with NET formation are NE and MPO. Most of the proteolytic activity of NETs is attributed to NE [38], which can target and degrade all ECM components [52] and activate MMPs [53]. NET-bound MPO on the other hand exerts its affects through the generation of ROS [50], and elevated levels are associated with poor prognosis in several cardiovascular disease states [65]. Additional granular proteins found in NETs include MMP-8 and MMP-9, which can also contribute to ECM degradation [49], and NGAL, the stabilizer of MMP-9 [54, 66]. The serine protease cathepsin G is also found in NETs and can process MMPs into their active form [47] and promote platelet activation and aggregation [48]. Together, this milieu of granular proteins contributes to NET-driven inflammation through the excessive degradation of the ECM and activation of pro-inflammatory signals.

NETs also contain proteins of nuclear origin including histones and chromatin-bound proteins. Histones are of particular importance in inflammation and tissue healing because they are recognized as DAMPs, leading to pro-inflammatory responses from immune cells [55]. Moreover, histones have been shown to directly induce epithelial and endothelial cell death that contributes to tissue destruction [67]. In addition, non-histone nuclear protein HMGB1 is also a DAMP with diverse functions in inflammation and immunity [68]. NET-bound HMGB1 has been shown to aggravate systemic lupus erythematosus [69], potentially participate in acute gouty inflammation [70], and induce NET release and pro-inflammatory responses in liver injury [28]. As such, these NET-bound nuclear proteins participate in the regulation of the inflammatory microenvironment with predominantly pro-inflammatory effects.

Besides proteins from defined neutrophil compartments, proteins that are not of neutrophil origin can also bind to NETs and play an important role in the response to NETs in tissue healing. The most noted example in literature is tissue factor, the primary initiator of the extrinsic coagulation cascade. Although some reports suggested that neutrophils can synthesize and secrete tissue factor [57, 71], more recent proteomics studies did not find tissue factor bound to NETs isolated from ultrapure populations of neutrophils [32-34, 36-38], suggesting that NET-bound tissue factor is not of neutrophil origin. Nonetheless, NET-bound tissue factor promotes thrombin generation [56] and has been shown to contribute to thrombosis in acute myocardial infarction as well as in antineutrophil cytoplasmic antibody associated vasculitis [29, 57]. Therefore, the ability of NETs to bind active tissue factor could be especially detrimental to biomaterial applications with blood-contacting biomaterials.

The diverse NET-bound proteins concentrate in NETs based on their interaction with the charged DNA fibers, but the source of the DNA from within the neutrophil is subject to debate. NET formation was originally described by the release of nuclear chromatin [27], but since the initial description, an additional type of NETs characterized by the release of mitochondrial DNA has been described [72, 73]. In one example, mitochondrial NETs were released from viable neutrophils after priming with GM-CSF and stimulation of TLR4 or complement factor 5a receptor [72]. Eosinophils are known to release mitochondrial DNA through a similar mechanism [74]. In another example, mitochondrial NET release was identified after traumatic injury and trauma surgery [73]. Most neutrophil biologists now accept that NETs can be composed of nuclear or mitochondrial DNA, which may impact the NET protein cargo, but the physiologic and mechanistic distinction remains unclear [75]. As such, there is potential that both nuclear and mitochondrial NETs are released in response to biomaterials, but this has yet to be specifically investigated. In our work, when abundant NETs are observed on electrospun biomaterials, there is an absence of intact nuclei, suggesting the NETs are primarily of nuclear origin [31, 76].

NETs are typically described as having a cloud-like morphology that can grow beyond the size of a neutrophil (Figure 3). However, the morphology can vary between cloud-like structures and elongated fibrous extrusions, but these differences are attributed to agitation during sample preparation rather than physiologically relevant, morphological differences [75]. The cloud-like morphology of NETs is likely related to their indiscriminate release from the cell, thought to be driven by entropic chromatin swelling, that has been observed both *in vitro* and *in vivo* using live microscopy [35, 77-79].

On our electrospun biomaterials imaged by fluorescence microscopy, NETs appear to randomly cover the surface of the biomaterial, which others have similarly observed [21, 31, 80]. Given their volume and ability to cover surfaces, it is easy to imagine that the extensively decorated DNA fibers can precondition a pro-inflammatory environment when released in response to stimuli other than invading pathogens.

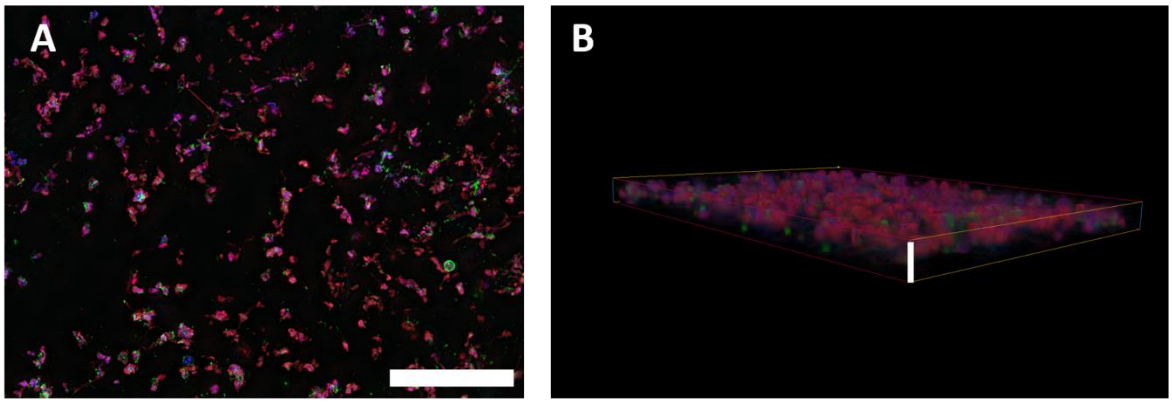

Figure 3. Fluorescent micrographs of NETs on electrospun biomaterials. Although they appear two-dimensional when viewed from (A) the top in epifluorescence microscopy, NETs are 3D structures with height and volume, which is evident when viewed in (B) a Z-stack of fluorescent micrographs. In these images, human neutrophils were cultured on the electrospun biomaterial for 3 hours. Extracellular chromatin is stained red with STYOX orange, cell membrane is green with Alexa Fluor™ 488 conjugated wheat germ agglutinin, and nuclei are blue with DAPI. (A) Scale bar is 100 µm. (B) Scale bar in the z-axis is 55 µm.

Stimuli and Pathways of NET Release

The release of NETs is a distinct, coordinated process that requires sequential steps to facilitate chromatin unraveling and ultimately the extrusion of NETs [81]. During nuclear NET release, the nuclear and granular membranes disintegrate, the nucleus decondenses, and the DNA mixes with cytoplasmic and granular components. The process culminates with rupture of the cell membrane and release of the protein-decorated NET into the extracellular space. However, the signaling pathways and involvement of critical enzymes, such as NOX2 production of ROS to free NE and MPO

from granules [82], activation of NF-κB [83], and PAD4 citrullination of histones to facilitate chromatin unraveling [63], vary greatly depending on the stimuli acting on the neutrophil. Additionally, the kinetics of NET release have been reported to vary from 10 minutes to 24 hours and are also stimuli dependent [84], which further emphasizes the importance of studying NET release within a specific disease state or lack thereof. Multiple non-physiological and physiological infectious, inflammatory, and immunologic stimuli are documented in the literature to trigger *in vitro* and *in vivo* NET release. Here, we highlight the stimuli and known signaling pathways most relevant for biomaterial and tissue engineering applications (Figure 4). Interested readers should reference Hoppenbrouwers *et al.* for a thorough list of stimuli, their studied concentration ranges, and their impact on NET release with corresponding references [84].

The most frequently used NET stimulus for *in vitro* studies is PMA, a plant-derived compound that bypasses receptor engagement and actives PKC to initiate its signaling cascade [27, 34, 85]. Downstream of PKC, PMA-induced NET release requires NOX2 production of ROS and PAD4 activation [77, 86]. The benefit of PMA as an *in vitro* stimulus is that it consistently triggers NET formation with reported 100% efficacy across a broad range of concentrations [84]. However, the detriment of PMA is that it is not physiologically relevant since it does not play a role in *in vivo* physiological processes. Therefore, it is now recognized that the use of PMA as an *in vitro* stimulus for NET formation should be approached with caution, especially in the context of biomaterials and the tissue repair program. If the goal is to study the neutrophil response during acute inflammation in an *in vitro* model or to evaluate potential inhibitors of NET release, PMA should not be used as a stimulus since it does not play a physiological role in acute

inflammation. Alternatively, if the goal is to stimulate maximum NET release for the purpose of quantifying NET formation *in vitro*, PMA may be an appropriate positive control. For example, our group uses PMA to represent 100% NET formation in our *in vitro* assay for quantification of biomaterial-induce NETs, and we express our results as a percentage of NET release relative to PMA [87, 88].

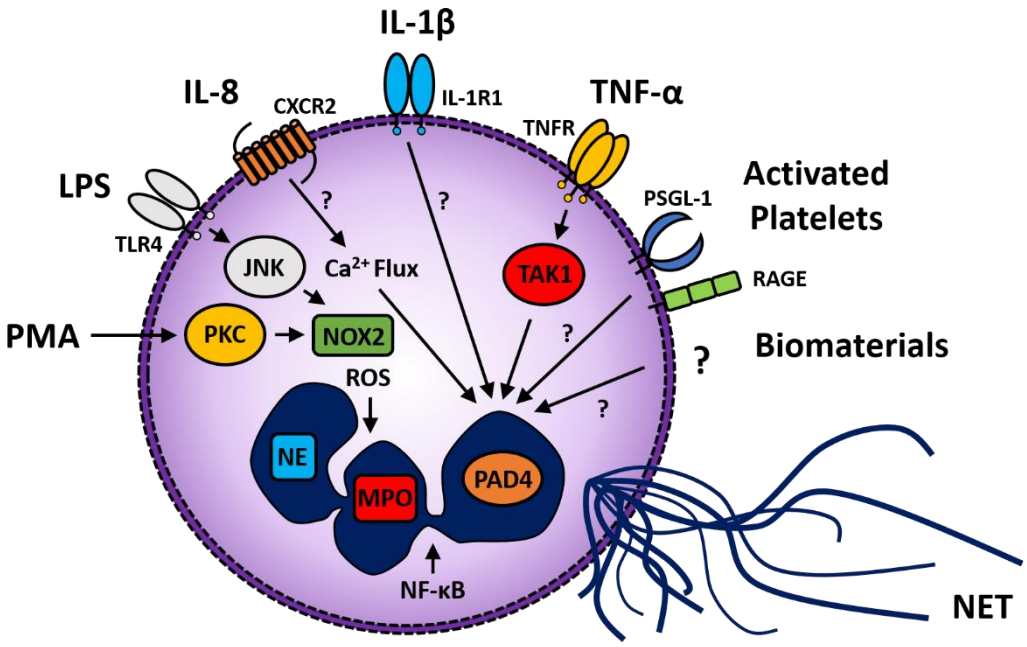

Figure 4. Stimuli and signaling pathways of NET release most relevant for biomaterials and tissue engineering applications. Question marks indicate pathways that have not been extensively investigated. PMA is the most widely used non-physiological NET stimulus requiring PKC, NOX2, and PAD4 for NET release [77, 86]. LPS, which is relevant in the context of infection, signals through JNK and also requires NOX2 and PAD4 [89]. The signaling pathways for IL-8, IL-1β, and TNF-α are not as well studied, but recent data indicates they do not require NOX2 for NET release [90, 91]. Data suggests IL-8 induced NET release requires calcium flux [92] whereas TNF-α signals through TAK1 [91]. Activated platelets can prime neutrophils for NET release through binding of P-selectin to PSGL-1 and directly stimulate NET release through HMGB1 binding to RAGE, although the signaling pathway has not been elucidated [93-95]. Biomaterials can also induce NET release, but the receptors and signaling pathways have yet to be evaluated and likely vary depending on the type of biomaterial. Finally, requirements for NF-κB activation and mobilization of NE and MPO are dependent on the stimuli, but have been found to participate in NET release [83, 96-99].

Similar to PMA, LPS is widely used as an *in vitro* NET stimulus and may or may not be appropriate in the context of biomaterials and tissue regeneration [27, 34, 86, 100, 101]. LPS has been shown to signal through TLR4 and JNK, though one group has demonstrated a TLR4-independent mechanism, and requires NOX2 production of ROS and PAD4 for NET release [87, 89, 102]. Derived from the outer membrane of gram-negative bacteria, LPS is composed of a lipid A component, a core containing an oligosaccharide, and an O-antigen that is the major basis for bacterial serotyping [103]. Thus, if NET release is being studied in an infected tissue environment, LPS may be an appropriate physiological control for assessing the efficacy of inhibitors. Unfortunately, contradicting data exists in the literature with some groups reporting LPS and neutrophil interactions trigger NET release while others report that they do not [100, 104, 105]. These different results can be primarily attributed to variability of the O-antigen between different types of LPS, which has been found to selectively regulate NET formation as a consequence of bacteria serotyping [102]. Moreover, the same study illustrated differential regulation *in vitro* under serum and platelet-free conditions, indicating that both the type of LPS and culture conditions should be carefully considered when studying LPS-induced NET release.

In addition, several pro-inflammatory cytokines and chemokines are efficient inducers of NET release and are important to consider for biomaterial-guided tissue regeneration. IL-8, the archetypal neutrophil chemoattractant secreted by damaged cells and neutrophils, has been shown to stimulate NET release at low concentrations but have no effect at high concentrations [27, 81, 90, 105, 106]. Likewise, IL-1β is released during acute tissue injury and can exacerbate tissue damage, which can be partially attributed to its ability to stimulate NET release [71, 107, 108]. TNF-α is also rapidly released after tissue

injury to enhance immune cell recruitment and stimulates NET formation [90, 108, 109]. While the signaling pathways for these pro-inflammatory mediators have been debated, recent data suggests that IL-8, IL-1β, and TNF-α signal through their respective receptors and trigger NET release in a ROS-independent manner [90, 91]. Given their involvement in acute inflammation, IL-8, IL-1β, and TNF-α should be considered important NET stimuli in tissue regeneration applications.

Activated platelets are a source of multiple growth factors and inflammatory mediators, which can activate neutrophils and trigger the release of NETs [93, 94, 110]. Alternatively, resting platelets cannot stimulate NET release [104], suggesting that the up-regulated expression of certain platelet receptors after activation and secretion of growth factors and inflammatory mediators are critical. In fact, platelet P-selectin has been found to prime neutrophils for NET release through binding to PSGL-1 [93], and platelet presentation of HMGB1 after activation also stimulates NET formation through RAGE in a NOX2-independent mechanism [94, 95]. The ability of activated platelets to stimulate NET release is intriguing for biomaterial-guided tissue regeneration since platelet rich plasma and platelet-derived growth factors have been found to resolve inflammation and enhance tissue healing in multiple tissue engineering studies [111]. It is possible that the high concentration of growth factors within platelet rich plasma overcomes the negative consequences of NET release in these scenarios, but this has not been investigated.

The last stimulator of NET release that is important for the application of biomaterials to tissue engineering and regeneration is the biomaterial itself. Our group and others have shown that a range of biomaterials stimulate NET formation, including electrospun biomaterials [31, 88], titanium [80], carbon and polystyrene nanoparticles [112],

Teflon™ [113], and a tissue-engineered trachea [30]. The stimulation of NET release is likely intimately related to the surface-adsorbed proteins on the biomaterial, which can vary greatly based on the surface chemistry and topography of the biomaterial [114]. Because investigations of NETs on biomaterials is a new consideration in tissue engineering, much work remains to determine variability between different types of biomaterials and the signaling pathways involved. Nonetheless, no matter the stimuli, exact kinetics, or signaling pathways, acute NET release is a significant preconditioning event occurring early in the tissue repair program that modulates the potential for tissue healing.

Inhibitors of NET Release

Similar to the stimuli triggering NET formation, multiple inhibitors can be used to block the release of NETs and their efficacy is dependent on the stimuli and signaling pathway. Because of the diversity of signaling pathways, it is unlikely that inhibition of one pathway abrogates all NET formation. Nonetheless, several common pharmacological targets (Table 2) exist due to their recurring involvement in NET release. While a plethora of inhibitors have been used specifically for elucidating the signaling pathways in NET release, here we focus on the targets and inhibitors of NET release with physiological implications.

Table 2. Common targets and inhibitors of NET release. Applications mentioning NET release were evaluated *in vitro* whereas applications mentioning a physiological impact were evaluated *in vivo.*

Target	**Inhibitor**	**Application**
PAD4	Cl-amidine	Protects against cardiac dysfunction in myocardial infarction [115]
		Reduces vascular damage in lupus [116]
		Suppresses colitis [117]
		Reduces arthritis [118]
		Reduces biomaterial-induced NET release [76]
	GSK484	Reduces ionomycin and *S. aureus* induced NET release [119]
ROS	Tempol	Reduces NET release induced by *Candida albicans* [120]
	TSG-6	Suppresses LPS-induced NET release [121]
	Luteolin	Suppresses arthritis [122]
	Kaempferol	Reduces tumor metastasis [123]
	Manuka honey	Reduces biomaterial-induced NET release [88]
Other Targets		
NE	GW311616A	Reduces tumor metastasis [96]
	Sivelestat	Rescues endotoxic shock [97]
	Secretory leukocyte protease inhibitor	Inhibits TNF-α and *S. aureus* induced NET release [124]
MPO	Anti-MPO antibody	Reduces NETS in response to influenza virus primed epithelial cells [98]
	AZM198	Attenuates endothelial damage [99]

Table 2 (Continued). Common targets and inhibitors of NET release. Applications mentioning NET release were evaluated *in vitro* whereas applications mentioning a physiological impact were evaluated *in vivo.*

Target	Inhibitor	Application
Other Targets		
NF-κB	Acetylsalicylic acid	Inhibits TNF-α induced NET release [83]
	BAY 11-7082	Inhibits TNF-α induced NET release [83]
	Ro 106-9920	Inhibits TNF-α induced NET release [83]
JAK	Tofacitinib	Reduces vascular damage [125]
Calcineurin pathway	Ascomycin	Attenuates IL-8 induced NET release [92]
	Cyclosporine A	Attenuates IL-8 induced NET release [92]
Autophagy	Chloroquine	Reduces hypercoagulability in cancer [126]
		Decreases acute pancreatitis severity [127]
Receptors	Anti-Mac-1 antibody	Inhibits LPS-induced NET release [128]
		Inhibits NET release in response to immobilized ICs [129]
	Anti-FcγRIIIb antibody	Inhibits NET release in response to immobilized ICs [129]
	Anti-FcγRIIa antibody	Inhibits NET release in response to endocytosed ICs [130]
	Roflumilast	Reduces IL-8, fMLP, and C5a induced NET release on fibrinogen surfaces [131]

The most frequently targeted enzyme for NET inhibition is PAD4 because its activity was initially described as essential for chromatin decondensation during NET release [132, 133]. Widely studied inhibitors of PAD4 include Cl-amidine, a general irreversible inhibitor of PADs [91, 132-134], and GSK484, a selective reversible inhibitor of

PAD4 [91, 115, 119]. Both have been used successfully *in vitro* and *in vivo* to attenuate NET release in several pathologies [116-118, 135]. Our group has even incorporated Cl-amidine into electrospun biomaterials to modulate biomaterial-induced NET release and showed that its local delivery could improve tissue integration and regeneration [76]. However, since NET release can occur independent of PAD4 as previously discussed [136, 137], PAD4 may not be a ubiquitous target for NET inhibition.

Down regulation of ROS has also been evaluated for blocking NET release since seminal studies in NET release used PMA, a powerful activator of NOX2 and ROS. Most studies have used ROS scavengers to quench ROS activity generated from various superoxide generating enzymes. Examples include Tempol, a stable redox-cycling drug [120], the anti-inflammatory protein secreted by stem cells, TSG-6 [121], and natural flavones and flavonoids [122, 123]. Recently, we used Manuka honey, which contains multiple flavones and flavonoids, to attenuate electrospun biomaterial-induced NET release [88]. Nonetheless, the requirement for ROS in NET release is also debated, and recent data indicates that ROS is likely not essential for NET formation but contributes to the process [91, 102, 137], which explains why ROS inhibitors may indirectly modulate NET release.

A variety of other signaling molecules and enzymes are involved in NET release and have been targeted to inhibit NET formation. Because most of the proteolytic activity of NETs is attributed to NE, several groups have evaluated inhibitors of NE [86, 96, 97, 124]. Likewise, antibodies or inhibitors of MPO have been investigated due to the contribution of MPO to NET release and tissue damage [98, 99, 138]. Additional targets include NF-κB [83], JAK [125], the calcineurin pathway [92], and autophagy [126, 127, 139]. Up-stream of all of these signaling molecules and enzymes are the receptors that initiated the outside-in signaling,

which have also been targeted to a lesser extent to modulate NET release. Blocking of Mac-1 [140] and FcγRs [129, 130] with neutralizing antibodies has been shown to reduce NET release, and indirect inhibition of platelet-neutrophil interactions with Roflumilast was also efficacious for reducing NETs [131]. Together, these data indicate that although the complexity of NET release has initially complicated our ability to demarcate specific signaling pathways, numerous pharmacological targets exist to down regulate NET release in a variety of pathologies, including biomaterial-induced NET release.

NETs in Inflammatory Pathologies

As the number of studies on NETs in *in vitro* systems and *in vivo* models has grown, so too has the number of physiological implications attributed to NETs. In line with their first described function, NETs are critical in the defense against bacteria, viruses, and fungi, especially in scenarios when the skin or mucosa are damaged [27, 102, 141, 142]. By trapping the invader in close proximity to the lytic anti-microbial compounds associated with the DNA structure, NETs efficiently kill the pathogen [27, 50]. Another interesting function of NETs that is attributed to their localized, toxic proteases is their anti-inflammatory action when clustered in aggregated NETs [143]. It is believed that the large aggregation of NETs around MSU crystals observed in gout actually attenuates inflammation by degrading cytokines and chemokines [144]. Nonetheless, the anti-inflammatory action of NETs seems to be highly specific to gout and infection prevention with the vast majority of investigations finding that NETs are typically pro-inflammatory and central to a number of inflammatory pathologies. Here, we will discuss the involvement of NETs in cancer, thrombosis, and fibrosis because of their relevance to biomaterials and tissue regeneration.

Cancer

Inflammation is a hallmark of cancer, and the proliferation of tumors has been described as wounds that fail to heal due to misappropriated mechanisms of inflammation in tissue regeneration [145, 146]. As such, an appreciation for the involvement of NETs in cancer could give important insight into the role of NETs in biomaterial-guided tissue regeneration applications. Most of the literature indicates that NETs facilitate cancer metastasis in a number of tissue environments, including breast, liver, pancreatic, ovarian, lung, and gastroesophageal metastases [147-151]. In these studies, the NETs function as structures that attract and capture circulating cancer cells to promote their adhesion [96, 148, 151]. Subsequently, NETs activate cancer-associated fibroblasts, which have a similar morphology to myofibroblasts in wound healing, and promote the deposition of a fibrous stroma in the developing metastasis [147, 152, 153]. Aside from metastasis, the contribution of NETs to primary tumor growth is not well understood, but some have speculated that NET release may propagate tumor cell proliferation by stimulating the recruitment of additional immune cells, fueling the pro-tumoral inflammatory environment [154]. Last, surgical stress has been shown to induce NET release that is enhanced in hypoxic tumors, suggesting that the hypoxic environment created by the surgical site around a biomaterial may also increase NET release [155]. Together, these studies indicate that NETs are important both as physical structures and activators of fibrous stroma deposition in tumor pathogenesis, resulting in misappropriated mechanisms of tissue healing.

Thrombosis

In addition to functioning as a scaffold for tumor proliferation, NETs contribute to cancer pathology by promoting thrombosis [126, 156, 157]. The procoagulant activity of NETs

has also been observed in myocardial infarction [29], antineutrophil cytoplasmic antibody associated vasculitis [57], deep vein thrombosis [85, 158, 159], heparin-induced thrombocytopenia [135], and sepsis [79]. The thrombogenicity of NETs is attributed to their ability to bind and expose functional tissue factor [29, 33, 57, 71] as well as promote platelet aggregation and stabilization through a positive feedback loop [29, 159, 160]. Additionally, NETs can disrupt the endothelium [161], which induces a more pro-coagulative endothelial cell phenotype characterized by retraction of cell-cell junctions [156]. Thus, the ability of NETs to initiate and support the coagulation cascade through multiple mechanisms is a concern for tissue engineering, especially for blood-contacting biomaterials where thrombosis can lead to detrimental consequences.

Fibrosis

Dysregulated NET release also promotes tissue fibrosis in multiple tissue and organ environments. Similar to fibrous stroma deposition in cancer [147, 152, 153], NETs activate lung fibroblasts and induce their differentiation into myofibroblasts, contributing to fibrosis [162, 163]. Likewise, NETs enhance the fibrotic potential of dermal fibroblasts in systemic lupus erythematosus [56] and cutaneous fibrosis in systemic sclerosis [164] and correlate with scar formation in post-epidural fibrosis [165]. Interestingly, in the case of gout where aggregated NETs seem to have an anti-inflammatory effect [35], the gouty tophi are surround by a fibrous capsule to isolate the stimuli from the microenvironment [166]. This may also explain why NETs lead to fibrosis in other scenarios where the body is attempting to wall off the inflammatory stimuli in an effort to restore homeostasis, an undesirable response in most biomaterial applications.

NETs in the Resolution of Inflammation

Since NETs retain their toxicity and proteolytic activity until degradation, NETs participate in the resolution of inflammation when their dismantling occurs efficiently during the acute inflammatory response, which can be skewed when their release is dysregulated [27]. NETs are primarily degraded by endonucleases, DNase I, and DNase I-like 3 [167]. Multiple studies have shown that exogenous DNase I treatment can abrogate the toxic effects of NETs in several pathologies, including thrombosis and fibrosis [163, 165, 168-170]. Moreover, accelerated NET degradation by DNase I has also been shown to improve neovascularization and vascular repair after stroke [169], highlighting that their degradation is central for the resolution of inflammation and progression in the tissue repair program. However, physiological concentrations of DNase I are not sufficient to completely degrade NETs, so macrophages engulf partially digested NETs in an immunologically silent manner, much like macrophage engulfment of apoptotic neutrophils [171, 172]. In contrast to their silent clearance, an overproduction of NETs during inflammatory pathologies can lead to pro-inflammatory responses from interacting macrophages [173]. Together, these data indicate that a fine balance between the presence of NETs and their degradation exists in order to avoid inflammation and tissue damage while propagating the tissue repair program.

NETs are also intimately related to the resolution of inflammation in their absence of release because neutrophils are then able to influence tissue healing through their active restorative functions [174, 175]. Examples of the pro-healing functions of neutrophils include phagocytosis of debris, release of growth factors, and the initiation of angiogenesis [17]. The contribution of neutrophils to the resolution of inflammation in

sterile tissue injuries has largely been studied in the context of ischemic injuries, where the purpose of the tissue repair program is to promptly initiate angiogenesis to restore blood flow. Angiogenesis is proceeded by neutrophil recruitment in many models, and these studies have found that neutrophil depletion significantly delays healing [176-179]. Moreover, these models have shown that neutrophils rapidly swarm to an injury within 25-40 minutes after its induction before clustering around the site of tissue damage, suggesting their integral involvement in tissue repair [12]. It is speculated that the absence of neutrophils delays proper healing in these sterile injuries because the resolution of inflammation is programmed for and requires the regulated activation and deactivation of neutrophils [180]. Alternatively, when inflammation is triggered by an unnatural stimulus, such as high glucose in diabetes, alcohol, autoimmune antibodies, or a biomaterial, neutrophils struggle to respond appropriately, which results in maladaptive effector functions [180]. Taken together, NET release and the resolution of inflammation are inherent programs within the neutrophil's molecular machinery, and understanding how to regulate them with immunomodulatory biomaterials may significantly enhance tissue regeneration by avoiding inadvertent neutrophil activation.

NETs and Biomaterials for Tissue Engineering and Regeneration

Engineering immunomodulatory biomaterials for controlling the immune response is not a new concept, but the application to regulating neutrophils and NET release to enhance tissue regeneration has only been realized in recent years. As with macrophages, the interest of tissue engineers in neutrophils increased with an increasing body of literature on neutrophil-driven angiogenesis and tissue remodeling in tumor biology [49, 181, 182]. As more studies revealed that NETs contribute to collateral tissue

damage and chronic inflammation, our interest has grown in understanding NET release as a preconditioning event in the response to biomaterials and the tissue repair program. Given that surgical stress, hypoxia, and trauma can trigger NET release [155, 183], it is easy to conceptualize that implantation of a biomaterial and its ability to induce NET release from swarming neutrophils [12] can contribute to a dysregulated inflammatory environment that is not conducive to functional tissue healing. Most investigations into biomaterial-induced NET release have focused on understanding how the composition, surface chemistry, and topographical features of the biomaterial regulate NET release to avoid their adverse effects. Here, we summarize what is known about NETs and biomaterials (Figure 5) in thrombosis, fibrosis, and tissue integration and conclude with future considerations for tissue engineering applications.

Thrombosis

Since NETs amplify platelet aggregation and bind active tissue factor [79, 85], NETs can synergistically promote coagulation with platelets in response to biomaterials. Recently, Sperling *et al.* evaluated the effects of biomaterial surface chemistry on NET release and thrombin generation [113]. The authors found that hydrophobic biomaterials

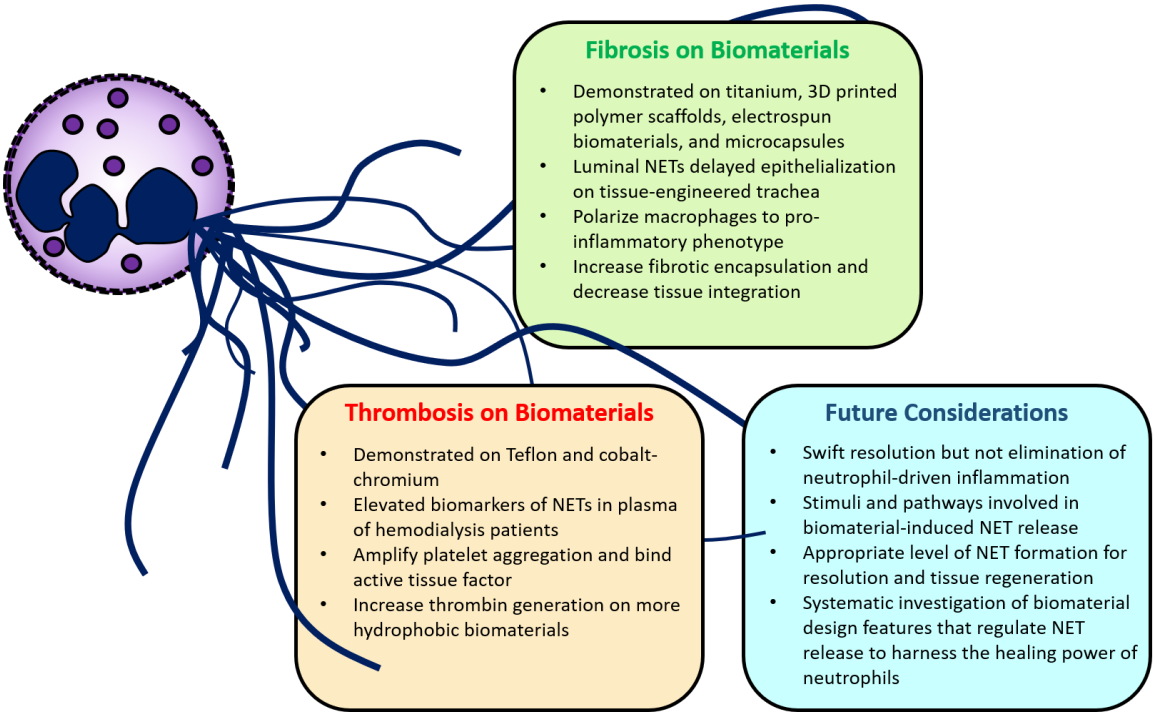

Figure 5. NET release on biomaterials regulates thrombosis, fibrosis, and tissue integration. Several studies illustrate that NETs enhance thrombin generation and coagulation on biomaterials, occurring more readily on hydrophobic biomaterials [113, 184], and elevated biomarkers are found in the plasma of hemodialysis patients [185]. Additionally, increased NET release on the surface of biomaterials polarizes macrophages towards an inflammatory phenotype [80, 186], up-regulates fibrosis and impairs tissue integration [21, 31, 186], which has been seen in the clinical application of a tissue-engineered trachea [30]. Finally, swift resolution of neutrophil-driven inflammation is needed for healing and an understanding of how to regulate NET release through immunomodulatory biomaterials may enhance biomaterial-guided tissue regeneration.

increased the release of NETs compared to hydrophilic surfaces [113]. Moreover, they demonstrated that NET release on hydrophobic Teflon™ AF resulted in elevated thrombin generation and coagulation, linking biomaterial-induced NET release and thrombogenicity to a clinically used biomaterial. Likewise, elevated biomarkers of NETs are found in the plasma of hemodialysis patients [185], which suggests that hydrophobic hemodialysis membranes may stimulate NET release and contribute to thrombosis seen in patients undergoing dialysis [187]. Similar work evaluating cobalt-chromium, an alloy commonly used in cardiovascular implants, illustrated that thrombin generation and NET

release occurred in the presence of platelets and can exacerbate endothelial cell dysfunction and coagulation [184]. Together, these studies link NET formation to biomaterial-induced thrombosis and emphasize the importance of assessing neutrophil activation when considering the hemocompatibility of biomaterials.

Fibrosis and Tissue Integration

Several groups have also focused on the impact of NETs in fibrosis and tissue integration. Vitkov *et al.* found that NETs are released in response to rough titanium biomaterials that stimulate osseointegration [188], but the impact of NETs on the inflammatory response and potential for tissue integration was not evaluated in this work. To address it, NET formation on smooth, rough, and rough-hydrophilic titanium surfaces was then studied to determine how the neutrophil response impacts macrophage polarization [80]. In these experiments, rough hydrophilic titanium biomaterials decreased pro-inflammatory responses and NET release whereas the smooth and rough hydrophobic titanium surfaces increased NET release, indicating that neutrophils sense the biomaterial surface and respond differentially. The authors then showed that the neutrophil conditioned media from the smooth and rough hydrophobic surfaces enhanced pro-inflammatory macrophage polarization, which was attenuated when the neutrophils were treated with NET inhibitors. Similarly, Won *et al.* eloquently demonstrated that 3D printed polycaprolactone biomaterials with hierarchical microchannels decreased NET release and enhanced macrophage polarization to the pro-healing phenotype, which correlated with increased angiogenesis and reduced fibrosis, compared to control 3D printed biomaterials [186]. Our group has also shown that both the polymer and topography of electrospun biomaterials can regulate NET release and that up-regulated NET release,

occurring on hydrophobic polydioxanone with a high surface area topography, correlates with fibrotic encapsulation [31]. Jhunjhunwala *et al.* obtained similar results with implanted microcapsules, observing NETs on the surface up to three days after implantation, and speculated that the surface-coating NETs nucleated fibrosis [21]. Last, in the only published clinical example to date, a decellularized cadaver trachea implanted into a 12 year old boy was found to have NETs on the luminal surface for the first 8 weeks after surgery, which the authors postulated delayed epithelialization [30]. Together, these data indicate that neutrophils sense the biomaterial and precondition the environment for differential immune cell activation and the subsequent tissue repair program, significantly impacting tissue integration and fibrosis.

Conclusion

NET release is an active process programmed into the neutrophil's molecular machinery to prevent infection. However, the dysregulated release of NETs contributes to multiple pathologies, including cancer, thrombosis, fibrosis, and biomaterial-related complications. Moreover, NET release prevents the neutrophil from exerting its pro-healing potential, further impairing tissue repair. Although the body of literature is still small, the release of NETs on biomaterials appears to be a significant preconditioning event that influences the potential for tissue healing with largely detrimental consequences. More extensive evaluations of neutrophils and NET release in response to biomaterials will likely aid in the development of immunomodulatory biomaterials that avoid maladaptive immune responses and improve the therapeutic potential of tissue-engineered biomaterials and their applications in the clinical setting.

CHAPTER 3

ELECTROSPUN TEMPLATE ARCHITECTURE AND COMPOSITION REGULATE NEUTROPHIL NETOSIS *IN VITRO* AND *IN VIVO*

Introduction

Biomaterials used in tissue engineering applications elicit a multifaceted and highly orchestrated, innate immune response, hallmarked by inflammation. On implantation, injury to surrounding tissues stimulates the release of chemical signals, and blood proteins immediately adsorb on the surface of the biomaterial [189]. After chemical signals trigger the immune response, the innate immune cells subsequently interact with the protein-coated material, recruit additional immune cells, and begin orchestrating either fibrosis or tissue repair and regeneration [190]. An emerging focus of tissue engineering is designing acellular tissue regeneration templates with architectures and compositions that harness the body's innate immune response and use it as a bioreactor to promote *in situ* regeneration of new tissues. Rather than designing inert scaffolds, the goal is to design temporary templates that dynamically initiate and guide the innate healing process through tissue integration and regeneration while preventing fibrosis [191].

Neutrophils, the sentinels of the innate immune system, are highly mobile phagocytes that are recruited rapidly and in large quantities by chemotaxis to a site of acute inflammation [192-194]. Historically, minimal attention was given to neutrophils and their role in tissue regeneration[194-196]. However, new evidence suggests that the neutrophil's activity and interaction with biomaterials deserve critical attention. Specifically, by adapting to microenvironmental cues and synthesizing and secreting an array of cytokines, chemokines, and MMPs, neutrophils exhibit multifaceted

physiological effects, including angiogenesis and regeneration [96, 192, 193, 197, 198]. Furthermore, research in the field of tumor biology has revealed that TANs have considerable plasticity of phenotype, displaying an N1 anti-tumor phenotype or an N2 pro-tumor phenotype, which is regulated by the tumor microenvironment and its constituent factors [181, 191]. These contrasting TAN phenotypes are synonymous with the macrophage M1 and M2 paradigm, which varies from the promotion of inflammation to the promotion of angiogenesis and tissue growth [181].

In addition to their ability to secrete potent factors like TIMP-free MMP-9 [182], neutrophils activated by microbial or chemical factors are able to expel their DNA along with granular contents to form NETs [27]. This process, deemed NETosis, was only discovered in 2004 and is not well understood [27, 81], especially its implications in *in situ* template preconditioning and guided tissue regeneration. On the decondensing of chromatin, aided by histone citrullination [132], and the disintegration of granules, the neutrophil cell membrane ruptures to extrude a cloud-like, fibrillary network of DNA, decorated with proteins and histones, into the microenvironment [104]. Neutrophils dying through the NETosis mechanism do not display ‘‘eat me’’ signals like apoptotic or necrotic cells do before cell membrane disruption. This prevents their pre-emptive clearing by macrophages and facilitates complete NET extrusion [199]. Furthermore, it has been proposed that NETosis is a response to noxious stimuli that are too large to be phagocytosed, such as biomaterials [21, 141], which is supported by findings that large particles like cholesterol crystals induce NETosis [70, 200]. Taken together, this suggests that NETs may be extruded on the surface of implanted tissue regeneration templates and precondition the ensuing innate immune response.

This article evaluates the hypothesis that NETs are generated in response to electrospun tissue templates and that the degree of template-bound NETosis is a function of template architecture (i.e., fiber diameter) and composition. PDO, COL, and a blend of the two polymers, PC, were electrospun with varying yet controlled architecture of SD and LD fibers and pores. NETosis was examined *in vitro* with freshly isolated, human peripheral blood neutrophils and *in vivo* with a subcutaneous implant rat model and analyzed based on template architecture, composition, and more specifically, architecture within a composition. Furthermore, NETosis was examined *in vitro* at multiple time points to elucidate its potential temporal regulation by template architecture and composition. Ultimately, understanding NETosis will facilitate design of electrospun templates and other biomaterials that harness the body's innate immune system as a bioreactor to promote, guide, and enhance *in situ* tissue integration and regeneration.

Materials and Methods

Fabrication and Characterization of Electrospun Templates

For this study, COL was isolated from rat tails following the protocol previously described by Rajan *et al.* [201]. Briefly, collagen type I obtained from rat tail tendons was dis- solved in acetic acid, frozen at -80°C, and lyophilized. PDO (Sigma Aldrich Co.) and COL were dissolved overnight in HFP (Oakwood Products, Inc.) at ratios of 100:0, 90:10, and 0:100 v/v at low (60 mg/ mL) and high (PDO 140 mg/mL and COL 110 mg/mL) concentrations to fabricate SD and LD regeneration templates, respectively.

Solutions of PDO, COL, and PC were placed in a syringe on a syringe pump (Model No. 78-01001; Fisher Scientific) with an 18-gauge blunt needle tip (2.5 cm length) attached to the positive voltage lead of a power supply (Spellman CZE1000R;

Spellman High Voltage Electronics Corp.). Solutions were dispensed at a rate 2 mL/h for COL LD, 3 mL/h for COL SD, 4 mL/h for PC SD and PDO SD, 5 mL/h for PC LD, and 6 mL/h for PDO LD with a voltage applied to the solution of ++22 kV for PDO SD and PDO LD, +25 kV for PC SD, PC LD, and COL LD, and +28 kV for COL SD. The airgap distance was 12.7 cm for all solutions. Fibers were collected on a grounded stainless steel rectangular mandrel (20 x 75 x 5 mm), rotating at 1250 rpm and translating 6.5 cm/s over 13 cm.

Templates were coated with 5 nm of gold palladium by sputter coating in an argon gas field before imaging via scanning electron microsopy (FEI NN650 FEG, Nova NanoSEM™ with field emission gun) at +20 kV with a working distance of 5 mm. Templates were characterized regarding fiber and pore diameters by analyzing the SEMs with FibraQuant™ 1.3 software (nanoTemplate Technologies, LLC). The average fiber diameter and pore diameter with corresponding standard deviations were calculated by averaging a minimum of 200 semi-automated random measurements per image and 60 random manual measurements per image, respectively.

Human Neutrophil Isolation

Neutrophils were isolated from blood obtained from healthy donors from Key Biological Services in accordance with protocols approved by the University of Tennessee Institutional Review Board. During disinfection and plating of the templates, fresh human peripheral blood neutrophils were isolated following a modified version of published protocols [202, 203]. Briefly, neutrophils were purified at room temperature from heparinized whole blood of healthy donors and collected from the pellet of an Isolymph density gradient (Gallard Schlesinger Chemical) under endotoxin-free conditions. The

contaminating erythrocytes were lysed in ice-cold hypotonic 0.2% sodium chloride solution for 30 seconds, and the solution was rendered physiological saline by addition of hypertonic 1.6% sodium chloride solution, resulting in neutrophil viability >98% as assessed by trypan blue dye exclusion. The neutrophils were washed once in 1x HBSS and resuspended at a density of 4 x 10^6 cells/mL in HBSS with 0.2% human serum and 10 mM HEPES.

Neutrophil Seeding

Before disinfection, pure COL templates were crosslinked in 25 mM EDC (Thermo Scientific Pierce™) in ethanol for 18 hours at room temperature [204]. Six 10-mm diameter discs (thickness 500 ± 100 µm) of each template type were punched and disinfected with a 30 minute ethanol soak, followed by three 10 minute washes with HBSS. The disinfected templates were then placed in a 48-well culture plate and kept hydrated with HBSS before seeding of neutrophils. Immediately following neutrophil isolation, templates were seeded with 150 µL of the cell suspension to generate 600,000 cells/well. After waiting for 10 minutes to allow the neutrophils to settle by gravity, an additional 150 µL of HBSS was carefully added to the wells. All templates were cultured under standard culture conditions (37°C and 5% CO_2) for 3 and 24 hours, after which the plates were placed on ice to inhibit further stimulation of the neutrophils. Supernatant was removed from the cellularized templates, and the cells were fixed in their wells on the templates with 10% buffered formalin. Fixed templates were stored in formalin at 4°C until analysis.

Fluorescent Detection of NETs

The surface of fixed, cellularized templates (n = 3, biological and technical replicates represented by three different donors seeded on templates) was imaged with fluorescent microscopy for quantitative analysis of the degree of NETosis in response to the templates. Templates were removed from formalin and stained with 100 nM SG extracellular DNA stain (Cat. No. S7020; Life Technologies) in DI water for 10 minutes at room temperature followed by DAPI fixed cell nuclei stain (Cat. No. R37606; Life Technologies) at stock concentration for 5 minutes at room temperature. Three DI water washes were performed between each step, and stained templates were covered with a glass coverslip.

Two images were taken randomly from different regions of each template with an Olympus microscope (Model BX43F) equipped with an Olympus DP73 high-performance digital color camera and fluorescent light source (DAPI and SG excited at 358 and 504 nm, respectively) at 20x magnification. Using cellSens® Standard 1.9 Digital Imaging software (Olympus Corp.), exposure times of each channel were kept at 200 ms to avoid saturated pixels. DAPI and SG images of the same region were overlaid, and the background was subtracted by defining a region of interest containing no cell nuclei or extruded NETs.

To determine the relative degree of NETosis, the B:G ratio, representing the area of an image occupied by intact cell nuclei compared to the area occupied by extruded NETs, respectively, was quantified. Using MATLAB® Release 2012a, the number of blue (DAPI), green (SG), and cyan (double staining of DAPI and SG) pixels in an image was quantified with a minimum threshold of 110 for all three colors. The number of cyan

pixels was subtracted from the number of green pixels, and the modified number of green pixels was used to formulate a B:G ratio. An average B:G ratio and corresponding standard deviation were calculated for each template type.

IR On-Cell Western Blot

An On-cell Western assay was performed to quantify template-bound CitH3. Fixed, cellularized templates were removed from formalin and rinsed with 1x PBS (HyClone™; GE Healthcare). Free aldehyde groups were quenched with three washes of 25 mM glycine in PBS for 5 minutes at room temperature and blocked with Odyssey® Blocking Buffer (Part no. 927-40000; LI-COR) for 1.5 hours at room temperature.

A standard curve was generated to quantify template-bound CitH3 using human histone H3 (citrulline R2 + R8 + R17) peptide (Product code ab32876; Abcam) spotted on an Immobilon®-FL PVDF membrane (Cat. no. IPFL00010; EMD Millipore Corporation) at 23.5, 11.7, 5.96, 2.93, 1.46, 0.73, 0.37, 0.18, 0.09, and 0.00 ng per spot in DI water. After allowing it to dry overnight, the spotted membrane was blocked with Odyssey Blocking Buffer for 1 hour at room temperature.

The templates (n = 3, biological and technical replicates) and membrane were incubated with anti-histone H3 (citrulline R2 + R8 + R17) antibody (Product code ab5103; Abcam) at a 1:200 dilution in Odyssey Blocking Buffer overnight at 4°C. All templates and membrane were washed five times with 0.1% Tween-20 in PBS for 5 minutes at room temperature with gentle shaking and subsequently incubated with IRDye 800CW donkey anti-rabbit (Part no. 926-32213; LI-COR) at a 1:20,000 dilution in Odyssey Blocking Buffer for 1 hour at room temperature, protected from light. Non-cellularized templates, serving as negative controls, were incubated with secondary

antibody only. After four washes with 0.1% Tween-20 in PBS and a fifth wash with PBS, the templates and membrane were scanned on the 800 nm channel of the Odyssey CLx IR Imaging System (LI-COR) with automatic intensity adjustment to obtain full-thickness template fluorescence and analyzed using Image Studio Version 5.x (LI-COR).

For the standard curve, fluorescent intensities were measured using circular markers encompassing the area of a spot. The intensities and corresponding mass of CitH3 were plotted and fit with a line of best fit. Then, the fluorescent intensities of the templates were measured using circular markers placed on the center of the template. The intensities were extrapolated to give total fluorescence for a 10 mm punch and converted to the mass of template-bound CitH3 using the standard curve.

***In Vivo* Study**

To elicit the most drastic responses as determined by the *in vitro* model, 10 mm diameter discs of SD and LD PDO templates were implanted on the dorsa of four Sprague-Dawley rats (250-300 g, male and female) following the protocol approved by the University of Memphis Institutional Animal Care and Use Committee. Templates were sterilized with peracetic acid (Product no. 77240; Sigma-Aldrich®) [205], and all materials were handled aseptically. Templates were hydrated for 10 minutes with sterile 1x PBS before implantation to minimize air within the template.

The rats were anesthetized by 5% isoflurane in an induction chamber, and anesthesia was maintained with 1-2% isoflurane delivered through a nose cone. Antisepsis was provided with iodine, and after creating incisions, four isolated subcutaneous pockets were tunneled on the dorsa of each animal by blunt dissection. One template lying flat was implanted per pocket to minimize void space around the template.

Four replicates per template type (n = 4) were implanted for the 24-hour time point, and two replicates per template type (n = 2) were implanted for the 7-day time point. The skin was closed with a single suture. The animals were euthanized 24 hours and 7 days after implantation. After euthanasia, the subcutaneous pocket was opened, templates were explanted (7-day templates excised with surrounding tissue), and subsequently fixed with 10% buffered formalin. Templates were stored in 10% buffered formalin at 4°C until analysis.

Template Staining and Evaluation

Fixed, excised templates were processed and stained to evaluate the *in vivo* response to the different template architectures. For cryosectioning, templates were soaked in 30% sucrose solution overnight, embedded in Tissue-Plus® O.C.T. Compound (Fisher HealthCare), frozen at -20°C, cryosectioned at a thickness of 15 µm, and mounted on glass slides. Replicates from 24 hours were stained with DAPI and SG following the same methods defined for the *in vitro* samples and with Shandon Kwik-Diff (Cat. no. 9990701; ThermoScientific) following the manufacturer's protocol. In addition, 7-day samples were processed and stained with H&E following standard protocol. Sections were qualitatively evaluated for cell migration through the template and the overall inflammatory response.

IR On-Cell Western Blot

Template-bound CitH3 was quantified on 24 hour templates (n = 4) following the On-cell Western assay protocol used for the *in vitro* templates.

Statistical Analysis

Statistical analysis was performed using Microsoft® Excel Real Statistics to determine significant differences at an *a priori* level of $p < 0.05$. For template characterization and quantification of template-bound CitH3, analysis of the data was conducted using a Kruskal-Wallis one-way ANOVA test and Tukey-Kramer HSD multiple comparison procedure. For the fluorescent detection of NETs, analysis of the data utilized a Welch's ANOVA test and the Games-Howell multiple comparison procedure.

Results

Template Characterization

SEM analysis confirmed that low and high polymer concentrations resulted in small and large fiber and pore diameters, respectively (Figure 6). All LD templates resulted in fiber diameters that were statistically larger than their SD counterparts (1.0-2.0 μm vs. 0.25-0.35 μm, $p < 0.05$). Similarly, all LD templates resulted in pore diameters that were statistically larger than their SD counterparts (6.0-8.0 μm vs. 1.0-1.25 μm, $p < 0.05$).

In Vitro Results

Fluorescent Detection of NETs

Fluorescent microscopy revealed varying degrees of NETosis in response to the different template architectures and compositions (Figure 7), which were evaluated with B:G ratios quantified by an image analysis algorithm written in MATLAB (Figure 8). Blue and green signify SG and DAPI staining. During NETosis, the plasma membrane maintains its integrity, while the nuclear and granular membranes disintegrate [206].

A

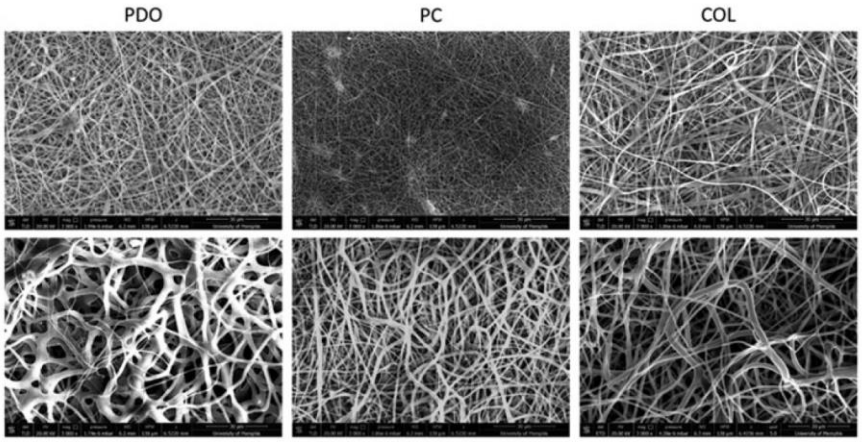

B

Template	Fiber Diameter (μm)	Pore Diameter (μm)
PDO SD	0.3 ± 0.1*	1.0 ± 0.3*
PDO LD	1.9 ± 1.0	8.1 ± 3.6
PC SD	0.3 ± 0.2*	1.2 ± 0.5*
PC LD	1.2 ± 0.6	6.7 ± 2.5
COL SD	0.3 ± 0.1*	1.1 ± 0.4*
COL LD	1.6 ± 0.9	6.6 ± 3.1

Figure 6. Processing solution concentration alters fiber diameter and pore diameter. (A) SEMs of electrospun templates (scale bar is 30 μm). (B) Resulting electrospun template fiber diameter and pore diameters. *Signifies a significant difference between SD and LD template counterparts ($p < 0.05$).

Because SG is unable to penetrate an intact plasma membrane [207], double staining of DAPI and SG, resulting in cyan, denotes cells that may be undergoing cellular changes, other than NETosis, that are associated with a compromised plasma membrane [206]. Therefore, blue, green, and cyan represent intact viable cells, extruded NETs, and intact cells with compromised cell membranes, respectively. To accurately quantify the degree of NETosis as the B:G ratio and obtain a true measurement of extruded NETs, cyan pixels were subtracted from the green pixels before calculating the B:G ratio. A B:G ratio greater than 1 signifies a larger area of the template occupied by intact cells than by extruded NETs, suggesting a relatively low degree of NETosis, with the inverse for a B:G ratio less than 1, suggesting a relatively high degree of NETosis.

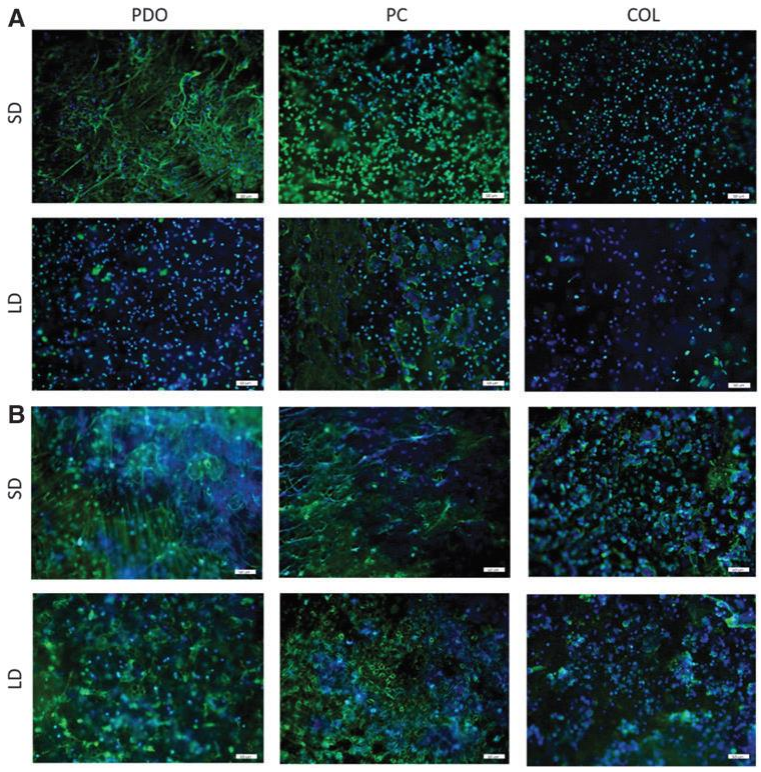

Figure 7. Representative fluorescent micrographs demonstrating varying degrees of NETosis in response to templates of different architectures and compositions. Images of *in vitro* cellularized templates at (A) 3 hours and (B) 24 hours stained with DAPI and SG (scale bar is 50 μm).

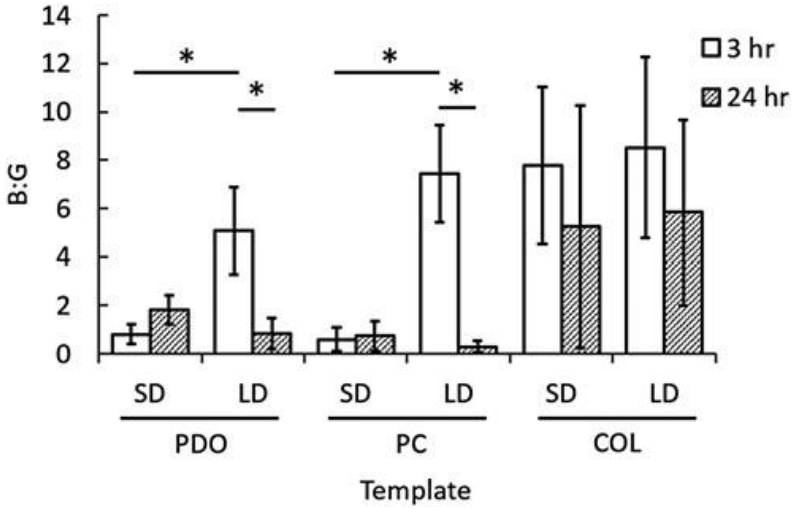

Figure 8. Template architecture and composition modulate NETosis as indicated by B:G ratios. B:G ratios quantifying NETosis at 3 and 24 hours. *Indicates a significant difference ($n = 3$, $p < 0.05$). No statistical differences were found between SD and LD template counterparts at 24 h.

Historically, extended *in vitro* experiments with isolated human neutrophils have not been considered feasible or reliable because of the neutrophil's brief half-life *in vitro* [208]; however, fluorescent microscopy revealed that a portion of the template-adhered neutrophils at 24 hours were stained with DAPI only (Figure 7B), indicating the maintenance of an intact cell membrane and thus cell viability. In addition, previous work has relied on artificial stimulation with manganese to enhance neutrophil adhesion [209]. Our studies did not utilize manganese stimulation, and neutrophil adhesion on the templates was evident at both 3 and 24 hours (Figure 7). These results are similar to previous experiments with mast cells, which were also thought to require stimulation for adhesion, but were found to adhere unassisted *in vitro* [210].

At 3 hours, all LD templates, regardless of composition, resulted in B:G ratios greater than 1 (Figure 8). For PDO and PC, SD counterparts resulted in B:G ratios less than 1. PDO LD and PC LD had significantly higher B:G ratios (6x and 12x increase, respectively) compared to their SD counterparts ($p = 0.003$, not indicated in Figure 8). These results suggest that a LD template primarily composed of PDO induces a lower degree of NETosis *in vitro* compared to SD templates.

In addition, all COL templates at 3 hours resulted in B:G ratios greater than 1. The B:G ratio for COL SD was significantly higher (10x increase) than the other SD templates ($p = 0.003$). Moreover, although not statistically greater ($p = 0.34$), the B:G ratios for all COL templates were higher than those for PDO LD and PC LD templates, which suggests that incorporation of COL, regardless of architecture, minimizes the degree of NETosis beyond that of PDO template architecture. Together, these data indicate that the degree of NETosis exhibited in response to a tissue regeneration

template in the critical, initial hours following implantation does not solely depend on the template architecture free from its composition, but rather depends on a specific template architecture for a given composition.

For all templates that had a B:G ratio greater than 1 at 3 hours, the B:G ratio decreased at 24 hours with significant differences between time points for PDO LD ($p = 0.002$) and PC LD ($p = 0.03$) (Figure 8). The decreased B:G ratios for templates exhibiting a low degree of NETosis at 3 hours suggest that the templates may be temporally modulating NETosis. In other words, these templates may be slowing the onset of NETosis. Inversely, for all templates that had B:G ratios less than 1 at 3 hours, the B:G ratio increased at 24 hours with no statistical differences. This may be the result of the delicate NETs degrading or detaching from the templates as time progresses.

IR On-Cell Western Blot

To quantify template-bound CitH3, the PVDF membrane spotted with CitH3 was scanned on the Odyssey system and analyzed. The standard curve revealed a linear relationship ($y = 3998.8x$, $R^2 = 0.9165$) between intensity and CitH3. Using the equation obtained from the standard curve, the total amount of template-bound CitH3 was quantified for each template type. The amount of extracellular CitH3 expressed on the templates appears to be largely dependent on template architecture and composition (Figure 9). Citrullination of histone H3 is a critical step during NETosis, allowing for the extrusion of an NET, and CitH3 is known to be contained within NETs after extrusion [128]. Because the cells were not permeabilized for the On-cell Western, increased CitH3 can be correlated to a high degree of NETosis, while decreased CitH3 can be correlated to a low degree of NETosis.

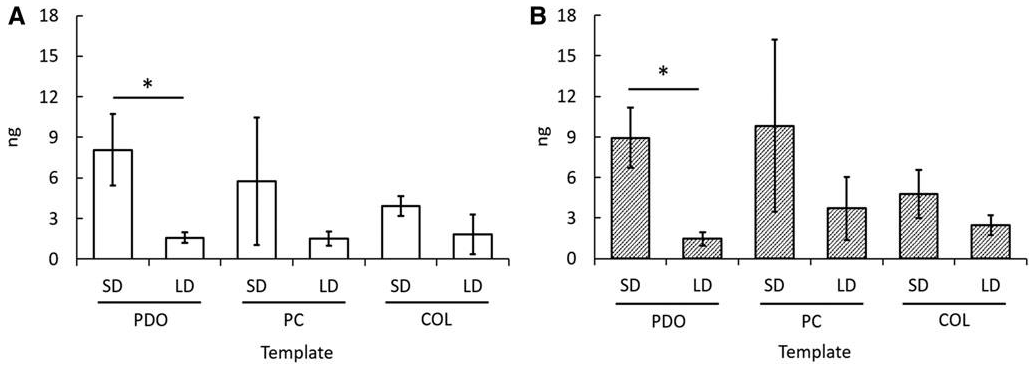

Figure 9. Template architecture and composition modulate NETosis *in vitro* as indicated by template-bound CitH3. Quantified template-bound CitH3 on templates at (A) 3 hours and (B) 24 hours. *Signifies a significant difference between SD and LD template counterparts ($n = 3$, $p < 0.05$).

At both time points, templates with smaller fiber diameters and pore diameters resulted in higher amounts of template-bound CitH3 compared to templates with larger fiber diameters and pore diameters, with a significant difference between PDO SD and PDO LD at both 3 and 24 hours ($p < 0.05$). Specifically, PDO SD expressed 8.06 ± 2.64 ng of CitH3 at 3 hours, which is five times the amount on PDO LD, and 8.94 ± 2.24 ng of CitH3 at 24 hours. This stark contrast again demonstrates, via quantification of extracellular, template-bound CitH3, that the degree of NETosis is regulated by template architecture. Furthermore, the COL SD template expressed 3.9 ± 0.73 ng of CitH3, significantly less than PDO SD, at 3 hours ($p < 0.05$), and 4.0 ± 1.8 ng of CitH3, also less than PDO SD, at 24 hours. This decrease in CitH3 again suggests that template composition also plays a crucial role in the degree of NETosis.

Interestingly, the amount of template-bound CitH3 did not decrease from 3 to 24 hours for PDO SD and PC SD, as anticipated based on the results from fluorescent microscopy (Figure 9B). This interesting finding suggests that the CitH3 may remain

template bound at later time points, even after the NETs have detached or been degraded. Considering the strong positive charge of histones and the largely negative charge of adsorbed proteins on the templates, it is possible that the attraction between CitH3 and the proteins is great enough to conserve the presence of CitH3 for extended periods of time.

In vivo Results

Template Staining and Evaluation

A preliminary *in vivo* study was executed to evaluate the physiological significance of the *in vitro* model. Cryosectioning and staining of the PDO SD and PDO LD templates from the rat subcutaneous pocket show that the overall response to the templates *in vivo*, as orchestrated by the acute confrontation of the neutrophil, varies significantly based on fiber diameter of the template. DAPI and SG staining (Figure 10A) and Shandon Kwik-Diff staining (Figure 10B) highlight the extreme differences between templates at 24 hours. A dense, cell layer can be seen surrounding the PDO SD templates, whereas the PDO LD templates possess an even distribution of cells throughout their thicknesses. Moreover, at 7 days, the H&E staining (Figure 10C, D) reveals the formation of a capsule-like tissue (i.e., pink staining) separating the SD template from the surrounding tissue. In contrast, the PDO LD template is partially integrated with the surrounding tissue and has high cellularity around its borders at 7 days. Since the only factor that varied in this initial *in vivo* study was template architecture, these results emphasize the importance of better understanding the innate immune response to a material and subsequent healing as modulated by material design.

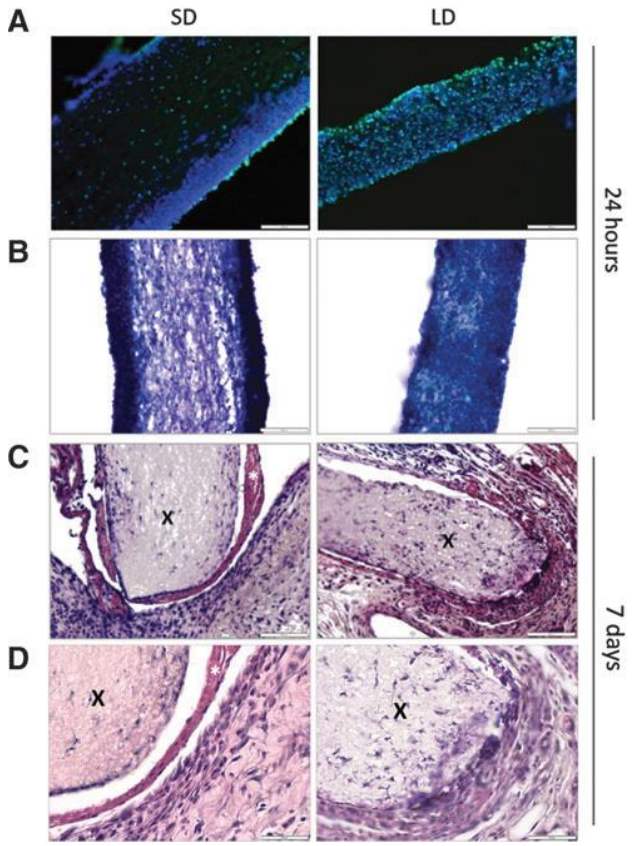

Figure 10. Fiber diameter modulates evoked cell distribution through PDO templates and marginal tissue integration *in vivo*. The white space between the template and surrounding tissue is an artifact of sectioning. Cross sections of SD and LD templates stained with (A) DAPI and SG and (B) Shandon Kwik-Diff stain at 24 hours and (C and D) H&E stain at 7 days (scale bars are 100 µm for (A–C) and 50 µm for D). It is important to note that a capsule-like tissue (*) separates the template (X) from the surrounding tissue for the SD templates, but not the LD templates.

IR On-Cell Western Blot

As seen with the *in vitro* templates, the degree of extracellular, template-bound CitH3 *in vivo* appears to be dependent on template architecture (Figure 11). PDO SD expressed 1376 ± 286 ng of CitH3, which is significantly greater than the mass of 422 ± 30 ng of CitH3 on PDO LD ($p = 0.02$). The three and a half-fold increase in CitH3 is indicative of a high degree of NETosis in response to PDO SD templates.

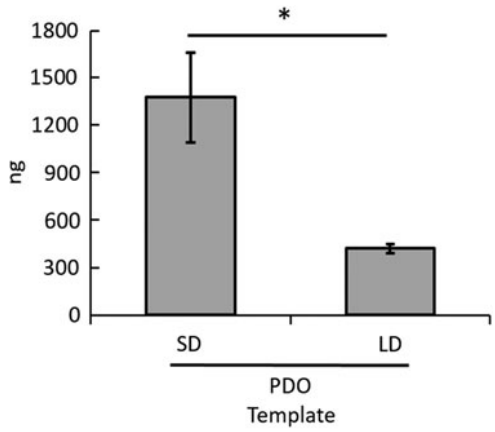

Figure 11. Electrospun PDO template architecture modulates NETosis *in vivo* as indicated by template-bound CitH3. Quantified template-bound CitH3 on templates at 24 hours *in vivo*. *Signifies significant difference between templates ($p < 0.05$).

In addition, the *in vivo* mass of extracellular template-bound CitH3 is one and two orders of magnitude greater than the *in vitro* mass on LD and SD PDO, respectively. In the *in vitro* model, the number of neutrophils was restricted to the seeding density, which inherently limited the mass of CitH3. In the *in vivo* model, the templates were implanted subcutaneously by blunt dissection, which resulted in an acute inflammatory response at the implant site and allowed for the recruitment of readily available, circulating neutrophils, thus giving rise to the increased mass of CitH3. Most notably, even with the restricted number of neutrophils *in vitro* and the complex response involving multiple cell types *in vivo*, the *in vitro* and *in vivo* models follow the same significant trends. In both cases, the mass of CitH3 is four to five times higher on PDO SD than PDO LD.

Discussion

Understanding the role of NETosis in priming electrospun templates may act as a guide for designing templates that promote synergy between neutrophils and other innate immune cells leading to innate immune system-guided *in situ* regeneration. Our objective

was to determine a relationship between template architecture and composition and the degree of NETosis. By electrospinning PDO, COL, and PC at low and high concentrations, resulting in statistically different templates with anticipated fiber morphologies and size distributions [211, 212], any variation in the degree of NETosis seen on SD and LD template counterparts can be considered a function of template architecture. Likewise, any variation in the degree of NETosis seen on templates with the same architecture, but varying compositions, can be attributed to the template composition.

Using freshly isolated human peripheral blood neutrophils, we demonstrated that it is possible to study neutrophil interactions with templates *in vitro* in non-TCP microenvironments that are more physiologically relevant and do not rely on artificial stimulation to facilitate neutrophil-template interactions. Notably, we demonstrated that both template architecture and composition affect the degree of NETosis in response to tissue templates, as evidenced by the variations between B:G ratios and extracellular, template-bound CitH3.

In general, we demonstrated that template architecture plays a significant role with more hydrophobic, synthetic polymer templates and that the incorporation of a more hydrophilic, natural polymer attenuates NETosis regardless of architecture. With both fluorescent microscopy and the On-cell Western blot, we showed that the incorporation of COL decreases NETosis, potentially by enhancing the bioactive surface functionality of the templates [212, 213], and thus biocompatibility. Furthermore, the incorporation of COL, segregated to the external surface of blended composition electrospun fibers [214],

increases the hydrophilicity of the template, which has previously been shown to improve the biocompatibility of electrospun templates [215].

For primarily PDO templates, an increased fiber diameter (i.e., micron-size) induces a significantly lower degree of NETosis compared to a decreased fiber diameter (i.e., nanosize), which is potentially the result of the associated non-restrictive pore sizes allowing for uninhibited cell migration into the template. Our data also suggest that there is a potential temporal modulation of the neutrophil's response via template architecture and composition, demonstrated by templates with a low degree of NETosis at 3 hours and a slightly increased degree of NETosis at 24 hours. Most importantly, the significant and notable trends regarding synthetic PDO templates were magnified *in vivo* using a rat subcutaneous pocket model, thus validating the methods used for the *in vitro* model.

Considering the *in vitro* and *in vivo* results, a high degree of NETosis appears to correlate to inflammation and fibrous encapsulation of a biomaterial, which is not surprising since excessive NET formation has been linked to a number of pathologies and diseases in recent years [216-220]. The PDO LD templates, which were integrated with the surrounding tissue after 7 days *in vivo*, stimulated a low degree of NETosis *in vitro*, while the PDO SD template, coated in CitH3 and other potent proteins contained within NETs, led to minimal marginal tissue integration. Thus, a low degree of NETosis and the associated neutrophil phenotype (i.e., N1 or N2) may better prime the microenvironment for tissue integration and regeneration by reducing inflammation and the presence of harmful factors, such as histones and granule proteins. Characterizing the cell population surrounding and infiltrating these templates may also provide valuable information regarding NETosis and the attenuation or promotion of the foreign body response. Most

importantly, the preliminary *in vivo* study suggests that there is a critical link between the neutrophil's acute confrontation and degree of NETosis, its temporal modulation, and the overall response to and integration of an electrospun template.

The mechanisms of NETosis are not yet fully understood because previous research has relied on pharmacological stimuli, such as PMA, or microbes to trigger NETosis; nonetheless, significant insight has been gained in recent years. In general agreement, various stimuli such as microbes and their by-products (i.e., LPS), cytokines (i.e., IL-8, TNF-α, and others), and ICs can induce NETosis via binding to TLRs (i.e., TLR2 and TLR4), FcγRs, cytokine receptors, complement receptors [221], and integrins (i.e., β2 integrin) [222]. Binding of stimuli to these receptors leads to an intracellular Ca^{2+} influx from the endoplasmic reticulum stores and opening of membrane channels, resulting in PKC activity, assembly of NOX2, and rupture of granular and nuclear membranes. Simultaneously, histones are citrullinated to facilitate chromatin decondensation, mixing of cellular contents, and final extrusion of NETs [223].

Clearly, there are many factors to consider and characterize in the complex neutrophil response to other biomaterials, including how the variation of template hydrophilicity and SAVR may be affecting the adsorption of serum proteins and binding of surface receptors [221, 222], triggering different degrees of NETosis. More direct approaches to modifying NETosis through the neutrophil's acute confrontation may be prevalent in the near future and would likely assume an important role in the subsequent design of biomaterials for optimal integration.

Nonetheless, one looming question that remains unanswered is the effects of the preconditioning event orchestrated by the initially interacting neutrophils. For this study,

we identified that PDO templates with a larger fiber and pore diameter reduce the degree of template-bound NETs. Because a PDO template with larger fiber and pore diameters is also known to shift macrophage phenotype toward the regenerative M2 phenotype and encourage angiogenesis [224], we conclude that a low degree of NETosis may correlate to a neutrophil N2 phenotype, subsequent macrophage M2 phenotype, and ultimately, angiogenesis and regeneration.

Conclusion

Taken together, it is evident that this preliminary, first-of-its-kind study yielding significant insight into neutrophil NETosis in response to biomaterials only scratches the surface of the highly complex innate immune response that drives inflammation and rejection of a biomaterial or integration and regeneration. Over the last decade, the macrophage has received significant attention as the key cell determining success or failure of tissue regeneration templates. In contrast, this work suggests that we must focus on the acute confrontation between the neutrophil and biomaterial if we wish to achieve tissue regeneration. Most significantly, we have demonstrated that NETosis is acutely modulated by electrospun template architecture and composition *in vitro* and *in vivo* and shown that a high degree of NETosis *in vivo* may result in a pro-inflammatory microenvironment that inhibits marginal tissue integration and angiogenesis. Further characterization of extruded NETs by immunoreactivity assays that colocalize CitH3 with other neutrophil granule contents contained within NETs may provide additional valuable information for further characterizing the response to electrospun templates and the microenvironment it creates. Our results thus far suggest that investigating the

neutrophil's specific response to electrospun templates and other biomaterials is an avenue of utmost importance.

CHAPTER 4

SURFACE AREA TO VOLUME RATIO OF ELECTROSPUN POLYDIOXANONE TEMPLATES REGULATES THE ADSORPTION OF SOLUBLE PROTEINS FROM HUMAN SERUM

Introduction

The greatest challenge for the clinical translation of biomaterials in tissue regeneration applications is guiding integrative and functional tissue regeneration. The cellular and molecular events immediately following implantation establish the microenvironment that determines the biological performance of implants. During the immediate innate immune response, lipids, ions, sugars, and soluble proteins from the blood rapidly adsorb on the surface of the biomaterial to facilitate cell interactions with the biomaterial. The instantaneous and dynamic adsorption of protein on a material surface is known as the Vroman effect [225]. In general, smaller low-molecular weight proteins and those present at high concentrations adsorb first on the surface of a material. As time progresses, these proteins may be displaced by larger, high molecular weight proteins that have a greater affinity for the material surface. Material surface properties, such as hydrophobicity or hydrophilicity, charge, roughness, surface area, and chemistry, all govern protein adsorption and potential conformational changes while providing some selectivity [16]. Protein adsorption, in turn, influences the recruitment and attachment of vascular, stromal, and inflammatory cells over the course of several hours to orchestrate the foreign body response, which ultimately culminates in fibrous tissue encapsulation or elusive, functional tissue regeneration. While it is generally well-accepted that the outcome is largely dependent on the extent of the foreign body response, it is becoming

increasingly recognized that the neutrophil and its interactions with the biomaterial play a central role in establishing the optimal microenvironment for functional tissue regeneration [17].

Neutrophils, the most abundant white blood cell in the blood, are the first dynamic line of defense interacting with surface-adsorbed proteins on the biomaterial within the first hour of the inflammatory response [8, 12]. Through outside-in signaling via receptors on the cell surface, the diverse stimuli from the surface-adsorbed proteins are transduced into intracellular signals, ultimately resulting in a cellular response. Neutrophil responses can include phagocytosis, degranulation, and the generation of ROS, which together create an intense attack that modulates the local microenvironment surrounding the biomaterial [23, 49]. In addition to these well-described mechanisms of defense, neutrophils can also release NETs through NETosis to trap and neutralize invading pathogens [27]. NETosis, a specialized form of anti-microbial cell death, results in the extrusion of a voluminous, 3D structure composed of decondensed chromatin, histones, various granule factors, and other anti-microbial proteins. While beneficial for combating infection, the dysregulated release of NETs is detrimental and associated with chronic inflammation, autoimmune disorders, tissue fibrosis, and thrombosis [134, 226, 227].

NETs are also released in response to various biomaterials including titanium plates, nanoparticles, and electrospun templates [31, 112, 188] Our group recently demonstrated that NETs are differentially released on the surface of electrospun PDO tissue regeneration templates [31]. Templates composed of SD fibers (0.2-0.4 μm) elicit a significantly greater release of NETs from interacting neutrophils compared to templates made of LD fibers (1.0-3.0 μm), suggesting that the microenvironment created by the

template architecture regulates the neutrophil response. More importantly, we also showed that the increased presence of NETs on the surface of the SD electrospun templates impairs tissue integration and promotes development of a fibrotic capsule *in vivo* in a rat subcutaneous implant model [31]. Given that neutrophils interact with the surface of the biomaterial through adsorbed proteins, the protein constituents and their quantities on the electrospun template surfaces may be intimately linked to differential release of NETs, thereby playing a central role in establishing a microenvironment conducive to functional tissue regeneration.

In this study, we evaluated the adsorption of eight proteins of interest: (1) albumin, (2) complement C1Q, (3) complement C3, (4) IgG, (5) IgM, (6) vitronectin, (7) fibrinogen, and (8) fibronectin on the surface of electrospun PDO templates. The purpose of the work was to characterize protein adsorption on the PDO templates in order to begin understanding how it may be linked to the differential engagement of neutrophil surface receptors leading to strikingly different NET responses [31]. PDO templates were electrospun with SD and LD fibers to generate materials with a high and low SAVR, respectively. We hypothesized that greater protein adsorption would occur on the SD templates with high SAVR. To replicate the culture conditions of our previous work, the templates were incubated with 0.2% human serum for different periods of time, and protein adsorption on the templates was quantified with *in situ* IR-based immunodetection to assess the effects of SAVR on protein adsorption. We found that SD templates with high SAVR adsorbed significantly more protein than LD templates with low SAVR. Furthermore, we determined that IgG adsorbs in the greatest quantity and most rapidly on the SD templates, suggesting it may play a role in signaling NET release.

Ultimately, understanding the constituents and dynamics of protein adsorption on electrospun tissue regeneration templates may provide insight into the potential mechanisms regulating NET release from neutrophils and their subsequent contribution to template-guided tissue regeneration.

Materials and Methods

Template Fabrication and Characterization

PDO (Bezwada Biomedical, LLC) was dissolved overnight in HFP (Oakwood Products, Inc.) at 67 and 135 mg/mL to generate SD and LD templates, respectively. The solutions were loaded into a 5 mL syringe (Becton, Dickinson and Company, Pro. No. 309646) and attached to a 22.5-gauge (Becton, Dickinson and Company, Pro. No. 305156) and 18-gauge blunt needle (Becton, Dickinson, and Company, Pro. No. 305196) for SD and LD templates, respectively, that was connected to the positive lead of a Spellman CZE1000R power source (Spellman High Voltage Electronic Corp.). The syringe was placed on a syringe pump (Fisher Scientific, Model No. 78-01001), and the 67 and 135 mg/mL solutions were dispensed at 0.5 and 4 mL/h with an applied voltage of +11 and +25 kV, respectively. The fibers were collected over an airgap distance of 10 cm for the SD templates and 27.9 cm for the LD templates on a grounded stainless steel cylindrical mandrel (2.5 cm diameter, 10 cm width), rotating at 1250 rpm and translating 6.5 cm/s over 13 cm.

To generate SEMs, the templates were sputter coated (Electron Microscopy Sciences, EMS 550) with 5 nm of gold-palladium in an argon gas field and imaged with a FEI Nova NanoSEM^{TM} at +20 kV with a working distance of 5 mm and spot size of 3. The SEMs were then characterized to determine template fiber diameter using

FibraQuant^{TM} 1.3 software (nanoTemplate Technologies, LLC) from a minimum of 250 semi-automated random measurements per image. The SAVR for 6 mm diameter punches of the SD and LD templates (n = 20) was then determined using Equations 1 and 2:

$$Equivalent\ fiber\ length\ [cm] = \frac{mass\ of\ the\ template\ [g]}{material\ density\ [\frac{g}{cm^3}] * \pi * (fiber\ radius\ [cm])^2} \quad (1)$$

$$SAVR\ \left[\frac{m^2}{cm^3}\right] = \frac{Equivalent\ fiber\ length\ [m] * 2 * \pi * fiber\ radius [m]}{template\ volume\ [cm^3]} \quad (2)$$

The material density of PDO (Equation 1) is 1.40 g/cm^3 as determined by standard pycnometry with a Quantachrome Instruments Ultrapyc 1200e pycnometer (Model MUPY-31). The volume of the templates (Equation 2) was determined by measuring the thickness of the 6 mm diameter punches and multiplying it by the area of a 6 mm diameter circle to generate cylindrical volume.

IR-Based Immunodetection Assay and Validation

To quantify the adsorption of protein, we developed an IR-based immunodetection assay using standard curves and validated the method. First, a standard dilution for each protein (Table 3) was generated on Immobilon-FL PVDF membrane (EMD Millipore Corporation) using a Bio-Dot Microfiltration Apparatus (BIO-RAD) according to manufacturer instructions. Briefly, 30 µL of protein (n = 3) diluted in HBSS was allowed to flow through the membrane by gravity for 45 minutes before applying the vacuum to draw through the remaining protein solution. The membranes were dried overnight before proceeding with processing and IR-based immunodetection.

Table 3. Protein was spotted onto a PVDF membrane to create standard curves for quantification of protein adsorption. Each point in the standard curves was produced from three replicates.

Protein	Upper Limit of Standard Curve [ng]	Lower Limit of Standard Curve [ng]	Dilution Factor
Human albumin (Novus Biologicals, Cat. No. NBP2-47623)	148	0.07	3
Human complement C1Q (Millipore Sigma, Cat. No. 2048761MG)	100	17.8	3/4
Human complement C3b (Millipore Sigma, Cat. No. 204860)	600	4.7	2
Human fibrinogen (Invitrogen, Prod. No. RP-43142)	800	4.1	2/3
Human fibronectin (ThermoFisher Scientific, Cat. No. 33016015)	150	20.0	3/4
Human IgG (Invitrogen, Prod. No. 31154)	1250	19.5	2
Human IgM (Millipore Sigma, Cat. No. 4017991MG)	900	0.11	2
Human vitronectin (Life Technologies, Cat. No. PHE0011)	35	2.6	3/4

Next, the standard dilutions were blocked with 5% non-fat milk (Nestle) in PBS for one hour at room temperature before overnight incubation with primary antibodies diluted in 5% milk at 4°C (Table 4). Following, three five-minute washes with 0.1% Tween-20 in PBS were performed at room temperature with gentle agitation. The standard dilutions were then incubated with secondary antibodies conjugated to IR dyes (Table 4) diluted in 5% milk with 0.1% Tween-20 and 0.01% SDS for one hour at room temperature to facilitate IR detection of adsorbed proteins. After two five-minute washes with 0.1% Tween-20 in PBS and a final five-minute wash with PBS, the standard

dilutions were scanned on the 680 and 800 nm channels of the Odyssey CLx IR Imaging System (LI-COR) with automatic intensity adjustment to generate fluorescence for each spot on the standard dilutions. Finally, using Image Studio version 5.x (LI-COR), relative fluorescent intensities of the spots were acquired by placing circular markers over the area of the spots.

To validate the method, known amounts of each protein (n = 3) within the working ranges of the standard curves (Table 5) were applied to the PVDF membrane, dried overnight, and processed for IR-based immunodetection as described for the

Table 4. Primary antibodies were paired for immunodetection of two adsorbed proteins per template via two-color IR detection. The paired primary antibodies were from different species while the secondary antibodies were from the same species.

Paired Protein Detection	Primary Antibody	Dilution	Secondary Antibody	Dilution
Albumin and IgG	Mouse anti-albumin (Abcam ab10241)	1:2000	IRDye 680LT goat anti-mouse (LI-COR, Part no. 926-68052)	1:20,000
	Rabbit anti-IgG (Abcam ab109489)	1:2000	IRDye 800CW goat anti-rabbit (LI-COR, Part no. 925-32211)	1:20,000
Complement C3 and Fibronectin	Mouse anti-complement C3 (Abcam ab11871)	1:1000	IRDye 680RD goat anti-mouse (LI-COR, Part no. 925-68070)	1:20,000
	Rabbit anti-fibronectin (Abcam ab32419)	1:1000	IRDye 800CW goat anti-rabbit (LI-COR, Part no. 925-32211)	1:20,000
Complement C1Q and IgM	Mouse anti-complement C1Q (Invitrogen MA1-83963)	1:2000	IRDye 680RD goat anti-mouse (LI-COR, Part no. 925-68070)	1:20,000
	Rabbit anti-IgM (Abcam ab212201)	1:1000	IRDye 800CW goat anti-rabbit (LI-COR, Part no. 925-32211)	1:20,000
Vitronectin and Fibrinogen α chain	Mouse anti-vitronectin (Abcam ab13413)	1:600	IRDye 680LT goat anti-mouse (LI-COR, Part no. 926-68050)	1:20,000
	Rabbit anti-fibrinogen α chain (Abcam ab92572)	1:2000	IRDye 800CW goat anti-rabbit (LI-COR, Part no. 925-32211)	1:20,000

standard dilutions. Only four standard curves were validated based on data indicating that four of the eight proteins of interest adsorbed on the electrospun templates, which is detailed below.

Table 5. Known amounts of each protein were adsorbed to PVDF to validate the standard curves. Each point was produced from three replicates.

Protein	Point 1 [ng]	Point 2 [ng]	Point 3 [ng]	Point 4 [ng]	Point 5 [ng]
Albumin	0	1	5	50	100
IgG	0	30	200	500	1000
IgM	0	1	50	400	800
Vitronectin	0	3	10	20	30

In Situ Protein Adsorption

For *in situ* protein adsorption, 6 mm diameter punches of the SD and LD templates (n = 6) were disinfected with a 30-minute ethanol (Fisher Chemical, Cat. No. A407-1) wash followed by three washes with 1x HBSS (Corning cellgro) for 10 minutes each. The disinfected templates were then placed in a 96-well cell culture plate, and 150 µL of 0.2% normal pooled human serum (MP Biomedicals, LLC, Cat. No. 0823201) in HBSS or 150 µL of HBSS were added to the templates. The templates were incubated at 37°C with 5% CO_2 for 0.25, 0.5, 0.75, 1, 2, 3, and 6 hours. After each time point, the serum solution was removed from the wells and discarded, and the templates were washed with 1x PBS for 5 minutes with gentle agitation at room temperature to remove non-adsorbed protein. The templates were then fixed and stored in 10% buffered formalin at 4°C overnight until analysis.

IR-Based Immunodetection of Adsorbed Proteins on Templates

The adsorbed protein on the electrospun templates was quantified using the standard curves for each protein. First, free aldehyde groups on the fixed templates were quenched with three five-minute washes of 100 mM glycine in PBS with gentle agitation

at room temperature. Then, the templates were processed for IR-based immunodetection as described for the standard curves. Each template was incubated with two primary and secondary antibodies to facilitate detection of two adsorbed proteins per template (Table 4). Relative fluorescence of the templates incubated with HBSS only was subtracted from the relative fluorescence of the templates incubated with serum to remove background fluorescence. Finally, protein adsorption was normalized to the mass of the 6 mm diameter punches.

Statistical Analysis

Data are presented as mean ± standard deviation. Fiber diameters and SAVRs were analyzed with a two-tailed t-test with Welch's correction. For the standard curves, nonlinear regression was performed, and goodness of fit was assessed with a replicates test for lack of fit. For validation of the IR-immunodetection assay, linear regression was performed, and the coefficient of determination was calculated. Analysis of protein adsorption was executed with a two-way ANOVA and Tukey multiple comparison procedure. All statistical analyses were performed in GraphPad Prism 6 at a significance level of 0.05.

Results

Electrospun Template Fiber Diameter Controls Surface Area

The low and high concentration PDO solutions resulted in electrospun templates with SD fibers and LD fibers, respectively (Figure 12A-B). The SD templates had significantly smaller ($p < 0.05$) fiber diameters with an average of 0.43 ± 0.20 μm compared to the LD templates with fiber diameters of 1.93 ± 0.72 μm (Figure 12C). The fiber diameters of the SD templates correlated to an average SAVR of 2.07 ± 0.33

m^2/cm^3, which is significantly greater ($p < 0.05$) than the average SAVR for the LD templates of 0.55 ± 0.07 m^2/cm^3 (Figure 12D). Because the SD templates have nearly 4-times the surface area per volume, these data indicate that the SD templates have significantly more surface area available for protein adsorption.

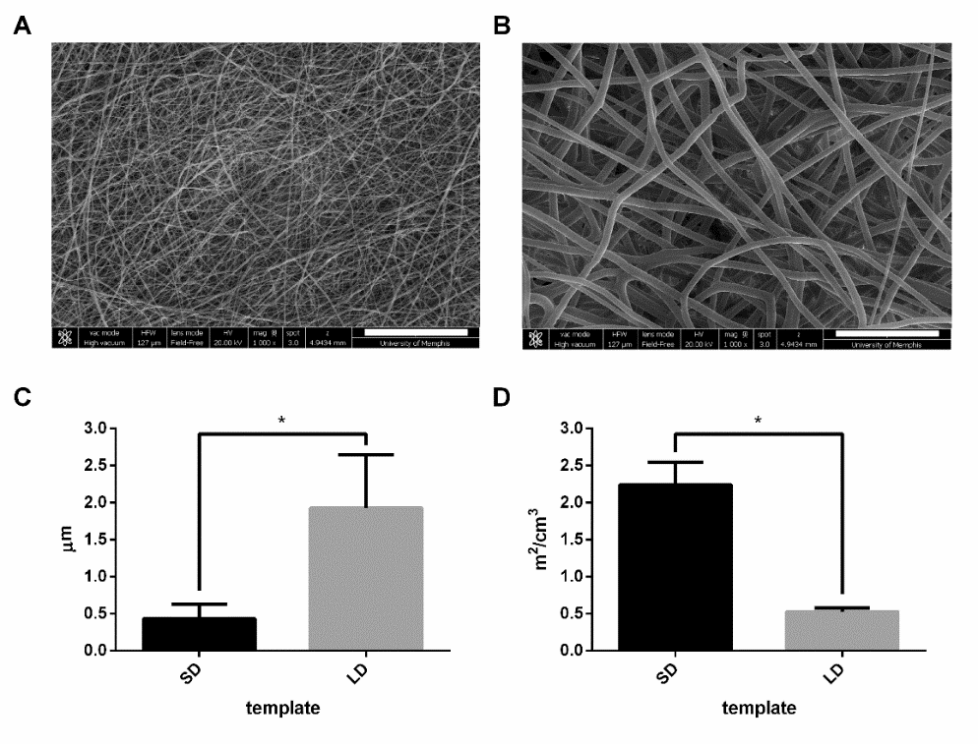

Figure 12. Electrospun SD and LD PDO templates. Representative SEMs of (A) SD and (B) LD electrospun PDO templates (magnification = 1000x, scale bars = 30 µm). (C) Fiber diameter of the SD templates is significantly smaller than the LD templates which correlates to significantly greater (D) SAVR. Graphs show mean ± standard deviation. * $p < 0.05$.

IR-Based Immunodetection Quantifies Protein Adsorption

For each protein, a standard curve was created to quantify adsorption through IR-based immunodetection. Figure 13 shows the standard curves with the nonlinear regression for vitronectin, IgM, albumin, and IgG. There was no adsorption of complement C1Q, complement C3, fibrinogen, and fibronectin detected on the electrospun templates, so these standard curves are not shown. For vitronectin (Figure

13A), the nonlinear regression (Equation 3) produced a well-fitting curve with no evidence of an inadequate model from the lack of fit test (p = 0.99). Similar results were obtained for IgM (Figure 13B, Equation 4, p = 0.98), albumin (Figure 13C, Equation 5, p = 0.62) and IgG (Figure 13D, Equation 6, p = 0.65).

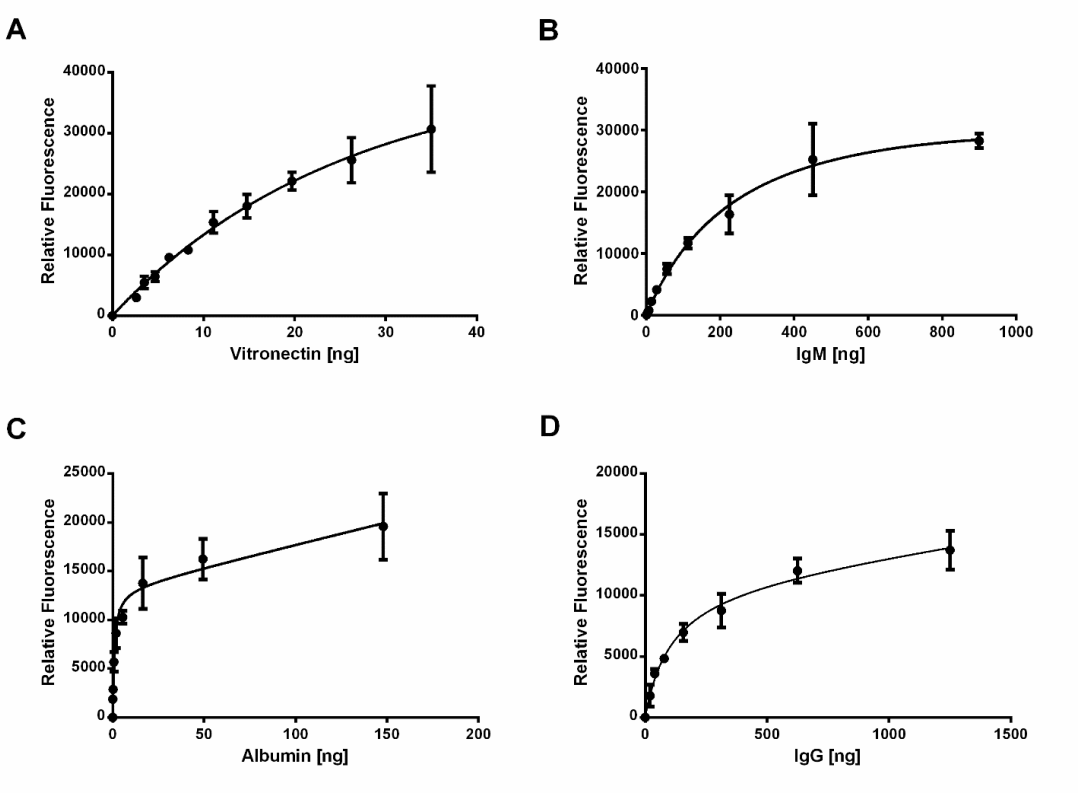

Figure 13. Standard curves generated from IR-based immunodetection. Dilutions of (A) vitronectin, (B) IgM, (C) albumin, and (D) IgG were vacuum blotted onto PVDF membranes, dried, and processed for detection with IR-based immunodetection. Each point in the standard curves was generated from three replicates. Error bars represent standard deviation.

$$y = \frac{115003x}{(57.53 + x)} - 373.6x \qquad y = \text{relative fluorescence, } x = \text{ng of vitronectin} \qquad (3)$$

$$y = \frac{43725x}{(292.1 + x)} - 5.052x \qquad y = \text{relative fluorescence, } x = \text{ng of IgM} \qquad (4)$$

$$y = \frac{13200x}{(0.89 + x)} + 45.83x \qquad y = \text{relative fluorescence, } x = \text{ng of albumin} \qquad (5)$$

$$y = \frac{11247x}{(107.2 + x)} + 2.84x \qquad y = \text{relative fluorescence, } x = \text{ng of IgG} \qquad (6)$$

Additionally, the assay was validated for albumin, IgG, IgM, and vitronectin (Figure 14) by adsorbing known amounts of each protein to PVDF membranes and assessing the interpolation from the standard curves. For all four proteins, the linear regressions for adsorbed protein versus the interpolated value from the standard curves have slopes near 1.0 and high coefficients of determination, indicating that the assay accurately quantifies the mass of adsorbed proteins. Together, these standard curves were used to quantify adsorption of vitronectin, IgM, IgG, and albumin on the templates based on relative IR fluorescence.

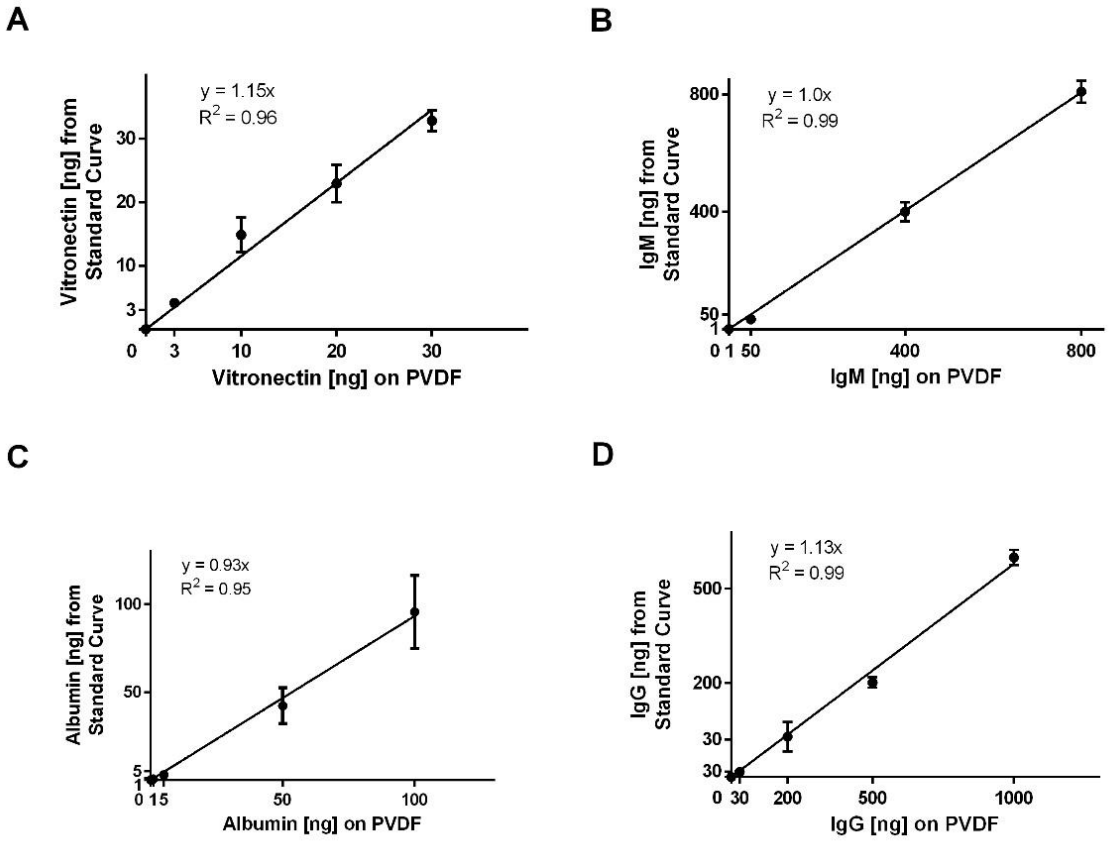

Figure 14. Validation of the IR-based immunodetection assay. Adsorption of known amounts of (A) vitronectin, (B) IgM, (C) albumin, and (D) IgG were plotted against the interpolated values from the standard curves. Each point was generated from three replicates. Error bars represent standard deviation.

SAVR Regulates *In Situ* Protein Adsorption

In order to highlight the differences in adsorption due to SAVR, the mass of adsorbed protein was normalized to mass of the 6 mm diameter template punches. Figures 15-18 show the results from the IR-based quantification of the *in situ* adsorption of vitronectin, IgM, albumin, and IgG. There was no detection of complement C3, complement C1Q, fibronectin, or fibrinogen. Notably, the Odyssey CLx Imaging System utilizes two IR lasers that penetrate through 3D structures. This facilitates full-thickness quantification of protein adsorption on the complex surface geometry of the electrospun templates.

For vitronectin (Figure 15), adsorption was not detected until the 1-hour time point for the LD templates and the 6-hour time point for the SD templates. Upon adsorbing on the LD templates, the mass of vitronectin did not change over time. Despite the delay on SD templates, the amount of vitronectin adsorption at 6 hours was significantly greater ($p < 0.05$) than on the LD templates, indicating that the high SAVR of the SD templates facilitated greater protein adsorption. Nonetheless, the adsorption of vitronectin on both templates was not detectable until at least 1 hour after exposure to serum. In the physiological environment, neutrophils have already swarmed to the site of inflammation, clustered around the biomaterial, and began interacting and responding within the first hour, which suggests that vitronectin adsorption may not play an integral role in the initial template-induced release of NETs [12].

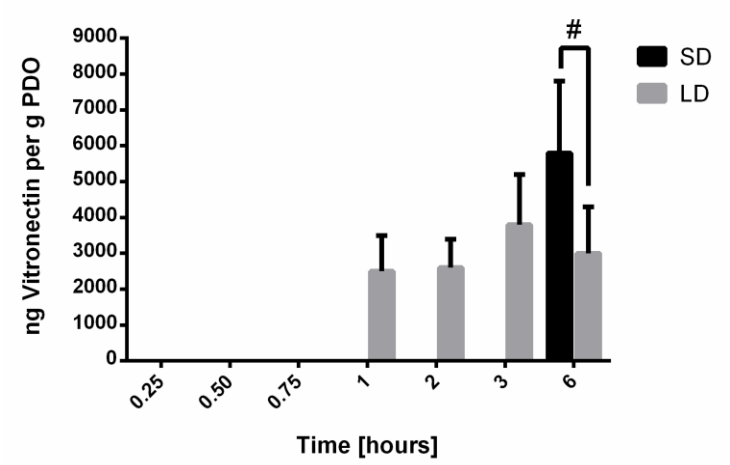

Figure 15. Vitronectin adsorption on electrospun PDO templates. Data shown as mean ± standard deviation from three independent experiments. # significant difference between SD and LD templates ($p < 0.05$).

Figure 16 shows the results from the IR-based quantification of IgM adsorption. The adsorption of IgM was not detected until the 0.50-hour time point for the SD templates and the 0.75-hour time point for the LD templates. Adsorption on the SD templates initially decreased between the 0.50 hour and 1 hour and then gradually increased between the 2-hour and 6-hour time points, suggesting that the dynamics of adsorption are temporal. At all time points, adsorption of IgM was greater on the SD templates, and by 3 hours, it was significantly greater ($p < 0.05$) on the SD templates compared to the LD templates. These results indicate that the high SAVR of the SD templates promote greater protein adsorption compared to the LD templates. Nonetheless, the relatively low levels of IgM adsorption, similar to those for vitronectin, suggest that IgM does not significantly contribute to the template-induced release of NETs.

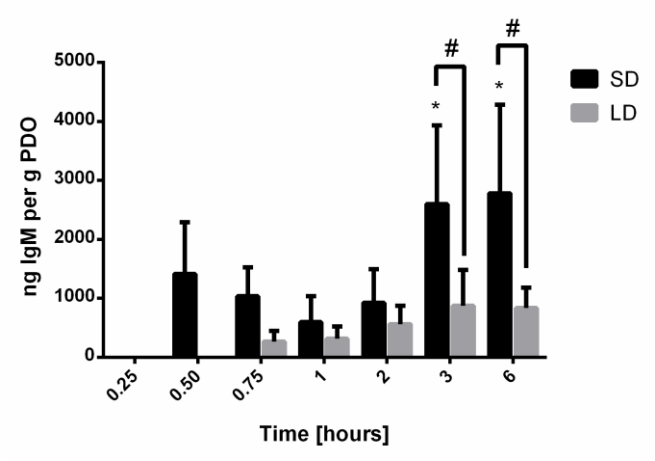

Figure 16. IgM adsorption on electrospun PDO templates. Data shown as mean ± standard deviation from three independent experiments. # significant difference between SD and LD templates ($p < 0.05$), * significant difference from 0.25 through 2-hour time points for SD ($p < 0.05$).

In contrast to vitronectin and IgM, albumin (Figure 17) was detected on the SD and LD templates at all time points and increased significantly over time for both templates. From 0.25 hours to 6 hours, there was greater adsorption on the SD templates compared to the LD templates, and by 6 hours, albumin adsorption was significantly greater on the SD templates compared to the LD templates ($p < 0.05$). While increasing on both, the rate of albumin adsorption on the SD templates was nearly 2-times greater, with an average increase of 270 ng per hour, compared to the LD templates, which increased on average by 110 ng per hour. These data suggest that the high SAVR of the SD templates accelerated the adsorption of albumin and resulted in greater total adsorption over time. Because it was detected at all time points, it is possible that the adsorption of albumin contributes to the regulation of the neutrophil response.

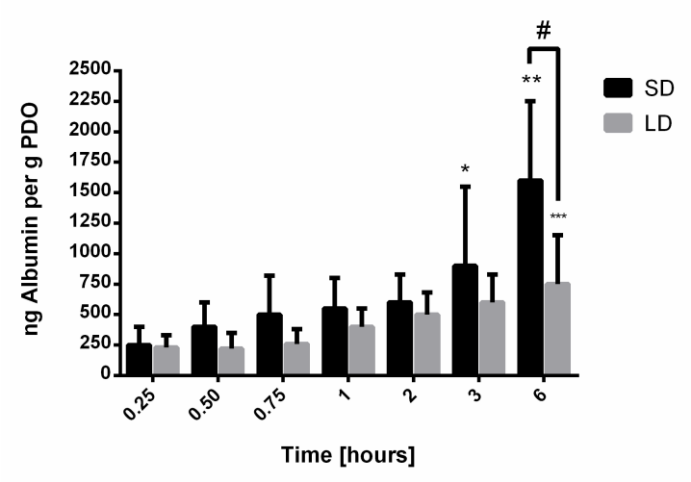

Figure 17. Albumin adsorption on electrospun PDO templates. Data shown as mean ± standard deviation from three independent experiments. * significant difference from 0.25, 0.50, and 0.75-hour time points ($p < 0.05$), ** significant difference from all other time points for SD templates ($p < 0.05$), *** significant difference from 0.25 through 1-hour time points for LD templates ($p < 0.05$), # significant difference between SD and LD templates ($p < 0.05$).

Similar to albumin, IgG (Figure 18) was detected on the SD and LD templates at all time points. However, by half an hour, adsorption of IgG was significantly greater on the SD templates compared to the LD templates ($p < 0.05$). Though it increased significantly on the SD templates, IgG adsorption did not significantly increase over time on the LD templates. The average rate of adsorption on the SD templates was 20,200 ng per hour compared to 5,400 ng per hour for the LD templates. The strikingly different rates of adsorption resulted in nearly 4-times greater IgG adsorption on the SD templates by half an hour. These results suggest that significantly more IgG is adsorbed on the SD templates in the critical first hour after exposure to serum, which may contribute to the contrasting cell responses to SD and LD templates. Furthermore, compared to albumin, IgG adsorption on the SD and LD templates over the first hour is 200-times greater and 100-times greater, respectively. Based on the high magnitude of IgG adsorption, these

data indicate that IgG may play a significant role in directing the differential release of NETs in response to electrospun polymeric biomaterials.

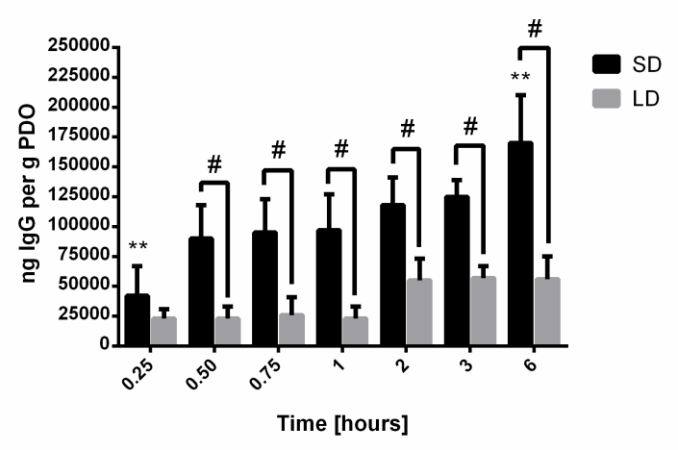

Figure 18. IgG adsorption on electrospun PDO templates. Data shown as mean ± standard deviation from three independent experiments. ** significant difference from all other time points for SD templates ($p < 0.05$), # significant difference between SD and LD templates ($p < 0.05$).

Finally, Figure 19 shows the total protein adsorption on the templates based on the detectable and quantifiable adsorption of vitronectin, IgM, albumin, and IgG. For all time points, total protein adsorption was greater on the SD templates compared to the LD templates, and by half an hour, the difference was significant ($p < 0.05$). While the average rate of adsorption on the LD templates was 14,000 ng per hour, the average rate of adsorption on the SD templates was 40,000 ng per hour. These data are dominated by the adsorption of IgG and suggest that in general, the high SAVR of the SD templates facilitates greater protein adsorption compared to the LD templates. Taken together, the IR-based immunodetection of our eight proteins of interest indicate that the significant adsorption of IgG on the surface of the electrospun SD templates is driven by SAVR, which may orchestrate outside-in signaling to stimulate NET release from interacting neutrophils.

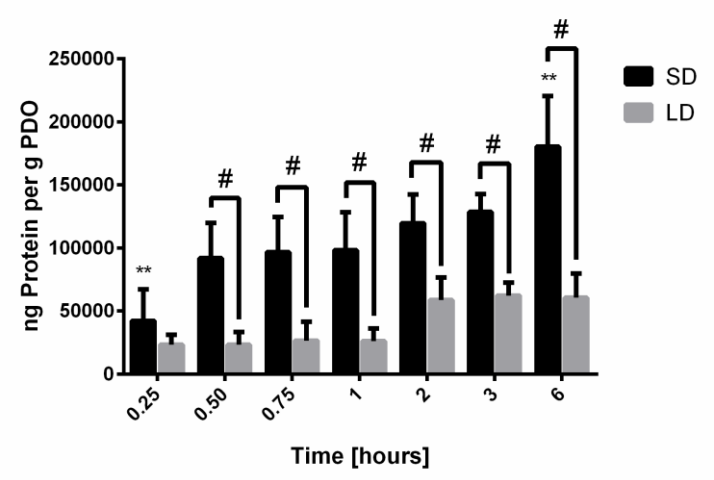

Figure 19. Total protein adsorption on electrospun PDO templates. The graph shows mean ± standard deviation from three independent experiments. ** indicates a significant difference from all other time points for SD templates ($p < 0.05$), # indicates a significant difference between SD and LD templates ($p < 0.05$).

Discussion

The neutrophil is increasingly recognized as a dynamic, central player in the foreign body response to a biomaterial. Recent work examining neutrophil interactions with electrospun tissue regeneration templates has shown that the architecture of the electrospun templates differentially regulates the release of NETs and that an abundance of NETs impairs tissue regeneration *in vivo* [31]. Because neutrophils represent the first line of defense interacting with and responding to an electrospun template, it is expected that their responses, including NET release, have significant implications in the microenvironment modulation around a biomaterial and the progression of template-guided *in situ* tissue regeneration. In this study, we aimed to characterize protein adsorption on SD and LD electrospun templates to begin understanding if protein adsorption drives the differential engagement of neutrophil receptors to regulate NET release.

Electrospun PDO templates were fabricated from low and high concentration solutions to generate SD and LD templates with significantly different fiber diameters and SAVRs. In order to make comparisons, the SD and LD templates for this study were fabricated with the same average fiber diameters of the templates used to evaluate NET release in our previous work [31]. The SD templates had a fiber diameter that was nearly 4-times smaller than the LD templates, correlating to a SAVR that was nearly 4-times greater. Therefore, the significantly smaller fiber diameter of the SD templates provided more surface area for the potential adsorption of protein per unit mass of the electrospun templates.

Using an IR-based immunodetection which was validated for protein quantification, we examined the adsorption of eight proteins: (1) albumin, (2) complement C1Q, (3) complement C3, (4) IgG, (5) IgM, (6) vitronectin, (7) fibrinogen, and (8) fibronectin. While other proteins are present in the serum which may be adsorbed to the templates, it is not feasible to study all protein constituents, and these eight proteins were selected for their high concentrations in serum and important roles in innate immunity. To replicate the methods from our previous experiments, we incubated the templates with commercially available 0.2% serum in HBSS that is produced by clotting [31]. Because our aim was to begin understanding how protein adsorption was regulated by SAVR and its potential implications in NET release, we did not quantify adsorption with purified protein solutions. Purified protein solutions would likely exhibit different adsorption profiles for each of the eight proteins, given that the Vroman effect is partly dependent on which proteins are present and their concentrations. Using purified solutions would undermine the complexity of an *in vitro* and *in vivo* microenvironment

with a milieu of proteins [228]. Additionally, the concentration of each protein in the serum was not quantified before the experiments because our goal was not to determine what percentage of available protein adsorbs to the templates. However, we did verify that the total protein concentration for the serum fell within the normal range of 6.0 – 8.0 g/dL [228].

The results indicate that there was no detectable adsorption of complement C3, complement C1Q, fibrinogen, or fibronectin on the SD and LD templates. Since the experiment utilized 0.2% serum, which is depleted of most fibrinogen and fibronectin during coagulation, a lack of fibrinogen and fibronectin adsorption onto the templates was not surprising [229]. In addition, neither complement C3 or complement C1Q adsorption was detected on the SD or LD templates. Despite their significant roles in innate immunity, the lack of complement adsorption may be due to their low affinity for the material surface and their relatively low concentrations in serum, which cannot compete with the high concentrations of other proteins such as albumin and IgG [228, 230-232]. For vitronectin, IgM, albumin, and IgG, the results indicate that SAVR regulates protein adsorption and that the high surface area of the SD templates adsorbs significantly more protein compared to the LD templates with low surface area. These results were anticipated since it is established that surface area regulates protein adsorption on biomaterial surfaces. Furthermore, no significant desorption of these proteins was observed over the 6-hour study, indicating that their affinity for the material surface was great enough to prevent competitive displacement by other high molecular weight proteins in this specified time frame.

Vitronectin, a low molecular weight glycoprotein, plays a role in cell adhesion and spreading. With regards to the neutrophil, it has been shown to modulate adhesion, contribute to pro-inflammatory processes, and inhibit neutrophil apoptosis through integrin-dependent signaling pathways [233-235]. The adsorption of vitronectin to the electrospun templates was delayed until 1 hour after exposure to serum on the LD templates and 6 hours after exposure to serum on the SD templates. In addition, the magnitude of adsorption was lower compared to other detected proteins. Given this information, the adsorption of vitronectin on the electrospun templates likely does not regulate template-induced NETosis, but may influence neutrophil viability and thus their ability to modulate the microenvironment through other cell responses such as degranulation and the secretion of cytokines and chemokines [23, 49].

Similar to vitronectin, the adsorption of IgM was delayed until half an hour after exposure to the serum for the SD templates and 0.75 hour after exposure to the serum for the LD templates with relatively low levels of adsorption occurring on both the SD and LD templates. Compared to other immunoglobulins, IgM only accounts for 10-15% of the antibodies present in the serum, which together with its affinity for PDO, may explain the delayed, low levels of adsorption [236]. Even though IgM can play a central role in complement activation and thus the neutrophil response to the biomaterial, our data suggest it is likely not a central player in the regulation of NET release on the surface of the electrospun templates [230].

Contrasting to vitronectin and IgM, both albumin and IgG adsorbed rapidly and readily to the surface of the SD and LD templates. Albumin adsorption increased over time on the templates and was significantly greater on the SD templates, suggesting that

the high SAVR facilitated greater protein adsorption. As a non-adhesive protein that plays an integral role in maintaining oncotic pressure, albumin has been reported to work synergistically with adhesive proteins to regulate cell adhesion and spreading by exposing binding sites on the adhesive proteins [237]. In the case of neutrophil interactions, albumin has been shown to promote adhesion but prevent spreading and the generation of hydrogen peroxide [238]. Recently, Neubert et al. showed that albumin actually inhibits NET release when neutrophils are treated with pharmacological stimuli and cultured in the presence of albumin [239]. Therefore, although significantly more albumin adsorbed to the surface of the SD templates, these data suggest that albumin does not play a direct role in regulating NET release, and another dominant protein on the surface of the material may be responsible for stimulating NETosis.

In fact, compared to albumin, 100- to 200-times more IgG adsorbed on the surface of the electrospun templates over the first hour, suggesting that the greatest proportion of the surface area is covered by IgG. These results are not surprising because IgG is the second most abundant protein in serum, present at a concentration of 11 mg/mL, and is the most abundant immunoglobulin in circulation [240]. The absorption was also significantly greater on the surface of the SD templates by half an hour, and the rate of adsorption over the 6-hour study was 4 times greater on the SD templates compared to the LD templates. These data indicate that IgG is the dominant protein on the surface of the SD templates, potentially regulating the outside-in signaling leading to the differential release of NETs.

We are not the first to quantify IgG adsorption on the surface of biomaterials. IgG has previously been shown to adsorb readily to the surface of biomaterials through strong

hydrophobic interactions that can alter its secondary structure [16]. These strong hydrophobic interactions inhibit its desorption from the surface of a material, which is consistent with previous work showing that the dynamics of the Vroman effect are not as prominent on hydrophobic surfaces like our PDO templates [241, 242]. On the surface of hydrophobic Teflon™, Vermeer *et al.* found that IgG adsorbs through denaturation of the Fab fragments, leaving the Fc fragment unperturbed for potential recognition by cell receptors and outside-in signaling [243].

The neutrophil expresses two types of FcγRs, which play a major role in mediating phagocytosis and the secretion of inflammatory mediators [244]. In resting neutrophils, FcγRIIIb binds most of the ligand on the surface of the antibody-coated substrate [245]. However, when a neutrophil is activated during inflammation, a high number of strongly signaling FcγRIIa receptors engage the IgG-covered target, working synergistically with FcγRIIIb to initiate inflammatory signaling [246]. Traditionally, this signaling promotes the phagocytosis of the noxious stimuli, but recent work has shown that opsonization of beads with IgG promotes a rapid increase in NET release that functions collaboratively with phagocytosis [67]. It is plausible that because our electrospun materials cannot be phagocytosed, all of the signals generated by FcγR ligation are transduced into rapid and abundant NET release on the IgG-coated SD templates. Moreover, recent work studying TLR-FcγR crosstalk in neutrophils has shown that engagement of TLR7/8 by soluble ICs induces shedding of FcγRIIa [247]. The shedding of FcγRIIa reduces the phagocytic capacity of neutrophils and shifts the signaling toward NETosis. Together, these studies support our finding that the SAVR-dependent adsorption of IgG may be the major polarizing event occurring on electrospun templates,

resulting in the engagement of cell receptors that up-regulate the release of NETs on SD templates.

In order to determine if IgG adsorption is intimately linked to biomaterial-induced NETosis, future work will include investigating how IgG adsorbs to the electrospun PDO templates and if the adsorption induces conformational changes. In addition, modulating the composition of the serum or inhibiting the activity of the FcγRs on the neutrophils will be critical for linking receptor ligation to NET release. Upon understanding the role of IgG, the surface properties of the electrospun templates can be modulated to regulate adsorption and possible induced conformational changes in the initial critical hours of the acute inflammatory response. In summary, we have shown that the adsorption of protein from human serum is regulated by electrospun template SAVR and that the high surface area of the SD templates significantly increases protein adsorption. Furthermore, we found that IgG adsorbs abundantly to the SD templates, which may drive outside-in signaling to up-regulate the release of NETs, a topic of further investigation. Due to the increasingly acknowledged role of the neutrophil in functional tissue regeneration, this work provides a foundation for the future development of biomaterials that harness the dynamic responses of the neutrophil to promote wound healing and accelerate their translation into the clinical setting.

Conclusion

The release of NETs on the surface of electrospun tissue regeneration templates may function as a significant preconditioning event that orchestrates the progression of the foreign body response and potential for functional tissue regeneration. Recent work shows that SD templates, which have high SAVR, up-regulate the release of NETs

compared to LD fibers, resulting in impaired tissue regeneration. In this study, we found that SD templates significantly increase the adsorption of soluble serum protein. Additionally, we showed that IgG adsorbs rapidly on the surface of SD templates and at the greatest quantity compared to other proteins. Given the role of IgG in innate immunity and the release of NETs, these findings suggest that IgG may be linked to the differential modulation of NETosis on electrospun templates as a function of SAVR. Ultimately, understanding how protein adsorption on electrospun templates regulates neutrophil interactions will enhance the design of immunomodulatory biomaterials that utilize the neutrophil as an initiator and driver of biomaterial-guided tissue regeneration.

CHAPTER 5

HUMAN NEUTROPHIL FCΓRIIIB REGULATES NEUTROPHIL EXTRACELLULAR TRAP (NET) RELEASE IN RESPONSE TO ELECTROSPUN POLYDIOXANONE BIOMATERIALS

Introduction

For several decades, electrospun biomaterials have been used to create ECM analogs for a variety of tissue engineering applications [2, 4, 11]. Because electrospinning systems are relatively easy to build and adapt to large-scale production, electrospinning is a cost-effective fabrication technique for producing non-woven substrates of continuous fibers in large quantities. Furthermore, electrospun biomaterials offer vast versatility and adaptability for tissue engineering, including *in vitro* and *in situ* tissue regeneration. For *in situ* tissue regeneration, the purpose of the electrospun biomaterial is to guide the body as a bioreactor to stimulate the regenerative capacity of autologous cells, tissues, and organs [1]. Given the reliance on autologous cells to infiltrate the biomaterial, the inflammatory and immune response to the electrospun biomaterial are of utmost importance for biomaterial-guided *in situ* tissue regeneration [26].

In recent years, our group has focused on characterizing and understanding the neutrophil response to electrospun biomaterials [17, 31, 76, 88, 248, 249]. Peaking in numbers near 24 to 48 hours after implantation, neutrophils are the first dynamic cell population recruited to an electrospun biomaterial [8]. Their rapid and numerous recruitment suggests an important role in preconditioning the inflammatory state of the local environment, which may have a long-term impact on the potential for tissue regeneration [181, 250]. At an

inflammatory site, neutrophils influence the tissue milieu through several effector functions, including the release of NETs [27].

NETs are extracellular structures composed of chromatin filaments, histones, and proteolytic enzymes normally found within the cytoplasm and granules [27]. Although they are integral to pathogen containment [27, 50, 141], NETs can also be tissue destructive, resulting in prolonged inflammation and pathogenesis due to aberrant enzyme release and histone toxicity [216, 223]. In fact, NETs have been implicated in several non-infectious inflammatory diseases, such as autoimmune disorders, thrombosis, cancer, and tissue fibrosis [100, 134, 162, 227, 251, 252]. Because of this, the potential deleterious effects of NETs have recently garnered attention in the field of biomaterials. Our group and others have shown that the release of NETs on the surface of a biomaterial is a significant preconditioning event that promotes inflammation and fibrosis [21, 31, 80]. In particular, we found that the fiber size of electrospun PDO regulates NET release with small fiber diameters significantly up-regulating NET release and fibrotic encapsulation relative to large fiber diameters. Together, these data suggest that one potential strategy to enhance biomaterial-guided *in situ* tissue regeneration is to regulate NET formation and its adverse effects through biomaterial design.

A variety of artificial and physiological stimuli have been shown to regulate NET release, including pharmacological compounds like PMA that act intracellularly and ligands that initiate outside-in signaling through various receptors [84, 136, 253]. Previously, we evaluated the adsorption of eight serum proteins on the surface of the electrospun PDO to begin elucidating the fiber size-dependent stimuli regulating NET formation on our biomaterials [114]. We found that nearly 2-times more IgG adsorbs to the surface of

small fiber biomaterials compared to the large fiber biomaterials within 15 minutes and that IgG adsorption was 100- to 200-times greater than any other protein, suggesting IgG signaling may increase the propensity to form NETs on small fibers. In fact, neutrophils constitutively express two FcγRs for IgG, FcγRIIa (CD32a) and FcγRIIIb (CD16b) [245]. Both have been found to participate in the release of NETs stimulated by ICs [129, 130, 135, 254, 255]. Moreover, activated neutrophils express FcγRI (CD64) within 4-6 hours of activation [256-258], and Mac-1 (CD11b/CD18) can cooperate with FcγRs in the release of IC-induced NETs [129]. Given the prominent surface adsorption of IgG on our electrospun biomaterials, we hypothesize that IgG and FcγR signaling may be intimately linked to biomaterial-induced NET release.

In this work, we explored the role of IgG and FcγR signaling in electrospun biomaterial-induced NET release with human neutrophils. The propensity to release NETs was increased and decreased by increasing and decreasing adsorbed IgG, respectively, suggesting a functional link between IgG and NET formation. Then, blocking of FcγRIIIb, but not FcγRI, FcγRIIa, or Mac-1 (CD11b/CD18), resulted in a decrease in fiber-size dependent NET release, indicating a specific receptor mediated neutrophil response. Finally, incubation with 5Z-7-oxozeaenol, an inhibitor of FcγRIIIb signaling through TAK1 [254], led to a decrease in NET formation on both biomaterials. Together, these data show for the first time that surface adsorbed IgG, ligation of FcγRIIIb, and activation of TAK1 are involved in biomaterial-induced NET release. Our results indicate that regulation of IgG adsorption and FcγR signaling in neutrophils may be used to modulate NET release in biomaterial-guided tissue regeneration applications.

Materials and Methods

Electrospinning Biomaterials

Biomaterials were fabricated from PDO by electrospinning as previously described [114]. Briefly, PDO (Cat. No. 6100, Bezwada Biomedical, Hillsborough, NJ, USA) was dissolved overnight in HFP (Cat. No. 003409-1KG, Oakwood Products, Estill, SC, USA) at 50 and 120 mg/mL and electrospun with optimized parameters (Table 6) from a 5 mL syringe connected to an 18-gauge and 5 cm long blunt needle. Fibers were collected on a stainless steel, 100 mm long x 25 mm diameter cylindrical mandrel that was grounded and rotating at 1250 rpm while oscillating horizontally at 6.5 cm/s over 13 cm. For experiments, 8 mm diameter discs of the biomaterials, ranging in thickness from 0.05 to 0.10 mm, were cut using a biopsy punch (Cat. No. P825, Acuderm Inc., Fr. Lauderdale, FL, USA) and stored in a desiccator until use. Prior to cell culture, the biomaterials were disinfected by ultraviolet irradiation using an 8 W lamp (Cat. No. EN280L, Spectroline, Westbury, NY, USA) at a working distance of 9.5 cm. The samples were disinfected for 10 minutes on each side in a sterile, laminar flow hood and kept disinfected for cell culture.

Table 6. Electrospun biomaterials were fabricated with optimized parameters.

Fiber Size	PDO Concentration (mg/mL)	Flow Rate (mL/h)	Airgap Distance (cm)	Applied Voltage (+ kV)
Small Fibers	50	0.55	28	25
Large Fibers	120	4.0	28	28

Biomaterial Characterization

SEMs were acquired and analyzed in FibraQuant 1.3 software (nanoTemplate Technologies, LLC) to quantify fiber diameter as previously described [76]. Briefly, 150

semi-automated random measurements per SEM were taken to determine the average and corresponding standard deviation for fiber diameter.

Isolation and Culture of Primary Human Neutrophils

Heparinized, whole peripheral blood was obtained by venipuncture from unidentified, healthy donors from Tennessee Blood Services. Since purchased or donated samples are not traceable back to the donor, it does not qualify as human subjects research as determined by the University of Memphis Institutional Review Board on November 22, 2016. Neutrophils were then isolated by density separation as previously described [31, 76, 259]. Once isolated, neutrophils were resuspended in HBSS without calcium, magnesium, or phenol red (Cat. No. 14175095, Thermo Fisher Scientific, Waltham, MA, USA) and with 10 mM HEPES and 0.2% autologous serum at a concentration of 1 million neutrophils/mL. After placing the disinfected biomaterials (n = 4) in a 96-well plate, 40 µL of the cell culture media were added to each well to hydrate the biomaterials. For TCP wells (n = 4), 30 µL of the cell culture media were added prior to cell seeding. Subsequently, 100 µL of the cell suspension containing 100,000 neutrophils were added to each well. All wells then received 10 µL of heparin (Cat. No. H3393, Sigma Aldrich, St. Louis, MO, USA) at a final well concentration of 10 U/mL to dissociate NET-associated MPO as previously described [50, 88]. The positive and negative controls were TCP with 100 nM PMA (Cat. No. P8139, Sigma Aldrich, St. Louis, MO, USA) and TCP with 0.15% DMSO, respectively. The neutrophils were cultured on the biomaterials at 37℃ and 5% CO_2 for 3 hours, and the TCP wells were cultured for 6 hours. Following culture, the samples were placed on ice for 10 minutes to inhibit neutrophil stimulation prior to fixing in 10% buffered formalin (Cat. No. SF1004,

Thermo Fisher Scientific, Waltham, MA, USA) for 1 hour at room temperature. Three experiments were performed with unique donors (2 males, between 18 and 40 years of age, and 1 female, 25 years of age), and the results were pooled for analysis.

Addition of IgG to Biomaterials

To examine the dose-dependent effects of IgG on NET release, the biomaterials (n = 4) were hydrated with 1, 100, or 440 µg of human IgG (Cat. No. 31154, Thermo Fisher Scientific, Waltham, MA, USA) in 40 µL of HBSS for cell culture. The mass of 1, 100, and 440 µg of IgG were selected to mimic the mass of IgG in 40 µL of cell culture media, the mass of IgG needed to saturate the biomaterial surfaces, and the mass of IgG at physiological concentration, respectively. Controls were biomaterials hydrated with 40 µL of cell culture media.

Depletion of IgG from Biomaterials

To reduce the mass of surface-adsorbed IgG, IgG was depleted from autologous serum using Dynabeads™ Protein G (Cat. No. 10004D, Thermo Fisher Scientific, Waltham, MA, USA) [260]. Prior to use, Dynabeads™ Protein G were dialyzed in 12,000-14,000 molecular weight cutoff dialysis tubing in 1 L of PBS for 48 hours at 4°C with gentle agitation. The PBS was refreshed every 12 hours. After dialysis, 100 µL of Dynabeads™ were added to the wells on a 96-well plate, placed on a handheld magnetic plate washer (Cat. No. NC1403679, Thermo Fisher Scientific, Waltham, MA, US), and washed five times with 250 µL of HBSS. Once the final wash was removed, 250 µL of 0.2% autologous serum in cell culture media was added to the Dynabeads™ and incubated for 30 minutes at room temperature with gentle agitation. Human IgG (Cat. No. 31154, Thermo Fisher Scientific, Waltham, MA, USA) diluted to a concentration of 0.2%

in HBSS was used as an isotype control to validate the depletion. After incubation, the IgG-depleted supernatant was collected and sterile filtered with a 0.2 µM sterile filter. Subsequently, the biomaterials (n = 4) were hydrated with 40 µL of the IgG-depleted cell culture media prior to seeding the neutrophils. Controls were biomaterials hydrated with 40 µL of complete cell culture media containing 0.2% serum.

Validation of IgG Depletion

The depletion of IgG from autologous serum and the biomaterial surface was validated using immunodetection to quantify IgG as previously described [114]. Briefly, 30 µL of 0.2% autologous serum, IgG-depleted autologous serum, 0.2% isotype control IgG, and IgG-depleted isotype control (n = 3) were vacuum blotted on Immobilon-FL PVDF membrane (IPFL00005, EMD Millipore Corporation, Burlington, MA, USA) and dried overnight before processing and immunodetection. Free aldehyde groups on the fixed biomaterials were quenched with 100 mM glycine, and the PVDF membranes and biomaterials were then blocked and incubated with rabbit anti-IgG (ab109489, Abcam, Cambridge, MA, USA) followed by IRDye 800CW goat anti-rabbit (Part No. 925-32211, LI-COR, Lincoln, NE, USA). After washing, the PVDF membranes and biomaterials were scanned on the 800 nm channel of the Odyssey CLx IR Imaging System (LI-COR). The relative fluorescence of biomaterials incubated with HBSS only was subtracted from the relative fluorescence of the biomaterials from cell culture to remove background fluorescence, and the mass of IgG was interpolated from a standard curve. For the biomaterials, IgG adsorption was normalized to the mass of the 8-mm diameter sample.

Receptor Blocking

To block receptors, neutrophils were incubated with 10 µg/mL Fab blocking fragments for FcγRI (Cat. No. 216-580, Ancell, Bayport, MN, USA), FcγRIIa (Cat. No. 181-580, Ancell, Bayport, MN, USA), and FcγRIIIb (Cat. No. 165-580, Ancell, Bayport, MN, USA) and a blocking antibody for CD11b (Cat. No. BDB553308, Fisher Scientific, Waltham, MA, USA) at 37°C for 10 minutes. IgG Fab (Cat. No. 278-580, Ancell, Bayport, MN, USA) and IgG (Cat. No 401401, BioLegend, San Diego, CA, USA) were used as isotype controls. After resuspending, neutrophils were seeded on the biomaterials (n = 4) that were hydrated with 40 µL of cell culture media. Untreated cells seeded on the biomaterials (n = 4) served as controls.

Inhibition of TAK1

In order to inhibit signaling through TAK1, neutrophils were incubated with 10 nM 5Z-7-oxozeaenol (Cat. No. 49-961-01MG, Fisher Scientific, Waltham, MA, USA) or 0.1% DMSO as a negative control on ice for 30 minutes [254]. After resuspending, neutrophils were seeded on the biomaterials (n = 6) that were hydrated with 40 µL of cell culture media. Untreated cells seeded on the biomaterials (n = 4) served as controls.

Quantification of NET Release

The release of NETs was quantified by measuring the concentration of NET-dissociated MPO in the cell culture supernatant using an MPO Human Instant ELISA Kit (Cat. No. BMS2038INST, Thermo Fisher Scientific, Waltham, MA, USA) [50, 88]. Briefly, the cell culture supernatants were transferred to a clean cell culture plate and centrifuged at 500 xg for 5 minutes to pellet any free neutrophils. Then, 50 µL of the centrifuged supernatant was collected and assayed using the MPO Human Instant ELISA Kit

following manufacturer instructions. To quantify percent NET release on the biomaterials, the concentration of MPO was normalized to the concentration of MPO in the TCP positive control at 6 hours, representing maximum NET release.

Fluorescence Microscopy

Samples were stained with 5 µM SYTOX orange (Cat. No. S34861, Thermo Fisher Scientific, Waltham, MA, USA) and NucBlue™ Fixed Cell ReadyProbes™ Reagent (DAPI, Cat. No. R37606, Thermo Fisher Scientific, Waltham, MA, USA) and imaged as previously described [88]. Samples were incubated sequentially for 5 minutes at room temperature with each stain. Three washes with PBS for 5 minutes each were performed between each stain. The stained cells and NETs were visualized on an Olympus BX43 fluorescent microscope, and images were acquired in cellSens Standard 1.9 (Olympus Corp.). After image acquisition, contrast was enhanced using the automated function in cellSens.

Statistical Analysis

Statistically significant differences between fiber diameters were determined using a Mann-Whitney test. Statistical differences for the depletion of IgG were determined using a Kruskal-Wallis test with Dunn's multiple comparisons procedure. All other differences were tested with an ANOVA and Holm-Sidak's multiple comparisons test. Statistical analyses were performed in Prism version 8.4.3 (GraphPad Software, San Diego, CA, USA) at a significance level of 0.05. Data are reported as mean ± standard deviation.

Results

Electrospun PDO Biomaterials Were Fabricated with Small and Large Fibers

PDO was electrospun to create small and large fibers (Figure 20A). The average fiber diameters for the small and large fibers are 0.38 ± 0.10 μm and 2.1 ± 0.36 μm, respectively (Figure 20B). The small fiber biomaterials up-regulate the release of NETs while absorbing 2-times more IgG on their surface compared to large fibers, suggesting a role for increased IgG signaling in biomaterial-induced NET release [31, 114]. As in our prior work, these small and large fiber electrospun biomaterials allow us to further probe the role of IgG in biomaterial-induced NET release.

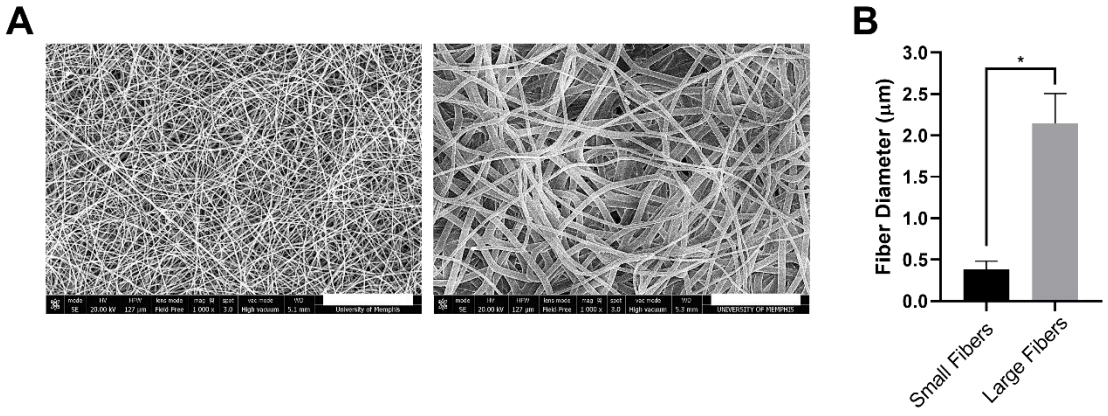

Figure 20. Electrospun PDO biomaterials were fabricated with small and large fibers. (A) Representative SEMs of the small and large fiber biomaterials. Micrographs were acquired at 1000x magnification and scale bars are 30 μm. (B) Fiber diameters of the electrospun biomaterials. Measurements (n = 150) were taken in FibraQuant 1.3 software. * $p < 0.0001$ was determined using a Mann-Whitney test.

IgG Increases NET Release

Neutrophils were isolated from the whole blood of healthy donors and seeded on electrospun biomaterials with increasing masses of IgG to examine the potential stimulatory role of IgG in biomaterial-induced NET release (Figure 21A). As expected,

neutrophils had an increased propensity to release NETs on the small fibers compared to the large fibers (Figure 21B) with nearly 2-times the release of NETs on small fibers. With the addition of 1 μg of IgG, the release of NETs was similar to the level of the controls on both small and large fibers. With the addition of 100 μg of IgG to saturate the surface of the biomaterials, NET release was significantly increased on both the small and large fiber biomaterials. Moreover, the release of NETs on the large fibers was increased to the level of the small fibers, indicating a stimulatory effect for IgG. The trends were similar with the addition of 440 μg of IgG, or IgG at physiological concentration, but there was no further increase in NET release observed. Together, these dose-response data indicate that IgG stimulates biomaterial-induced NET release.

Depleting IgG Decreases NET Release

In addition to stimulating NET release with the addition of IgG, we also examined if the depletion of IgG from autologous serum would attenuate NET release. First, we developed a method to deplete IgG using Dynabeads^{TM} protein G (Figure 22A). For both an isotype control of IgG and the autologous serum, our depletion protocol resulted in greater than 97% reduction in IgG concentration. For the isotype control, the concentration dropped from 11.1 ± 4.02 mg/mL to 0.30 ± 0.03 mg/mL. For the autologous serum, the concentration was reduced from 10.9 ± 2.78 mg/mL to 0.08 ± 0.05 mg/mL. To verify that this reduction translated to a reduction in biomaterial surface-adsorbed IgG, we quantified IgG adsorption on the small and large fibers after culture with neutrophils (Figure 22B). As expected, nearly 2-times the mass of IgG was adsorbed on the small electrospun fibers compared to the large fibers when the biomaterials were hydrated with cell culture media containing 0.2% autologous serum. However, when the

biomaterials were hydrated with the IgG-depleted serum, the adsorption of IgG was significantly reduced on both small and large fibers, verifying that the depletion of IgG from the cell culture media translates to reduced surface adsorption. We then quantified the release of NETs in response to the decreased IgG adsorption (Figure 22C) and found that the release of NETs trended towards a decrease on the small fibers, but did not change on the large fibers (Figure 22D).

Blocking FcγIIIb Decreases Biomaterial-Induced NET Release

Next, we blocked FcγRI, FcγRIIa, FcγRIIIb, and CD11b to test their potential contribution to NET release. On the small fiber biomaterials (Figure 23A and C), of the control whereas blocking of FcγRI, FcγRIIa, and CD11b resulted in no change in NET release. Contrastingly, NET release was near equivalent on the large fiber biomaterials with no change in NET release upon blocking any of the receptors (Figure 23B and D). Given that blocking of FcγRIIIb on the small fiber biomaterials reduced NET release to the level of the large fiber biomaterials, the data suggest that ligation of FcγRIIIb and its subsequent signaling are involved in biomaterial-induced NET release.

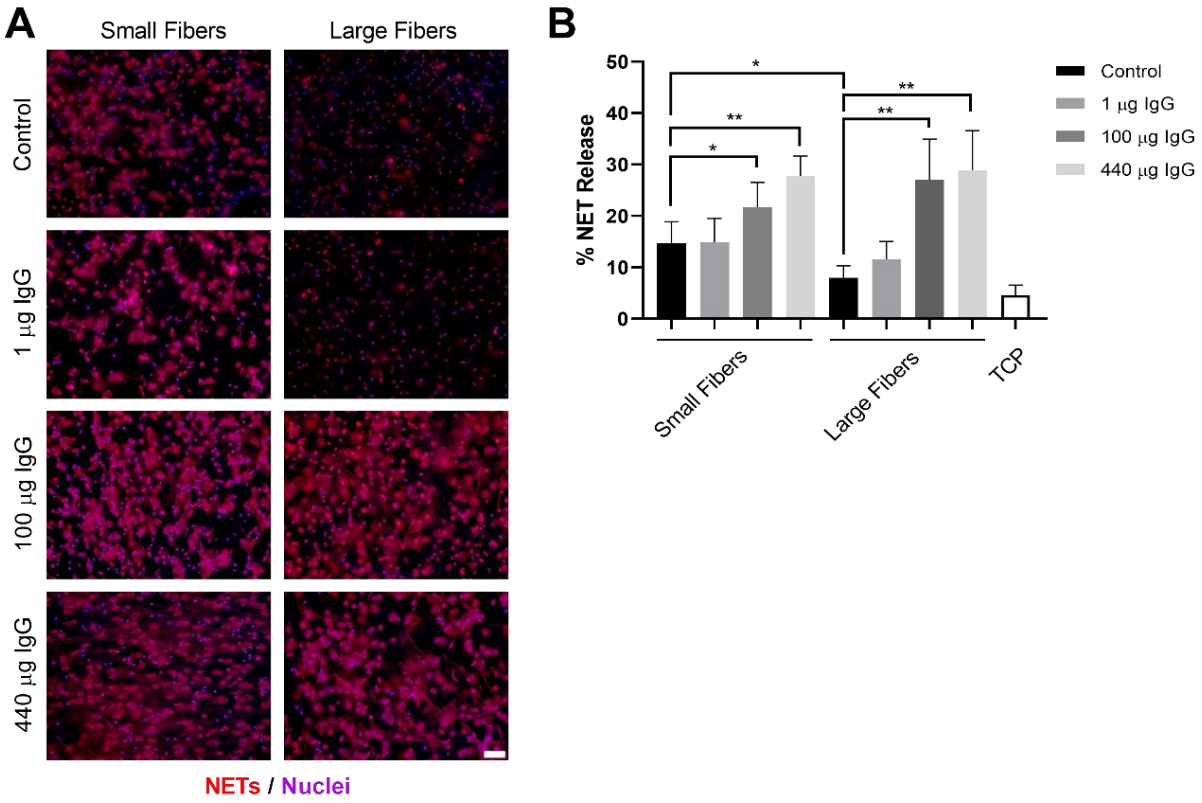

Figure 21. Increasing IgG on the electrospun biomaterials increases NET release. (A) Fluorescent micrographs of neutrophils on the electrospun biomaterials at 3 hours after seeding. Staining of NETs (red) and nuclei (purple) reveals that increasing IgG up-regulates NET release independent of electrospun fiber size. Scale bar is 50 μm. (B) Percent NET release at 3 hours as quantified by the ELISA for NET-disassociated MPO. The quantification of percent NET release (n = 4) indicates that increasing IgG on the biomaterials stimulates NET release with a maximum stimulatory effect upon saturation of the material surface with 100 μg of IgG. The data represent the mean ± standard deviation of three independent experiments with unique donors. * $p < 0.05$ and ** $p < 0.0001$ were determined using an ANOVA and Holm-Sidak's multiple comparisons test.

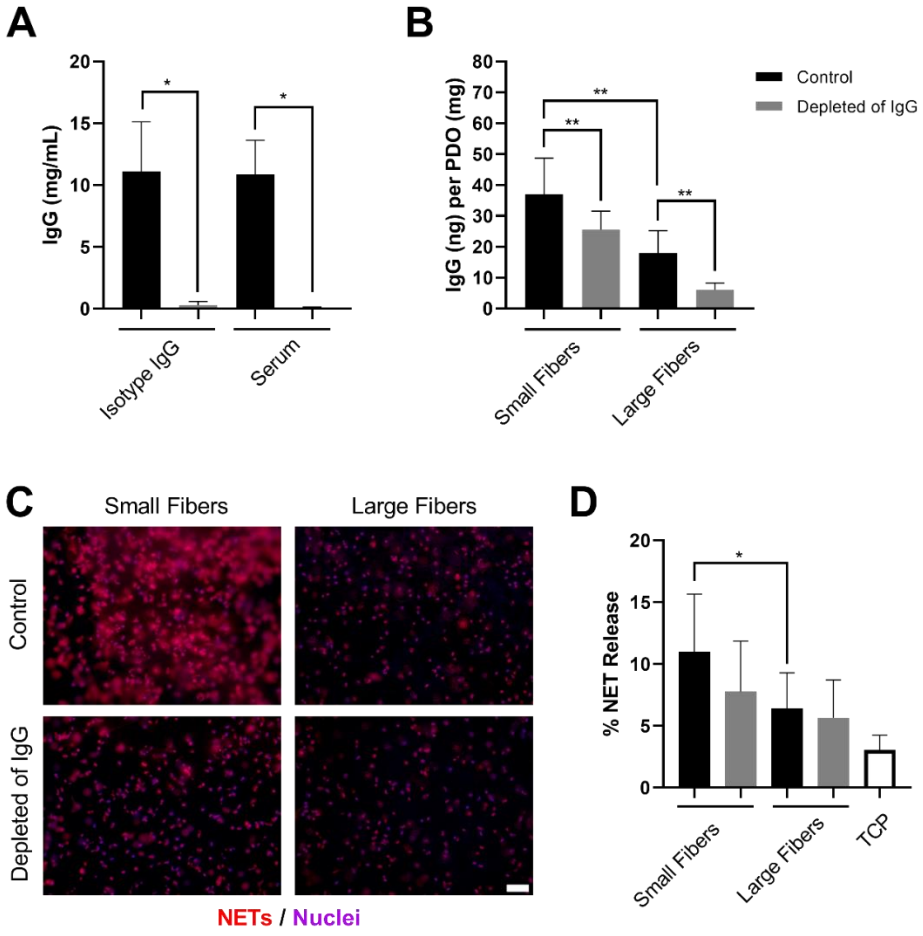

Figure 22. Decreased IgG adsorption decreases NET release on the small but not large fiber electrospun biomaterials. (A) Concentration of IgG in isotype control (n = 3) and serum (n = 3) before and after depletion with Dynabeads^{TM} protein G. The depletion procedure reduced the concentration of IgG by 97.4% and 99.3% for the isotype control and serum, respectively. The stock concentration of the isotype control was 11 mg/mL. * $p < 0.05$ was determined using a Kruskal-Wallis test with Dunn's multiple comparisons procedure. (B) IgG adsorption on the electrospun biomaterials after 3-hour culture with neutrophils. The controls hydrated with cell culture media (n = 4) adsorbed significantly more IgG compared to the samples hydrated with IgG-depleted cell culture media (n = 4). ** $p < 0.0001$ was determined using an ANOVA and Holm-Sidak's multiple comparisons test. (C) Fluorescent micrographs of neutrophils on the electrospun biomaterials at 3 hours after seeding. Staining of NETs (red) and nuclei (purple) reveals that decreasing IgG down-regulates NET release on small fibers. Scale bar is 50 µm. (D) Percent NET release at 3 hours as quantified by the ELISA for NET-disassociated MPO. The quantification of percent NET release (n = 4) indicates that decreasing IgG on the small fiber biomaterials decreases NET release. * $p < 0.05$ was determined using an ANOVA and Holm-Sidak's multiple comparisons test. For all graphs, the data represent the mean ± standard deviation of three independent experiments with unique donors. blocking of FcγRIIIb led to a significant reduction in NET release to approximately half

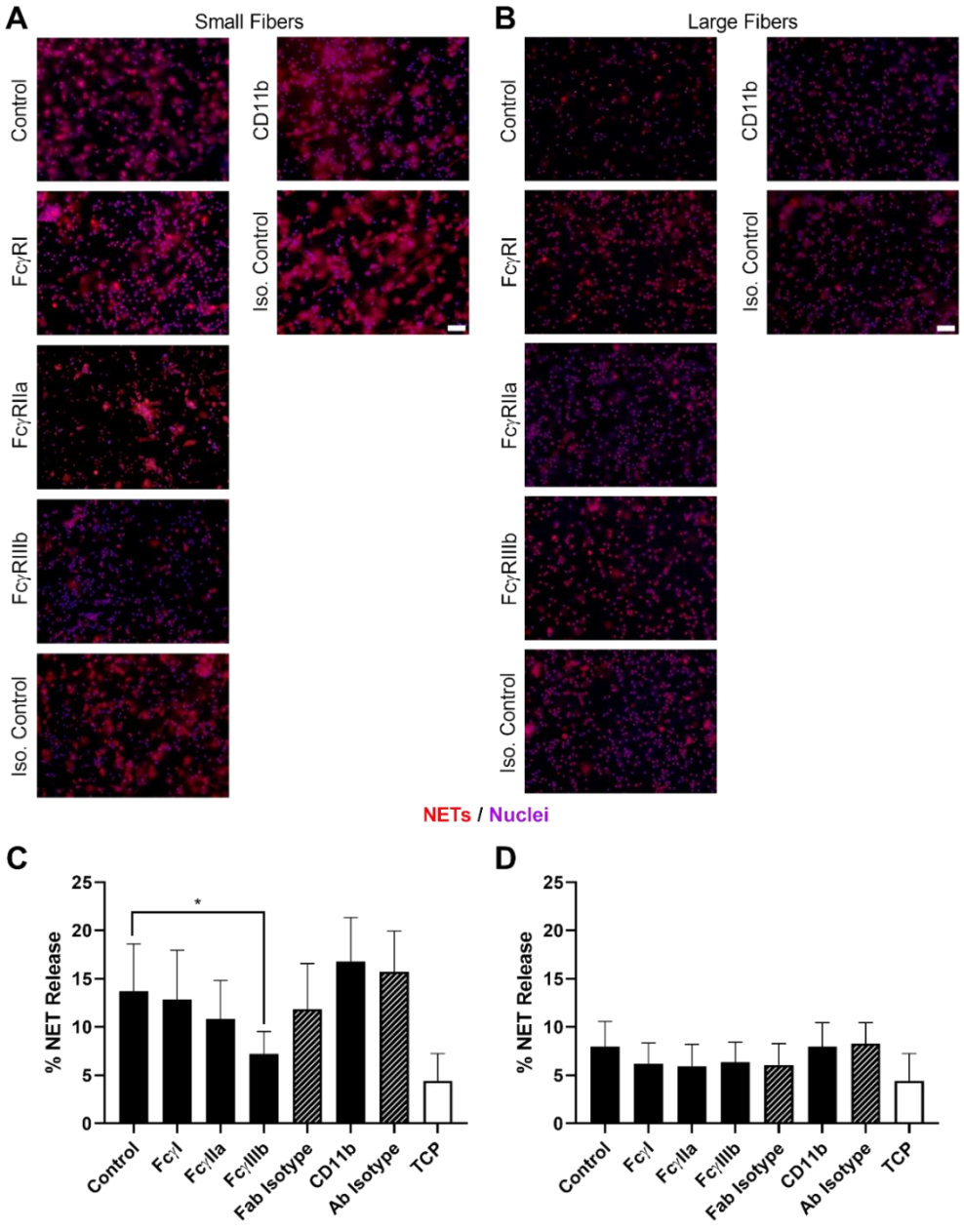

Figure 23. Blocking FcγIIIb decreases biomaterial-induced NET release on small but not large fiber biomaterials. (A and B) Fluorescent micrographs of neutrophils on the electrospun biomaterials at 3 hours after seeding. NETs are shown in red and nuclei in purple. Scale bars are 50 μm. (C and D) Percent NET release at 3 hours as quantified by the ELISA for NET-disassociated MPO. The quantification of percent NET release (n = 4) indicates that blocking FcγIIIb on the small fiber biomaterials significantly reduces NET formation whereas no effect is observed on the large fiber biomaterials. The data represent the mean ± standard deviation of three independent experiments with unique donors. * $p < 0.05$ was determined using an ANOVA and Holm-Sidak's multiple comparisons test.

Inhibition of FcγRIIIb Signaling through TAK1 Attenuates NET Release

To further verify the involvement of FcγIIIb in biomaterial-induced NET release, we inhibited TAK1, an enzyme required for FcγIIIb signaling in NET release [254]. Inhibition of TAK1 with the selective inhibitor 5Z-7-oxozeaenol led to a significant reduction in NET release on both the small and large fiber biomaterials (Figure 24A and B). On the small fibers, NET release decreased from 13.5 ± 4.65% to 4.28 ± 2.67%, a two-fold decrease. On the large fibers, the release of NETs was reduced from 7.24 ± 1.97% to 3.30 ± 0.62%, which is roughly the same level of NET release as the TCP control. Taken together, these data indicate ligation of FcγIIIb with IgG and subsequent signaling through TAK1 participate in electrospun biomaterial-induced NET release.

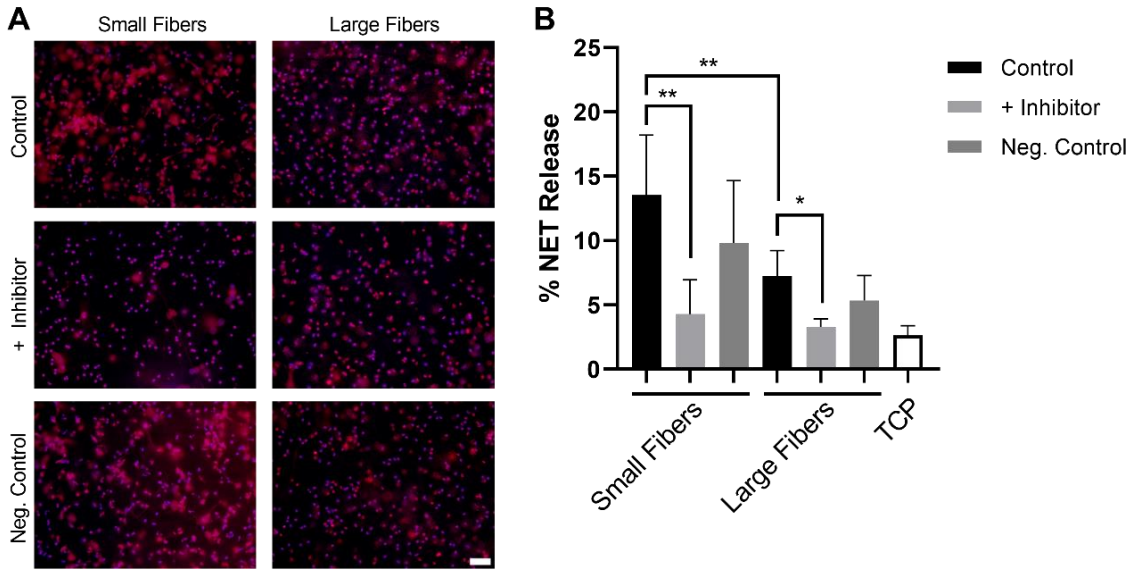

Figure 24. Inhibition of FcγIIIb signaling through TAKI attenuates NET release on both small and large fiber biomaterials. (A) Fluorescent micrographs of neutrophils on the electrospun biomaterials at 3 hours after seeding. NETs are shown in red and nuclei in purple. The scale bar is 50 µm. (B) Percent NET release at 3 hours as quantified by the ELISA for NET-disassociated MPO. The quantification of percent NET release (n = 6) indicates that inhibition of TAKI reduces NET formation on both the small and large fiber electrospun biomaterials. The data represent the mean ± standard deviation of three independent experiments with unique donors. * $p < 0.05$ and ** $p < 0.0001$ were determined using an ANOVA and Holm-Sidak's multiple comparisons test.

Discussion

Electrospun biomaterials offer putative advantages for *in situ* tissue engineering applications because of their versatile biomimetic structure, relatively simple fabrication, and cost-effectiveness. However, understanding the inflammatory and immune response to these biomaterials for guided tissue regeneration is a challenge that requires further investigation for translation into the clinical environment. Recently, our group and others have investigated the activation of neutrophils and release of NETs in response to biomaterials [21, 31, 80, 186]. The dysregulated release of NETs contributes to inflammation and fibrosis in several pathologies and has been described for thrombosis, cancer, and biomaterials *in vivo*, including our electrospun biomaterials [21, 31, 100, 134, 162, 186, 227, 251, 252]. In addition, multiple inflammatory diseases are linked to IC-induced NET release, including systemic lupus erythematosus [77], rheumatoid arthritis [261], anaphylaxis [262], and small vessel vasculitis [263]. Previously, we showed that greater IgG adsorption occurs on biomaterials that up-regulate NET release [114], but it remained unclear whether this surface-adsorbed IgG is responsible for stimulating biomaterial-induced NET formation similar to IC-induced NET release. Here, we demonstrate for the first time that IgG adsorption, binding to FcγRIIIb, and signaling through TAK1 stimulates and regulates the release of NETs from human neutrophils on the surface of electrospun PDO biomaterials.

The binding of neutrophils to ICs and biomaterials is an important mechanism for innate immunity, the activation of neutrophils, and inflammation. IC-induced NET release requires opsonization of the antigen or pathogen with IgG to mediate FcγR binding and has been shown to occur in the context of soluble and immobilized ICs and

IgG-coated beads [129, 130, 264]. In this work, we found that increasing the surface-adsorbed IgG on our biomaterials up-regulated the release of NETs, which occurred independent of electrospun fiber size. When the concentration of IgG exceeded the mass needed to saturate the material surface, no further increase in NET release was observed, indicating that the IgG must be bound to the material surface to have a stimulatory effect. Indeed, the high concentration of IgG in circulation does not stimulate NET release from circulating neutrophils, and others have shown that free Fc fragments not bound to a substrate and free IgG were unable to stimulate NET formation in the context of ICs [264, 265]. Likewise, we also showed that decreasing the surface-adsorbed IgG down-regulated the release of NETs, but this occurred in a fiber size dependent manner. Reduced IgG adsorption on the small fibers, but not the large fibers, significantly reduced NET release, suggesting that other stimuli, whether surface adsorbed or secreted by the neutrophils in an autocrine loop, may also participate in stimulating NET release on our biomaterials [136]. Nonetheless, given the magnitude of IgG adsorption on the biomaterial surface, our data provide evidence for IgG as the predominant stimulatory and regulatory protein in electrospun biomaterial-induced NET release.

Several FcγRs can bind IgG and induce outside-in signaling to trigger the release of NETs. Both FcγRIIa and FcγRIIIb have been implicated in IC-induced NET release through their independent engagement and cooperative signaling [129, 130, 135]. Additionally, Mac-1 has been found to participate in FcγRIIIb-induced NET formation both through its activation and crosstalk with other receptors through shared signaling molecules [129]. Although it is not constitutively expressed, FcγRI is up-regulated within several hours of neutrophil activation, indicating it may also bind IgG during an inflammatory response

[256-258]. In our experiments, we found that blocking of FcγRIIIb significantly attenuated NET release on the small fiber biomaterials to the level of the large fibers whereas blocking of FcγRI, FcγRIIa, or CD11b had no significant effect. Despite the decrease observed on the small fiber biomaterials, we found that blocking of FcγRIIIb had no effect on the large fiber biomaterials, suggesting another stimulus or compensatory mechanism of NET release when FcγRIIIb is blocked [136]. This may also explain why NET release was reduced but not completely abrogated on the small fiber biomaterials upon blocking FcγRIIIb. Moreover, the release of NETs is an active process that occurs after direct neutrophil contact with the stimulus, and others have demonstrated the ability of the neutrophil to modulate its response based on the stimuli, their size, and their valency [130, 141].

FcγRIIIb is a GPI-linked receptor that lacks transmembrane and cytoplasmic domains [266]. Compared to FcγRIIa, FcγRIIIb is 4- to 5-fold more abundant on the neutrophil membrane and is highly mobile with the ability to protrude further due to its GPI anchor [267, 268]. Despite lacking a transmembrane and cytoplasmic domain, FcγRIIIb signaling for NET release occurs through TAK1 and is dependent on NOX2 and ERK activation [129, 254, 269]. To further demonstrate the involvement of FcγRIIIb in biomaterial-induced NET release, we blocked TAK1 and showed a significant decrease in NETs on both small and large fiber biomaterials. The decrease in NET release on both biomaterials was unexpected because we did not observe a decrease in NETs on the large fibers when surface adsorbed IgG was reduced. However, TAK1 can be activated by other receptors, including Toll like receptors, indicating that signaling pathways may participate in biomaterial-induced NET release [136, 270]. When NOX2 is activated downstream of TAK1,

ROS are produced, which can in turn activate PAD4 to citrullinate histones and enhance NET generation [63]. We previously showed that citrullinated histones are found in biomaterial-induced NETs and that we could inhibit biomaterial-induced NET release using Cl-amidine, an inhibitor of PAD4, but were unable to explain the pathway leading to PAD4 activation [31, 76]. Given that ligation of FcγRIIa has been found to activate PAD4 [135], our present study suggests that for our electrospun biomaterials, PAD4 activation is linked to IgG engagement of FcγRIIIb and signaling through TAK1, although the precise mechanism remains to be explored.

The adsorption of IgG to the surface of biomaterials has long been considered significant in the design of biocompatible biomaterials that regulate inflammation, and IgG adsorption is consistently observed on many different biomaterial surfaces [271-275]. Prior work has focused on the adsorption of IgG as an activator of complement and monocytes [271, 276], but one group has explored IgG adsorption on expanded polytetrafluoroethylene and its impact on neutrophil activation and phagocytosis for preventing infection [272, 273]. To our knowledge, we are the first to explore the role of IgG adsorption in biomaterial-induced NET release in tissue engineering applications. Because we now know that neutrophils are important effector cells in the response to biomaterials [17], our work highlights the importance of considering IgG adsorption in the context of preconditioning biomaterial-neutrophil interactions. Future investigations are needed to determine if IgG adsorption can be regulated independent of fiber size and how altering the protein adsorption profile impacts NET release and the potential for tissue healing *in vivo*. Ultimately, we have demonstrated that surface adsorbed IgG, ligation of FcγRIIIb, and activation of TAK1 are involved in electrospun biomaterial-induced NET

release, and modulation of this pathway may have beneficial therapeutic effects for regulating neutrophil-mediated inflammation, fibrosis, and *in situ* tissue regeneration.

Conclusion

Electrospun biomaterials have great potential for a variety of *in situ* tissue engineering applications, but regulating the neutrophil-driven inflammatory response to promote tissue regeneration remains a challenge. In our prior work, we found that IgG adsorption on electrospun PDO is 100- to 200-times greater than the adsorption of other serum proteins and that it may be linked to the increased propensity to form NETs on electrospun biomaterials. The results presented here demonstrate that IgG adsorption does in fact stimulate and regulate biomaterial-induced NET release through FcγRIIIb and activation of TAK1. While the present study only investigated electrospun PDO with differing fiber sizes in the context of tissue engineering, these data garner important insights that are applicable to the design of other biomaterials, including degradable and non-degradable devices. More broadly, an understanding of how adsorbed proteins regulate NET formation during the acute inflammatory response can facilitate the design of new biomaterials for the desired biological outcome, set in motion by the neutrophil and its effector functions.

CHAPTER 6

LOCALIZED DELIVERY OF CL-AMIDINE FROM ELECTROSPUN POLYDIOXANONE TEMPLATES TO REGULATE ACUTE NEUTROPHIL NETOSIS: A PRELIMINARY EVALUATION OF THE PAD4 INHIBITOR FOR TISSUE ENGINEERING

Introduction

When a biomaterial template is implanted in the body, a highly orchestrated series of events is triggered that ideally harnesses the body as a bioreactor, resulting in *in situ* tissue regeneration. Almost instantly, soluble blood serum proteins adsorb on the surface of the biomaterial. The neutrophils swarming into the local microenvironment around the template interact with these proteins and other cells to begin orchestrating the complex responses leading to tissue integration, repair, and regeneration or fibrosis. Regulating the body's innate immune response to an acellular template to harness it as a bioreactor to promote *in situ* tissue regeneration is an emerging focus of tissue engineering. Instead of designing inert materials, tissue engineers aim to develop temporary templates that prevent fibrosis while dynamically guiding tissue integration and regeneration, driven by the innate immune system.

In terms of biomaterial-guided *in situ* tissue regeneration, the critical link between the innate immune response and the healing outcome may be the neutrophil. Historically, neutrophils have been regarded as the rapidly cleared, suicidal killers of the innate immune response. They functioned to simply clean up the microenvironment around a biomaterial before undergoing apoptosis and swift removal by macrophages. However,

insightful research in the last decade suggests that the neutrophil is capable of much more than previously understood with regards to biomaterial-guided tissue regeneration [17].

Neutrophils adopt distinct phenotypes, similar to macrophages, which are influenced by their microenvironment [181]. They release signals through degradation of the ECM and rapidly secrete pre-packaged granules that can modulate their phenotype and influence the recruitment of additional cells [23, 277]. Additionally, neutrophils are able to survive significantly longer after extravasation than once accepted [278], suggesting their ability to synthesize and secrete factors for early-stage immune system modulation that may have long-term effects. Finally, several recent studies have identified that neutrophils can actually reverse migrate from an area of inflammation, relocating to new areas of the body to potentially educate the immune system [279, 280].

Importantly, neutrophils are able to expel their DNA along with granular contents to form NETs through a specialized form of anti-microbial cell death called NETosis [27]. During NETosis, chromatin within the nucleus decondenses while the nuclear envelop and granule membranes disintegrate, resulting in a mixing of the potent granule cargo and DNA. Eventually, a cloud-like, fibrillary network of DNA that is decorated with anti-microbial proteins, proteases, and histones is extruded into the microenvironment. Importantly, NETing neutrophils are protected from pre-emptive clearing by macrophages, resulting in NETs that are difficult to contain [141].

During NETosis, chromatin decondensation occurs with deimination of histone H3 to CitH3 by the enzyme PAD4 [128, 132]. The basic amino acid residue, arginine, is converted to a neutral citrulline residue, which weakens the interaction between the histone and chromatin, leading to an unraveling of chromatin. When the activity of PAD4

is blocked with an inhibitor or eliminated in a mouse knockout model, the production of NETs is severely reduced for anti-bacterial immunity and in pathological deep vein thrombosis [119, 133, 134].

While functioning as a classic anti-microbial response, NETosis has also been implicated in various forms of tissue fibrosis, thus making it a prominent therapeutic target. In particular, neutrophils have been linked to pulmonary fibrosis, fibrosis after myocardial infarction, and atherosclerosis [281-283]. Dysregulated release of NETs appears to contribute to the overproduction of dense fibrotic matrix in tissue fibrosis. In terms of tissue regeneration, our group has recently demonstrated that the excessive presence of NETs inhibits tissue integration with an electrospun biomaterial and may promote fibrotic encapsulation [31]. In the study, we electrospun PDO, a synthetic resorbable biomaterial, to create two distinct material architectures, templates with SD (0.3 ± 0.1 μm) or LD (1.9 ± 1.0 μm) fibers and pores. Using fresh human peripheral blood neutrophils *in vitro* and a subcutaneous rat implant model, we showed that the microenvironment created by the template architecture differentially modulates NETosis and formation of fibrotic tissue *in vivo*, respectively.

In the present work, we confirmed the experiments of our previous study and extended them by incorporating varying concentrations of Cl-amidine, a haloacetamidine-based compound that irreversibly inhibits PAD4 [284], into the electrospun templates. Cl-amidine covalently modifies the cysteine residue in the active site that is critical for PAD4 enzymatic activity and functions in a dose-dependent manner [118]. The purpose of this study was to incorporate Cl-amidine into electrospun PDO templates for local delivery, measure its activity, and further assess the potential of the drug elution to

inhibit PAD4-mediated citrullination of histone H3 and reduce template-induced NETosis. We hypothesized that elution of Cl-amidine from the templates would attenuate NETosis with the greatest effect seen on SD templates. SD and LD templates were fabricated with 0-5 mg/mL Cl-amidine, and NETosis was evaluated in response to the templates *in vitro* with freshly isolated, human peripheral blood neutrophils and *in vivo* with a subcutaneous implant model in a rat. The results were analyzed based on the temporal degree of NETosis in response to the template architectures and Cl-amidine concentrations. Ultimately, regulating the release of template-preconditioning NETs from the interacting neutrophils may modulate the early-stage innate immune response, promoting or even enhancing guided tissue regeneration.

Materials and Methods

Activity of Cl-amidine After Solvent Exposure

Cl-amidine (trifluoroacetate salt) (Cayman Chemical, Item No. 10599, Batch No. 0468497-71) activity was quantified by a PAD4 Inhibitor Screening Assay (Cayman Chemical, Item No. 700560) following manufacturer protocol to evaluate activity after exposure to the organic electrospinning solvent HFP (Oakwood Products, Inc.), simulating processing. Cl-amidine was suspended in HFP, and 1x HBSS to result in final assay concentrations of 147.8, 29.5, 5.9, 1.18, 0.24, 0.047, and 0 μM. 40 μL of each HFP sample (n = 4) were pipetted into the wells of a 96-well culture plate, and the plate was placed in fume hood to allow evaporation of HFP overnight at room temperature. Then, the drug was resuspended in 40 μL of HBSS for detection. 5 μL of the HBSS and resuspended HFP samples were assayed according to manufacturer protocol and were read on a SpectraMax i3x Multi-Mode Microplate Reader (excitation 410 nm and

emission 475 nm) to determine fluorescent intensity. After taking the log transform of molarity, the average fluorescent intensity and standard deviation for each sample were plotted against Cl-amidine concentration.

Template Fabrication and Characterization

PDO (Sigma Aldrich Co.) was dissolved overnight in HFP at varying concentrations (Table 7) ranging from 65 to 100 and 170 to 200 mg/mL to create SD and LD templates, respectively. 0, 1, 2.5, or 5 mg/mL of Cl-amidine was added to the polymer solution and dissolved for 2 hours with gentle agitation before electrospinning. Solutions were loaded into a syringe with an 18-gauge blunt needle tip attached to the positive lead of a power source (Spellman CZE1000R, Spellman High Voltage Electronics Corp.) and placed on a syringe pump (Model No. 78-01001, Fisher Scientific). Solutions were electrospun with optimized flow rate, airgap distance, and applied voltage (Table 7). Fibers were collected on a grounded, stainless steel rectangular mandrel (20 x 75 x 5 mm) that was rotating at 1250 rpm and translating 6.5 cm/s over 13 cm. The templates (thickness 0.10 - 0.25 mm) were stored at -20°C until analyses.

For scanning electron microscopy, templates were coated with 5 nm of gold-palladium by sputter coating in an argon gas field. The materials were then imaged with a FEI Nova NanoSEM 650 with field emission gun at +20 kV with a working distance of 5mm to generate SEMs. Fiber diameter and pore diameter were characterized by analyzing the SEMs in FibraQuant 1.3 software (nanoTemplate Technologies, LLC). Average fiber and pore diameters with corresponding standard deviations were determined from a minimum of 250 semi-automated random measurements per image and 60 random manual measurements per image, respectively.

Table 7. Electrospun templates were fabricated with optimized parameters. Polymer and Cl-amidine concentration were varied to create two distinct groups of SD and LD templates.

Fiber Size	Polymer Concentration [mg/mL]	Cl-amidine concentration [mg/mL]	Flow Rate [mL/h]	Airgap Distance [cm]	Applied Voltage [+kV]
SD	65	0	2	13	22
	100	1	2.5	15	18
	100	2.5	2.5	15	18
	100	5	2.5	15	18
LD	170	0	6	13	22
	200	1	3	18	28
	200	2.5	3	18	28
	200	5	3	18	28

Cl-amidine Template Elution

Electrospun templates were characterized for the delivery of Cl-amidine into supernatant over 5 days. 10 mm diameter discs of the templates (n = 6) were placed in a 48-well culture plate, and 300 μL of HBSS were added to each well. After incubation at 37°C for 15, 30, 45 minutes, 1, 2, 3, 6, 12 hours, 1, 2, 3, 4, and 5 days, the supernatant was removed and refreshed with 300 uL of HBSS. The collected supernatant was frozen and stored at -20°C until analysis. Activity of Cl-amidine was detected using the PAD4 Inhibitor Screening Assay following manufacturer protocol, and the resulting fluorescent intensities were used to determine Cl-amidine concentration within the samples. An average and standard deviation were determined for each template type.

***In Vitro* Evaluation with Fresh Human Peripheral Blood Neutrophils**

Neutrophils were isolated from blood obtained from healthy donors from Tennessee Blood Services in accordance with protocols approved by the University of Tennessee Institutional Review Board as previously described [31]. Informed and written consent was obtained by Tennessee Blood Services. After isolation, neutrophils were resuspended at a density of 2.4 x 10^6 cells/mL in HBSS without calcium and magnesium

and with 10mM HEPES and 0.2% autologous serum. 10 mm diameter discs of the PDO templates (n = 4) were disinfected by ultraviolet irradiation with a Spectroline handheld lamp (8 watt, Part No. EN280L) for 10 minute per side in a sterile laminar flow hood with 365 nm wavelength at a working distance of 9.5 cm. The templates were placed in a 48-well culture plate and hydrated with 50 μL of sterile HBSS. Immediately following hydration, 250 μL of the cell suspension containing 600,000 cells were pipetted onto the templates, and the templates were cultured at 37°C and 5% CO_2. After 3 and 6 hours, the plates were placed on ice, inhibiting further stimulation of the neutrophils. Supernatant was carefully removed, and the cells were fixed in the wells with 10% neutral buffered formalin. Cellularized templates were stored in 10% formalin at 4°C until analysis.

Fluorescence Quantification of NETs

Fluorescence microscopy of the templates (n = 4) was used to quantify the degree of NETosis as previously described [31]. Briefly, templates were stained with 100 nM SG extracellular DNA stain (Life Technologies, Cat. No. S7020) in DI water for extruded NETs followed by DAPI fixed cell nuclei stain (Life Technologies, Cat. No. R37606) at stock concentration for intact nuclei. To determine the relative degree of NETosis, the B:G ratio, representing the area of intact cell nuclei to extruded NETs, within an image was quantified using MATLAB Release 2012a. The B:G ratios were normalized to cell number within an image, and an average and standard deviation were calculated for each template type.

IR Scanning and Quantification of CitH3

An On-cell Western assay was performed to quantify template-bound CitH3 as described [31]. Briefly, human histone H3 (citrulline R2 + R8 + R17) peptide (Abcam,

Product code ab32876) was spotted on an Immobilon-FL PVDF membrane and dried overnight to create a standard curve. The standard curve and cellularized templates (n = 4) were blocked with 5% non-fat milk for 1 hour at room temperature, then incubated with rabbit anti-human histone H3 (citrulline R2 + R8 + R17) antibody (Abcam, Product code ab5103) at a 1:200 dilution in 5% milk overnight at 4°C. After incubation with primary antibody, three washes were performed with 0.1% Tween-20 in HBSS for 5 minutes at room temperature with gentle agitation. Following, the standard curve and templates were incubated with IRDye 800CW donkey anti-rabbit (LI-COR, Part no. 926-32213) at a 1:20,000 dilution in 5% milk with 0.1% Tween-20 and 0.01% SDS for 1 hour at room temperature. Non-cellularized templates were incubated with secondary antibody only, serving as negative controls. After two washes with 0.1% Tween-20 in HBSS and one final wash with HBSS, the standard curve and templates were scanned on the 800 nm channel of the Odyssey CLx IR Imaging System (LI-COR) to generate full-thickness template fluorescence. The scans were analyzed with Image Studio Version 5.x (LI-COR).

For the standard curve, relative fluorescent intensities were acquired by placing circular markers over the area of a spot. The average and standard deviations were plotted against the mass of CitH3 to create a standard curve. For the templates, the relative fluorescent intensities were measured by encompassing the area of the sample and extrapolating it to the area for a 10 mm diameter disc, which was normalized to template thickness. The final relative fluorescent intensity was converted to mass of CitH3 using the standard curve, and an average and standard deviation were generated for each template type.

In Vivo Rat Subcutaneous Implant Model

Ten-millimeter diameter discs of the templates (n = 3) were implanted on the back of Sprague-Dawley rats (300-325 g, male) following the protocol approved by the University of Memphis Institutional Animal Care and Use Committee as previously described [31]. Briefly, templates were disinfected with ultraviolet irradiation for 10 minutes on each side, and all materials were handled aseptically. One template lying flat was implanted per subcutaneous pocket, and the skin was closed with 2-3 staples. Four templates were implanted randomly on the back of each rat (Figure 25A). Additionally, to ensure drug-eluting materials exerted their effects locally without diffusion or convection to adjacent samples, two SD templates with 0 mg/mL Cl-amidine were implanted between four SD templates with 5 mg/mL Cl-amidine (n = 3), and two SD templates with 0 mg/mL Cl-amidine (n = 3) were implanted alone (Figures 25B,C). One day after implantation, the animals were euthanized, the subcutaneous pockets were opened, and the templates were explanted, fixed, and stored in 10% neutral buffered formalin at 4°C.

Fixed templates were processed, sectioned at 10 μm, and stained with H&E following standard protocol. The sections were evaluated and scored by a board-certified veterinary pathologist blinded to sample identity for presence of surface DNA, invasion into the template, and degree of neutrophil degeneration (Table 8). The presence of surface DNA was evaluated based on prevalence of DNA on the surfaces of the templates seen as a blue-stained acellular layer, invasion into the templates was scored based on number of invading neutrophils and depth of invasion, and the degree of neutrophil

degeneration was assessed based on the abundance of neutrophils showing degenerative, morphological changes (i.e., loss of lobulated nuclei, fragmentation, apoptotic bodies, etc.). Finally, the surface of the 1-day templates were evaluated for template-bound CitH3 through an On-cell Western blot following the *in vitro* protocol.

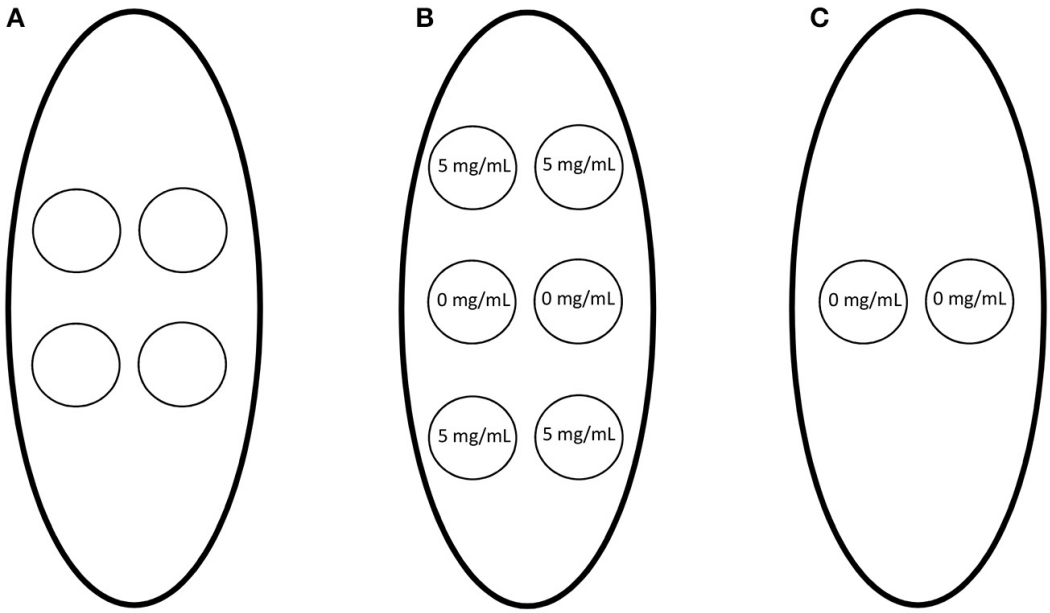

Figure 25. Electrospun templates with 0-5 mg/mL Cl-amidine were implanted subcutaneously on the dorsa of rats. (A) One template was implanted randomly per subcutaneous pocket. In addition, to determine if the drug-eluting materials had systemic effects due to diffusion or convection, (B) SD templates with 0 mg/mL Cl-amidine were implanted between SD templates with 5 mg/mL Cl-amidine and (C) SD templates with 0 mg/mL Cl-amidine were implanted alone.

Table 8. Electrospun templates were evaluated by a veterinary pathologist in a blinded fashion at 1 day after implantation in a subcutaneous rat implant model.

Score	Presence of Surface DNA	Invasion into the Template	Degree of Neutrophil Degeneration
1	DNA adherent to some surfaces of the template	Slight invasion into the template near a fold or defect	Most invading non-degenerate
2	DNA adherent to most surfaces of the template	Slight invasion into the template	Many invading non-degenerative
3	Dense DNA layer adherent to some surfaces of the template	Moderate invasion with reduced invasion towards the center	Occasional invading non-degenerative
4	Dense DNA layer adherent to most surfaces of the template	Moderate invasion throughout the thickness of the template	Few non-degenerating neutrophils not deeply invaded
5	Conspicuous, dense DNA layer adherent to the surfaces of the template	Dense invasion throughout the thickness of the template	Diffuse degenerating neutrophils near surface

Statistical Analysis

Significant differences in Cl-amidine activity were determined by an unpaired t-test to compare activity for each concentration. The plot of average fluorescent intensity against Cl-amidine concentration was fit with a four-parameter logistic regression, and a lack of fit test was executed. The plot of relative fluorescence against mass of CitH3 was fit with a linear regression. For all other *in vitro* methods, analysis of data was conducted using a two-way ANOVA and a Tukey multiple comparison procedure. All *in vitro* statistical analyses were performed in GraphPad Prism 6 at a significance level of 0.05.

For the *in vivo* methods, the data sets were resampled (n = 1,000) using bootstrapping and then evaluated with a two-way ANOVA and a Tukey multiple comparison procedure to ensure the data did not violate the assumptions of normality [285, 286]. Resampling and analyses were performed in SAS 9.4 and GraphPad Prism 6, respectively, at a significance level of 0.05.

Results

Cl-amidine Retains Activity During Template Production

Before incorporating the drug into the electrospun templates, the activity of Cl-amidine was verified after exposure to the harsh organic solvent, HFP, that is used during electrospinning. Figure 26 shows the four-parameter regression curve for the HFP samples along with the HBSS samples. As the concentration of drug increases, the relative fluorescence decreases, signifying an increase in the inhibition of PAD4. The assayed drug concentrations were selected to provide a range that includes the inhibitory concentration 50 of Cl-amidine against PAD4, which is 5.9 μM in an *in vitro* model [284]. Exposure of Cl-amidine to HFP significantly reduced its activity against PAD4 at two concentrations, 5.9 and 29.5 μM ($p < 0.0001$). However, the drug was still active producing a sigmoidal curve similar to that of the HBSS samples. This loss of Cl-amidine activity upon exposure to HFP was reproducible and therefore could be compensated for by increasing the drug concentration. Nonetheless, the drug retained efficacy after exposure to HFP and inhibited PAD4 activity at concentrations as low as 1.2 μM, demonstrating the potential to incorporate it into electrospun templates for release and activity against PAD4.

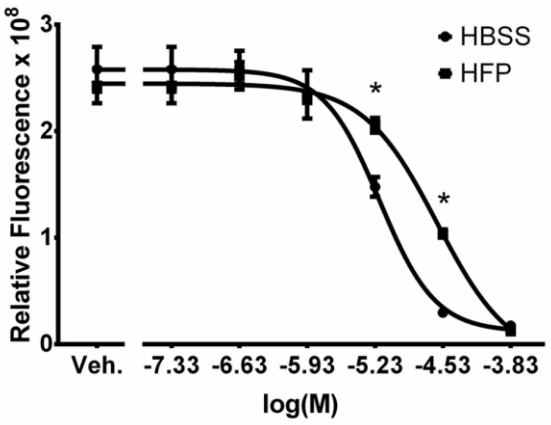

Figure 26. Cl-amidine retains activity after exposure to HFP. Plot of drug concentration against relative fluorescence for HBSS and HFP exposed samples. Veh. is HBSS only. The four-parameter regression of the HFP exposed samples has no evidence of lack of fit ($p = 0.28$). *Significant difference in relative fluorescence ($p < 0.05$) (mean ± standard deviation, $n = 4$).

In addition to determining the activity of Cl-amidine, the samples exposed to HFP were used to create a standard curve for quantifying unknown Cl-amidine concentrations. The four-parameter logistic regression of the HFP exposed samples (Equation 7, x = logarithmic transform of Cl-amidine concentration and y = relative fluorescence) has an R^2 value of 0.996, and there is no evidence of an inadequate model from the lack of fit test ($p = 0.28$).

$$y = \frac{2.65}{1+10^{5.25+1.14x}} \quad (7)$$

Template Characteristics Incorporating Cl-amidine

Low and high polymer concentration solutions incorporating Cl-amidine resulted in two distinct templates groups, SD and LD templates, which had uniform fiber and pore morphologies comparable to SD and LD templates without drug (Figures 27A,B). During electrospinning, the addition of a charged entity to the solution reduces fiber diameter, so we increased polymer concentration to prevent reduction in fiber diameter for Cl-amidine templates [287]. Figures 27C,D show the results of the fiber and pore diameter analyses,

respectively. Within the SD and LD template groups, the templates did not have significantly different fiber diameters between 0 and 5 mg/mL Cl-amidine. At each drug concentration, the SD templates had significantly smaller fiber diameters with an average of 0.36 ± 0.16 μm compared to the LD templates with average fiber diameters of 1.82 ± 0.59 μm ($p < 0.05$). Similarly, the pore diameters of the SD and LD templates were not different between templates with 0-5 mg/mL Cl-amidine, but at each drug concentration, the SD templates had significantly smaller pore diameters near 1.76 ± 0.79 μm compared to the LD templates with average pore diameters of 7.34 ± 2.42 μm. Together, these data indicate that the increase in polymer concentration for SD and LD templates compensated for the addition of Cl-amidine to produce templates with consistent fiber and pore diameters.

Elution Kinetics of Cl-amidine From Templates

The electrospun templates eluted Cl-amidine to varying degrees based on fiber diameter and drug content over 5 days (Figures 28A–D). At 3 0min, the SD template with 5 mg/mL Cl-amidine eluted significantly more drug than the LD template, and from 45 minutes to 6 hours, the SD templates with 2.5 and 5 mg/mL Cl-amidine eluted more drug

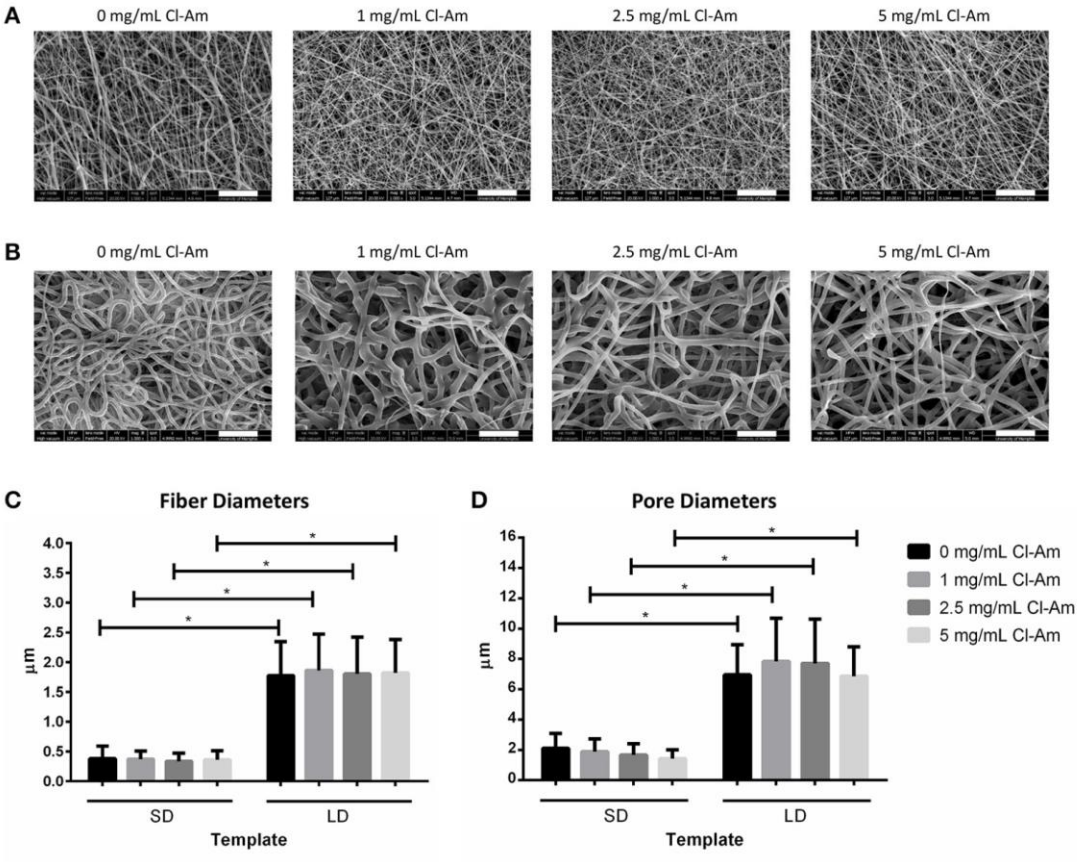

Figure 27. PDO electrospins at low and high concentrations with Cl-amidine. Representative SEMs of (A) SD and (B) LD templates with 0–5 mg/mL Cl-amidine (scale bars = 20μm). For all drug concentrations, all SD and all LD templates have statistically equivalent (C) fiber and (D) pore diameters; however, at each drug concentration, SD templates have significantly smaller (C) fiber and (D) pore diameters than the LD templates. *Significant difference ($p < 0.05$). (mean ± standard deviation, $n > 250$ for fiber diameter analysis and $n = 60$ for pore diameter analysis).

than the LD templates ($p < 0.05$) (Figures 28A,B). These significant trends were seen over the 5-day period (Figures 28C,D), and by 2 days, all of the SD templates eluted significantly more Cl-amidine than the LD templates ($p < 0.05$). Because HFP reduces the activity of Cl-amidine, there is potential that some Cl-amidine was eluted from the fibers and not detected in the activity assay. In addition, it is likely that some Cl-amidine was retained within the fibers and had yet to elute from the templates in the 5-day period.

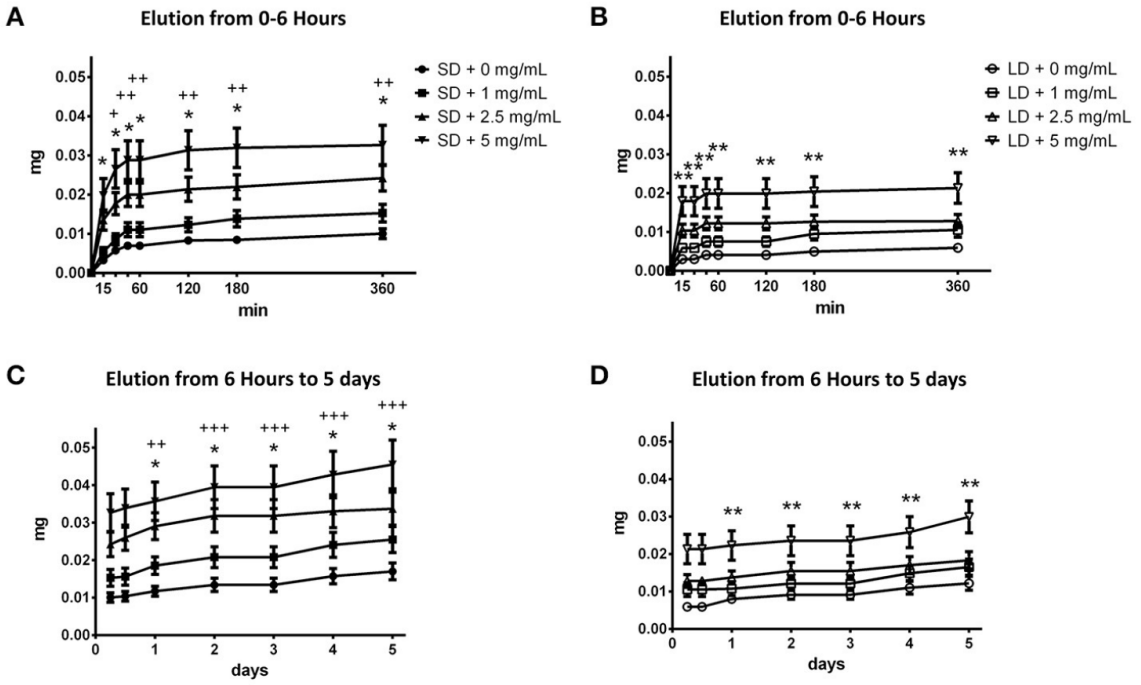

Figure 28. SD and LD templates elute Cl-amidine over 5 days. From 0 minutes to 6 hours, the (A) SD templates eluted significantly more drug than the (B) LD templates. This trend was observed from 6 hours to 5 days for the (C) SD and (D) LD templates. *Significant difference between 2.5 mg/mL Cl-amidine and 5 mg/mL Cl-amidine from 0 mg/mL Cl-amidine templates ($p < 0.05$). **Significant difference between 5 mg/mL Cl-amidine from 0 mg/mL Cl-amidine templates ($p < 0.05$). +Significant difference between SD and LD templates with 5 mg/mL Cl-amidine ($p < 0.05$). ++Significant difference between SD and LD templates with 2.5 mg/mL and 5 mg/mL Cl-amidine ($p < 0.05$). +++Significant difference between all SD and LD templates ($p < 0.05$) (mean ± standard deviation, n = 6).

The potential effects of low-level elution from the templates after the initial critical hours is negligible due to the short half-life of Cl-amidine *in vivo* [284].

At 3 hours, the SD templates with 1, 2.5, and 5 mg/mL Cl-amidine had eluted the drug to reach concentrations of 108.7 ± 16.5, 172.4 ± 24.2, and 250.6 ± 39.5 μM Cl-amidine. Contrastingly, the LD templates with 1, 2.5, and 5 mg/mL Cl-amidine only eluted the drug to reach concentrations 74.4 ± 12.2, 99.2 ± 13.3, and 160.1 ± 30.2 μM Cl-amidine. Despite the equivalent drug content during fabrication, these differences result from the high SAVR of the SD templates, leading to a more significant burst release of

Cl-amidine. Because the SD templates elicit the highest degree of NETosis, the greater elution of Cl-amidine from the SD templates at 3 hours may counteract template-induced NETosis [31]. Furthermore, by 3 hours, the SD and LD templates eluted nearly 60% of the drug released over the 5-day period. This burst release is due to the characteristic segregation of the charged drug to the outer surface of the electrospun fibers [214]. Since the swarming of neutrophils to the site of inflammation occurs in the first 3 hours, the substantial local release in the initial hours may be desired to regulate the critical interaction that directs the ensuing response [12].

Templates Eluting Cl-amidine Modulate NETosis *In Vitro*

Fluorescence microscopy revealed contrasting degrees of NETosis in response to the different template fiber diameters and drug concentrations at 3 and 6 hours (Figures 29 and 30). Blue (DAPI) stains condensed chromatin, and green (SG) stains decondensed NET chromatin, respectively. SG cannot penetrate an intact cell membrane [288]. Therefore, cyan, an overlap of DAPI and SG staining, indicates cells with an intact nucleus but compromised cell membrane. Because the cells retain their plasma membrane integrity while the nuclear and granular membranes disintegrate, these cyan stained neutrophils have compromised cell membranes and may be undergoing cell death other than NETosis. The varying degrees of NETosis were quantified with a B:G ratio using a MATLAB image analysis algorithm (Figures 31A,B). A B:G ratio >1 indicates that more image area of the template is covered by intact cells than extruded NETs, signifying a low degree of NETosis, with the inverse for a B:G ratio <1, signifying a high degree of NETosis.

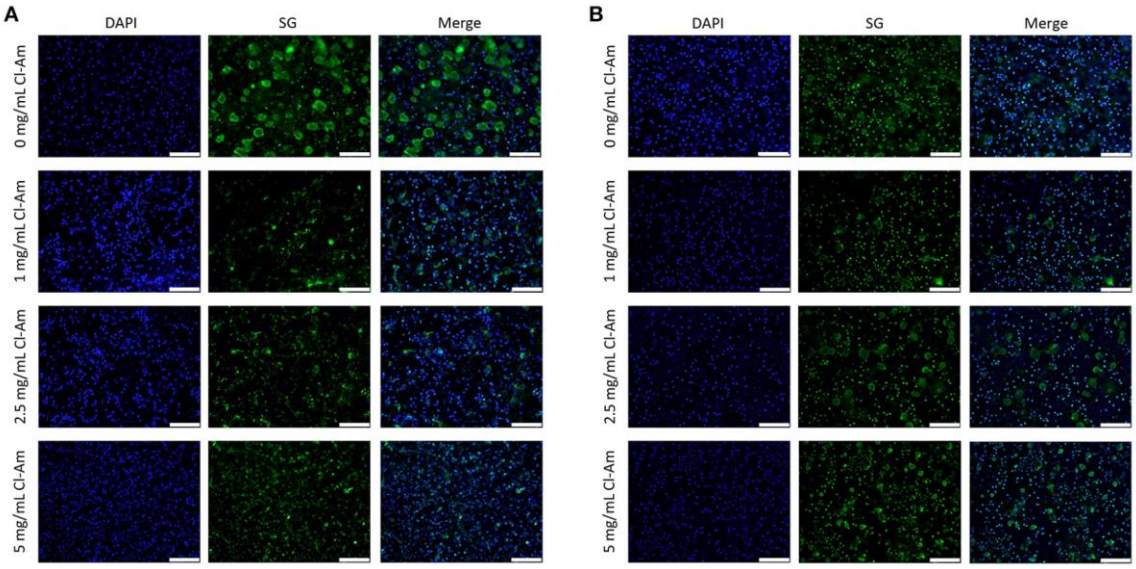

Figure 29. Neutrophils interacting with Cl-amidine eluting templates exhibit different degrees of NETosis at 3 hours. Representative fluorescent micrographs of (A) SD and (B) LD templates indicate different degrees of NETosis based on drug content (scale bars = 100 μm). Blue is DAPI. Green is SG.

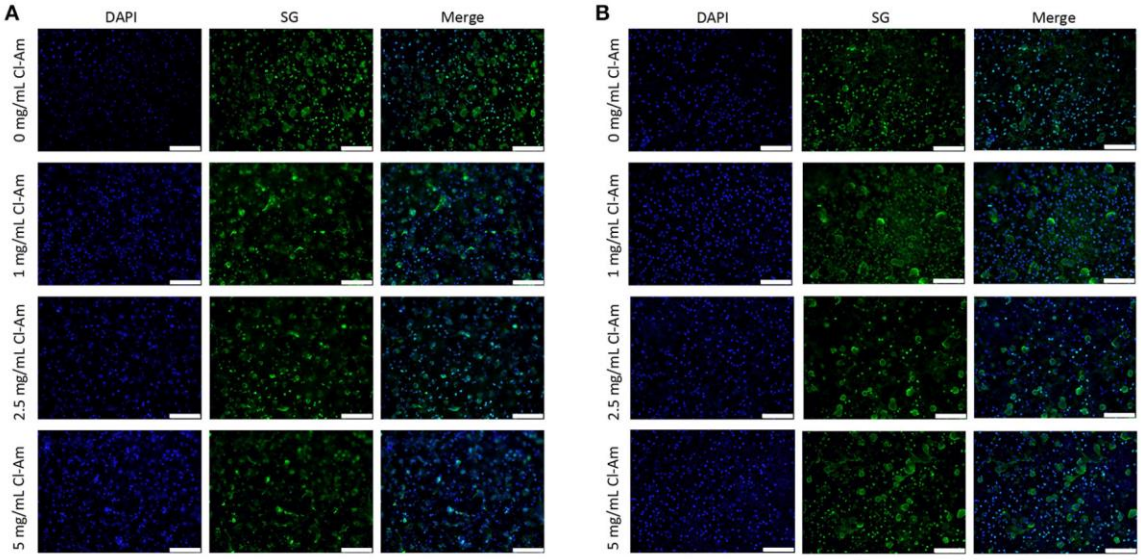

Figure 30. Neutrophils interacting with Cl-amidine eluting templates exhibit equivalent degrees of NETosis at 6 hours. Representative fluorescent micrographs of (A) SD and (B) LD templates indicate near equivalent degrees of NETosis based on drug content (scale bars = 100 μm). Blue is DAPI. Green is SG.

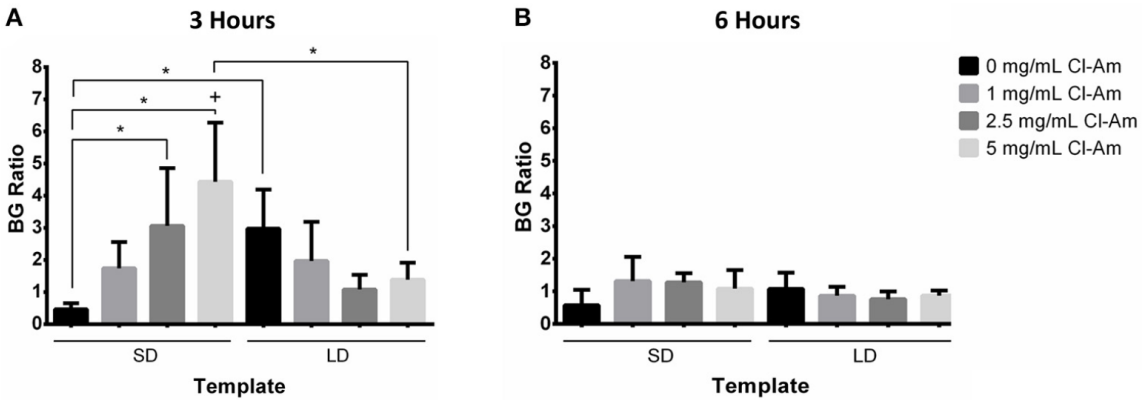

Figure 31. Cl-amidine significantly decreases NETosis on SD templates. The B:G ratio for templates at (A) 3 and (B) 6 hours indicate that template architecture modulates NETosis. In addition, the elution of Cl-amidine significantly affects NETosis at 3 hours with minimal effects at 6 hours. *Significant difference ($p < 0.05$). +Significant difference between 3 and 6 hours ($p < 0.05$) (mean ± standard deviation, n = 4).

At 3 hours, the SD templates with 0 mg/mL Cl-amidine elicited a statistically higher degree of NETosis, with a B:G ratio of 0.47 ± 0.19, than the LD template with 0 mg/mL Cl-amidine, which had a B:G ratio of 2.98 ± 1.21 ($p < 0.05$). These results were anticipated and replicate, to the same magnitude, those of our previous experiments where we showed that SD PDO templates increase NETosis *in vitro* while LD PDO templates led to a significant reduction [31]. As seen in Figure 31A, with increasing Cl-amidine concentration, the degree of NETosis in response to the SD templates significantly decreases in a dose-dependent manner. The SD templates with 5 mg/mL Cl-amidine have a B:G ratio of 4.4 ± 1.84, nearly 10 times greater than the SD templates without drug ($p < 0.05$). These results suggest that the addition of Cl-amidine to the SD templates attenuates NETosis through the inhibition of PAD4, and that these effects are concentration dependent.

For the LD templates at 3 hours, the incorporation of Cl-amidine into the templates decreases the B:G ratio in a dose-dependent manner down to 1.39 ± 0.52 for

the templates with 5 mg/mL Cl-amidine. While not significant, this trend is opposite of the SD templates and suggests that in the microenvironment created by the LD templates with Cl-amidine, NETosis is increased. Nonetheless, the B:G ratio for all of the LD templates with Cl-amidine is >1, indicating that there is still more surface area on the template covered by intact neutrophils than extruded NETs. Taken together, these contrasting effects of Cl-amidine at 3 hours *in vitro* suggest that there may be another mechanism in addition to PAD4-regulated NETosis that modulates the generation of NETs based on the template architecture. By 6 hours, the B:G ratios for the SD and LD templates decreased to values around 1, suggesting that there is an equivalent amount of area covered by viable neutrophils and extruded NETs on the templates (Figure 31B).

As a concomitant method to quantify NETosis, an On-cell Western assay was used to quantify template-bound CitH3 at 3 and 6 hours *in vitro* (Figures 32A,B). Histone H3 is citrullinated by PAD4 during NETosis, generating CitH3, which is then complexed with released NETs [128]. Previously, we showed that detection of CitH3 can be used in addition to fluorescence microscopy to quantify the degree of NETosis in response to electrospun templates [31]. The linear regression of mass of CitH3 against relative fluorescence (Equation 8, x = mass in ng of CitH3 and y = IR intensity) has an R^2-value of 0.966, which indicates a well-fitting line, and linear relationship that can be used to quantify CitH3.

$$y = 91.1x \tag{8}$$

At 3 hours, SD templates with 0 mg/mL Cl-amidine had significantly more template-bound CitH3 than the LD templates with 0 mg/mL Cl-amidine ($p < 0.05$). The SD templates had 8.1 ± 2.2 ng CitH3, nearly 4 times greater than the LD templates with

2.2 ± 0.4 ng. These results suggest a high degree of NETosis on the SD templates, which is supported by the results from fluorescence microscopy. In Figure 32A, Cl-amidine significantly decreased the amount of detectable CitH3 on SD templates, which suggests a decrease in NETosis similar to the results from fluorescence microscopy ($p < 0.05$). Likewise, for the LD templates, the templates with Cl-amidine correlated to higher amounts of template-bound CitH3. All of the LD templates with drug had more detectable CitH3 than their SD template counterparts. These similar results were also observed at 6 hours (Figure 32B). However, while it increased on the LD templates, the amount of template-bound CitH3 did not increase on the SD templates with Cl-amidine. Clearly, the elution of Cl-amidine from the electrospun PDO templates regulates NETosis from the interacting neutrophils in a dynamic manner dependent on the template microenvironment.

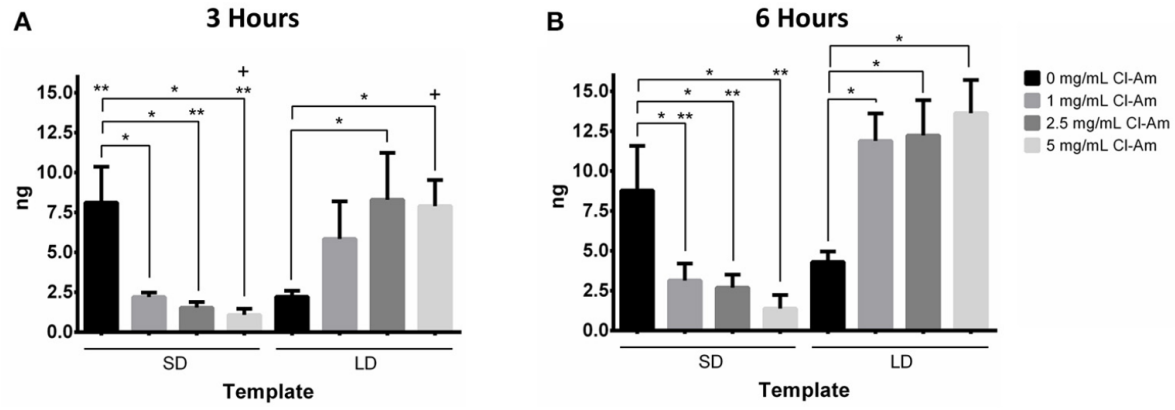

Figure 32. Cl-amidine significantly decreases template-bound CitH3 on SD templates. Template-bound CitH3 at (A) 3 and (B) 6 hours suggests that template architecture and Cl-amidine concentration regulate NETosis. *Significant difference ($p < 0.05$). **Significant difference between SD and LD templates ($p < 0.05$). +Significant difference between 3 and 6 hours ($p < 0.05$) (mean ± standard deviation, n = 4).

PDO Templates Eluting Cl-amidine Modulate NETosis *In Vivo*

Next, the Cl-amidine eluting electrospun templates were implanted subcutaneously on the back of rats. H&E staining of templates after 1 day (Figures 33A,B) indicated that SD and LD templates initiated differing responses based on template architecture and drug content, which were quantified by a veterinary pathologist in a blinded fashion. At 1 day, the presence of surface DNA, invasion into the template, and degree of neutrophil degeneration were evaluated (Figures 34A-C). The presence of surface DNA (Figure 34A) scored significantly higher on SD templates with 0 mg/mL Cl-amidine at 3.7 ± 0.5 compared to LD templates with 0 mg/mL Cl-amidine at 1.7 ± 0.5 ($p < 0.05$). A dense DNA layer was adherent to most surfaces on the SD the templates whereas only some DNA was adherent to the LD template surfaces, similar to the trends seen *in vitro*. For the SD templates, Cl-amidine significantly decreased the scores for the presence of surface DNA, while for LD templates, the opposite was observed ($p < 0.05$). Again, these data reflect the fluorescence microscopy results *in vitro*, suggesting that Cl-amidine elution results in similar effects in a physiological environment. Interestingly, for the SD templates with 5 mg/mL Cl-amidine, the score for surface DNA was greater than the score for 1 and 2.5 mg/mL Cl-amidine, but the score was still significantly lower compared to SD templates with 0 mg/mL Cl-amidine.

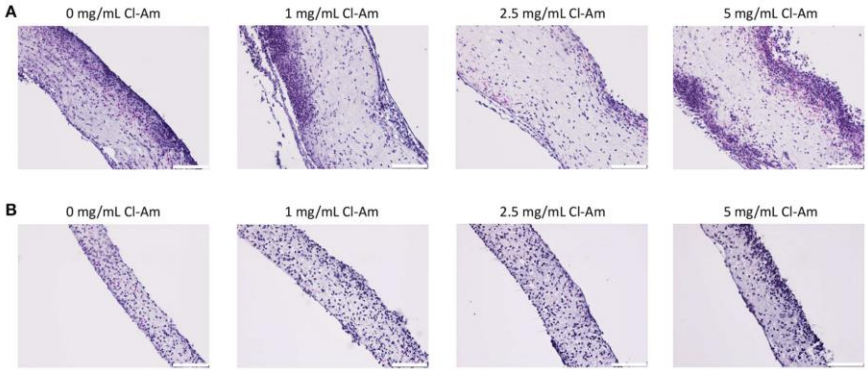

Figure 33. Cl-amidine eluting electrospun templates modulate neutrophil behavior *in vivo*. Representative light microscopy images of H&E stained sections of (A) SD and (B) LD templates removed after 1 day (scale bars = 100 μm).

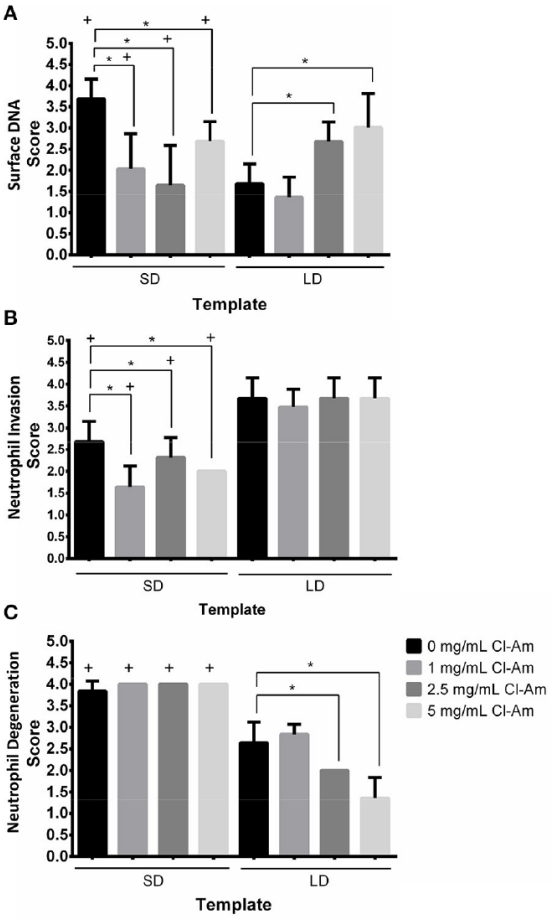

Figure 34. Cl-amidine eluting templates modulate cell behavior *in vivo*. Histological scores obtained from a blinded, veterinary pathologist for (A) presence of surface DNA, (B) invasion into the template, and (C) degree of neutrophil degeneration after 1 day implantation. *Significant difference ($p < 0.05$). +Significant difference between SD and LD templates ($p < 0.05$) (mean ± standard deviation, n = 3).

Invasion of neutrophils into the templates (Figure 34B) was also modulated by architecture and drug concentration. LD templates scored significantly higher with moderate invasion throughout the thickness of the template compared to SD templates with slight invasion into the template ($p < 0.05$). Because of the restrictive pore diameters of the SD templates, which are 3 times smaller than the LD template pore diameters, it is not surprising that the SD templates exhibited less invasion. Interestingly, the elution of Cl-amidine from SD templates significantly decreased invasion into the templates compared to the SD template with 0 mg/mL Cl-amidine ($p < 0.05$). This is not observed for the LD templates, which all scored with moderate invasion.

The degree of neutrophil degeneration (Figure 34C) was significantly different in response to the templates after acute interaction *in vivo*. As noted, the degeneration of neutrophils was classified by the degree of morphological changes. All of the SD templates scored significantly higher at 4.0 ± 0.2 compared to LD templates at or below 2.6 ± 0.5 ($p < 0.05$). This equates to minimal non-degenerating neutrophils that are not deeply invaded and many invading, non-degenerative neutrophils, respectively. Importantly, with increasing Cl-amidine concentration, the LD templates scored significantly better for neutrophil degeneration, decreasing from 2.6 ± 0.5 for 0 mg/mL Cl-amidine to 1.3 ± 0.5 for 5 mg/mL Cl-amidine ($p < 0.05$). The decreasing scores suggest that with increasing Cl-amidine concentration, a greater portion of the interacting neutrophils are viable and exerting their potential long-term effector functions to modulate the early-stage innate immune response.

In addition to pathological evaluation, the templates excised after 1 day were evaluated for template-bound CitH3 (Figure 35). The results show that the SD templates

with 0 mg/mL Cl-amidine had significantly more template-bound CitH3 with 7.3 ± 0.4 ng compared to the LD templates with 0 mg/mL Cl-amidine at 3.6 ± 0.3 ng ($p < 0.05$). With increasing drug concentration, the amount of template-bound CitH3 significantly decreased on the SD templates, while the opposite was observed on LD templates ($p < 0.05$). However, the SD templates with 5 mg/mL Cl-amidine resulted in more CitH3 compared to 1 and 2.5 mg/mL Cl-amidine. These significant trends validate the scores categorized by the pathologist for presence of surface DNA on the templates, indicating that the Cl-amidine eluting templates modulate NETosis *in vivo*.

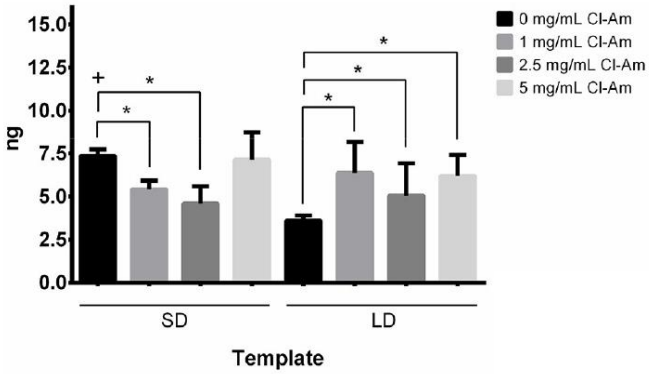

Figure 35. PDO templates eluting Cl-amidine modulate NETosis *in vivo*. Cl-amidine attenuates NETosis as indicated by CitH3 on SD templates while increasing NETosis on LD templates. *Significant difference ($p < 0.05$). +Significant difference between SD and LD templates ($p < 0.05$) (mean ± standard deviation, n = 3).

To ensure the Cl-amidine eluting templates exhibited only local inhibition of PAD4, SD templates with 0 mg/mL Cl-amidine were implanted between templates with 5 mg/mL Cl-amidine (Figure 25). SD templates with 0 and 5 mg/mL Cl-amidine were selected to maximally challenge the effects of Cl-amidine through its high and rapid release from the SD templates. The SD templates with 0 mg/mL Cl-amidine adjacent to templates with 5 mg/mL Cl-amidine were compared to SD templates with 0 mg/mL Cl-amidine that were implanted alone (Figure 25). After 1-day, histological scores were not significantly different for presence of surface DNA, invasion into the template, and

degree of neutrophil degeneration for the SD adjacent templates and the SD template controls ($p < 0.05$). The presence of DNA scored 2.0 ± 0.8 and 2.3 ± 0.8, the invasion into the templates scored 3.0 ± 0.7 and 3.0 ± 0.9, and the degree of neutrophil degeneration scored 4.2 ± 0.4 and 4.2 ± 0.2 for the SD adjacent templates and the SD template controls, respectively. Together, these data verify that the Cl-amidine eluting templates only exert local effects in the first 24 hours *in vivo* and do not affect the response to adjacent materials through diffusion or local convection.

Discussion

The unregulated release of NETs from the acute neutrophil response may inhibit biomaterial-guided tissue regeneration. Aggregated NETs have been shown to degrade the potent cytokines and chemokines secreted by neutrophils to direct wound healing, impairing the healing response and potential for tissue regeneration [143]. Moreover, NETs are linked to the formation of fibrotic tissue [227]. In particular, the up-regulation of NETosis contributes to the formation of dense, fibrotic tissue in pulmonary fibrosis, fibrosis after myocardial infarction, and atherosclerosis [281-283]. Riehl *et al.* linked NETs to fibrosis through NET-bound, histone-induced activation of platelets resulting in TGF-β secretion and the differentiation and activation of myofibroblasts [227]. Indeed, our initial work evaluating the neutrophil response to electrospun templates indicates that abundant template-preconditioning NETs induce fibrotic tissue formation *in vivo* and impair tissue integration with the biomaterial [31].

We attempted to modulate the degree of NETosis by incorporating Cl-amidine into electrospun templates for local delivery into the template microenvironment. Cl-amidine, which irreversibly inhibits PAD4, has a short half-life *in vivo* of < 15 minutes

and preferentially antagonizes the active form of PAD4 through covalent binding, which together reduces off target effects outside of an inflammatory environment [119, 284]. We are not the first to use Cl-amidine to inhibit NETosis through irreversible inhibition of PAD4-mediated histone H3 citrullination. Kusunoki et al. used intraperitoneal injections of Cl-amidine to reduce NETosis in a mouse model of small-vessel vasculitis [289]. In another study, subcutaneous injections of Cl-amidine were used to attenuate NETs in a model of obesity-associated, low-grade chronic inflammation [290]. However, we are the first, to our knowledge, to incorporate it into a delivery vehicle for local elution into a biomaterial-induced, inflammatory microenvironment.

First, we demonstrated that Cl-amidine can be incorporated into electrospun templates, creating templates with distinct architectures that have been shown to polarize macrophages and previously regulate NETosis [31, 224]. Next, we showed that Cl-amidine eluted from the templates rapidly, which is characteristic of electrospun materials incorporating charge carries (i.e., Cl-amidine) that segregate to the outer surface of the fibers [214]. The burst release is highly desired for this application because the swarming of neutrophils to a site of inflammation occurs in the first 3 hours after injury. After 3 hours, swarming has nearly ceased so that the neutrophils can begin exerting their effector functions [12]. Thus, our delivery vehicle ideally released most of its potent payload in the critical window of neutrophil-template interactions.

With freshly isolated human peripheral blood neutrophils, we evaluated the neutrophil interactions with the electrospun templates *in vitro* for 3 and 6 hours. The LD templates with 0 mg/mL Cl-amidine significantly attenuated NETosis compared to the SD templates, which was quantified with fluorescence microscopy and template-bound

CitH3. As the concentration of Cl-amidine increased in the SD templates, the degree of NETosis was significantly reduced in a dose-dependent manner. Intriguingly, the opposite effect was observed for the LD templates.

By 6 hours *in vitro*, all of the SD and LD templates triggered nearly equivalent degrees of NETosis, regardless of drug content. Those templates that attenuated NETosis at 3 hours were unable to inhibit it at 6 hours, which may be an artifact of *in vitro* culture from decreased neutrophil viability. Interestingly, while the fluorescent quantification reflects the increase in NETs on SD templates with Cl-amidine at 6 hours, the IR detection of template-bound CitH3 did not. Considering the increase in NETosis on LD templates with Cl-amidine, these data suggest that template-induced NETosis may also be occurring independent of PAD4-mediated histone H3 deimination.

Three models of NETosis have been proposed: suicidal NETosis dependent on ROS, vital NETosis independent of ROS, and vital NETosis dependent on ROS [291]. While the mechanisms are not yet fully understood, suicidal NETosis depends on ROS for deimination of histone H3 by PAD4 [119]. This is the model that we speculated is involved in template-preconditioning NETosis. Contrastingly, both forms of vital NETosis can occur independent of histone citrullination [72, 292]. Therefore, our data suggest that they may also be involved in the neutrophil response to PDO templates.

The different types of NETosis are in part regulated by receptor signaling through TLRs, complement receptors, cytokine receptors, and integrins [27, 69, 95, 293]. Because these same receptors interact with soluble proteins adsorbed on the template surface, variation in ligand binding and activation of outside-in signaling likely contributes to the activation of the different mechanisms triggering NETosis. We hypothesize that protein adsorption

and the conformational changes regulate outside-in signaling for template-induced responses. Particularly, we anticipate greater protein adsorption on SD templates (i.e., high SAVR) that is dynamic as described by the Vroman effect, and that exposure of protein domains through conformational changes induced by hydrophobic interactions engage different signaling pathways, topics of further investigation [294]. This type of regulation provides an explanation for the contrasting affects of Cl-amidine based on fiber diameter. The ability of Cl-amidine to inhibit template-induced NETosis may be intimately linked to protein adsorption on the template and the engagement of neutrophil surface receptors, which will be addressed in future studies.

The results of the subcutaneous rat implant model were similar to the *in vitro* evaluation with freshly isolated human neutrophils and indicated dose-dependent trends modulating the early-stage innate immune response. With the addition of Cl-amidine to the SD templates, the degree of NETosis significantly decreased, except for the SD templates with 5 mg/mL Cl-amidine, and the opposite was observed for LD templates. We anticipated that the dose-dependent effects observed *in vitro* would translate to the *in vivo* model. Therefore, this interesting discrepancy for SD templates with 5 mg/mL Cl-amidine between the *in vitro* and *in vivo* data suggests that the physiological complexity of the *in vivo* microenvironment masks the dose-dependent effects of Cl-amidine for the SD templates.

Despite the increase in NETosis, all of the LD templates had significantly greater neutrophil invasion compared to the SD templates after 1 day *in vivo*. Invasion into the templates may be a critical driving force for tissue integration and regeneration. Neutrophils secrete potent pro-angiogenic factors in large quantities, like TIMP-free

MMP-9, to guide and direct the growth of new blood vessels [49]. Without neutrophils, Lin *et al.* found vascularization of their biomaterial abrogated [295]. Regulating NETosis and neutrophil invasion may work in tandem to enhance tissue integration and regeneration.

We previously suggested that the restrictive pores of the SD templates may be increasing NETosis due to the decreased invasion of neutrophils into the templates [31]. However, considering the histological scores for the presence of surface DNA and invasion, the restrictive pore diameters are not a factor that could be increasing NETosis with the LD templates incorporating Cl-amidine. Since neutrophils have been shown to sense size and selectively release NETs, it may be the diameter of the fibers (i.e., micron-sized) that are up-regulating NETosis on the LD templates eluting Cl-amidine [141].

Importantly, the templates modulated acute neutrophil degeneration *in vivo* with all of the SD templates significantly increasing degeneration compared to LD templates. Degeneration was ranked based on the proportion of neutrophils showing degenerative signs, such as loss of lobulated nuclei and fragmentation. Thus, the SD templates promote significant degeneration at 24 hours *in vivo*. Because the scores for the presence of DNA improved with Cl-amidine, these data suggest that the cells interacting with the SD templates may be dying through other forms of cell death in addition to NETosis, like rapid apoptosis or necrosis. Moreover, the degeneration scores for the LD templates eluting Cl-amidine decreased significantly in a dose-dependent manner, despite an increase in the presence of surface DNA. Therefore, a greater portion of the neutrophils that are interacting with the template, invading it, and surviving are able to employ their long-term effector functions like the secretion MMP-9 for biomaterial-guided angiogenesis [296]. Taken together, these data suggest that engineering a Cl-amidine

delivery vehicle with the pore diameters of the LD templates and the fiber diameters of the SD templates may create the ideal microenvironment for regulated NETosis.

While PAD4 is a prominent therapeutic target that can be antagonized with Cl-amidine to regulate NETosis, there are many mechanisms involved in the NETosis response to biomaterials that provide other targets for intervention [251, 297]. Our preliminary evaluation suggests that other pathways may be regulating the release of NETs in the presence of Cl-amidine and that the complexity of the physiological environment should be considered. The deimination of substrates by PAD4 may be linked to TNF-α signaling, suggesting that synergistically targeting cytokine and chemokine production may further modulate NETosis [298]. Another recent study identified that PAD4 inhibition could impact neutrophil cytokine secretion, which may impact neutrophil polarization and the release of innate immune regulators [299]. Future work should examine how fiber and pore diameters regulate NETosis independently, other mechanisms that may be regulating NETosis in the template microenvironment, and how Cl-amidine elution effects neutrophil polarization. Extended *in vivo* studies should also be performed to understand the long-term effects of PAD4 inhibition by Cl-amidine in tissue regeneration. Clearly, local delivery of Cl-amidine modulates neutrophil NETosis *in vitro* and *in vivo* and may have significant implications in biomaterial-guided tissue regeneration and other medical devices that fail through fibrotic encapsulation.

Conclusion

Our preliminary evaluation of Cl-amidine eluting, electrospun PDO templates demonstrates that Cl-amidine can be used to modulate NETosis in response to a biomaterial, thereby regulating acute inflammation and the early innate immune response.

We demonstrated the efficacy of using electrospun templates to deliver Cl-amidine locally as well as its ability to regulate NETosis in a dose-dependent manner *in vitro* with fresh human peripheral blood neutrophils and *in vivo* with a rat subcutaneous implant model. It is evident that the innate immune response is highly complex and much remains to be characterized. However, we have shown the significance of designing immunomodulatory biomaterials that regulate the neutrophil interaction to potentially improve tissue integration and regeneration. Further investigation of the neutrophil response to biomaterials and the therapeutic potential of Cl-amidine is needed and will likely yield significant insight in the field of tissue engineering and regenerative medicine.

CHAPTER 7

ELECTROSPUN POLYDIOXANONE BIOMATERIALS LOADED WITH CHLOROQUINE MODULATE TEMPLATE-INDUCED NET RELEASE AND THE INFLAMMATORY RESPONSE FROM HUMAN NEUTROPHILS

Introduction

Biomaterial-guided *in situ* tissue regeneration utilizes a tissue engineering approach to guide the regeneration of diseased, damaged, or missing tissues [1]. However, compared to exogenous delivery in traditional tissue engineering, *in situ* tissue regeneration relies on the body's endogenous cells and signals to drive the repair and regeneration processes. Electrospun biomaterials have great potential for guiding *in situ* tissue regeneration because their ECM-mimicking fibers can be fabricated from a variety of biocompatible polymers and modified to suit tissue-specific applications [2, 4]. Additionally, fabrication of electrospun biomaterials is relatively simple, cost-effective, and easy to scale up for mass production. As such, electrospun templates are an excellent platform for developing biomaterials that guide *in situ* tissue regeneration with the potential for a far-reaching clinical impact.

Independent of location, the implantation of a biomaterial quickly initiates a tissue repair program to restore homeostasis that is initially characterized by an influx of neutrophils [8, 300]. During the acute inflammatory response, neutrophils condition the microenvironment through multiple mechanisms before recruiting additional immune cells in the tissue repair program. Two of their most significant effector functions include the extrusion of NETs and the secretion of soluble signals [17, 27, 301]. Together, these

mechanisms shape the microenvironment for resolution and healing or further perturbations of homeostasis.

NETs are composed of DNA that is complexed with anti-bacterial neutrophil-derived proteins, including histones, NE, and MPO [27]. They are released in response to bacterial signals for the purpose of killing pathogens and are also released in response to inflammatory mediators, such as IL-8 and TNF-α, activated endothelial cells, and platelets [104, 109, 128, 302]. While they are indispensable for preventing pathogen dissemination, the dysregulated release of NETs is associated with aberrant effects in sterile inflammation due to the localization of noxious cargo that can damage host cells [109, 162, 223, 303]. Of particular interest to tissue engineers is the ability of NETs to initiate thrombosis and fibrosis, both of which can be detrimental to functional tissue regeneration [85, 94, 134, 162, 227, 303]. In fact, our group has previously shown that NETs are released in response to the surface area-dependent, topographical cues of electrospun PDO biomaterials, functioning as a pre-conditioning event in the tissue repair program [31].

Similar to the release of NETs, neutrophil degranulation and the secretion of soluble signals are meant to neutralize pathogens and initiate the tissue repair program, but they can become dysregulated, leading to tissue damage [17, 301]. The combination of neutrophil recruitment and tissue damage is typically attributed to the release of proteinases that breakdown the ECM, such as MMP-9, and the release of pro-inflammatory chemotactic factors, such as IL-8 [304-308]. With continual neutrophil recruitment and degranulation, the acute response can develop into a non-resolving, chronic response through a perpetual cycle of recruitment and activation [306, 308]. Despite these potential deleterious outcomes, neutrophil degranulation and the secretion of

signaling molecules have also been shown to be tissue-restorative and pro-angiogenic [49, 174, 182]. Neutrophils secrete VEGF-A and HGF, both of which support and guide angiogenesis [309, 310]. Moreover, MMP-9 is also pro-angiogenic and has been shown to initiate and guide endothelial cell sprouting [49, 311]. Taken together, these data suggest that regulating neutrophil NET release and their secretion of signaling molecules at the onset of the tissue repair program is pertinent for regulating acute neutrophil-driven inflammation [21, 175, 295, 312].

In this work, we evaluated chloroquine diphosphate as an electrospun biomaterial additive to regulate *in vitro* NET release and the secretion of pro-inflammatory and pro-healing mediators from human neutrophils. Chloroquine is an FDA-approved, anti-malarial drug that has more recently been investigated as an immunomodulatory and anti-thrombotic drug for treating rheumatoid arthritis, systemic lupus erythematosus, and cancer [313-316]. Furthermore, chloroquine has been shown to inhibit NET formation, indicating its potential benefit as an additive for regulating biomaterial-induced NET release and inflammation [126, 127, 317, 318]. Here, we show that electrospun PDO biomaterials loaded with chloroquine modulate template-induced NET release and the inflammatory response from human neutrophils. We found that chloroquine suppresses NET release in a surface area-dependent manner at early time points while modulating pro-inflammatory and healing signals at both early and late time points. Ultimately, our findings demonstrate a novel repurposing of chloroquine as a template additive for *in situ* tissue engineering that modulates the *in vitro* acute inflammatory response to biomaterials.

Materials and Methods

Biomaterial Fabrication

PDO (Cat. No. 6100, Bezwada Biomedical, Hillsborough, NJ, USA) was dissolved overnight in HFP (Cat. No. 003409-1KG, Oakwood Chemical, Estill, SC, USA) at varying concentrations (Table 9) to generate biomaterials composed of small and large fibers, previously shown to regulate NET release through their surface area-dependent, topographical cues [31, 76]. Chloroquine diphosphate (Cat. No. 0219391910, MP Biomedicals, Solon, OH, USA) was added to the solutions at a concentration of 0.07 mg/mL and dissolved for 1.5 hours with gentle agitation before electrospinning. Following, the solutions were loaded into a syringe with a 22.5-gauge blunt needle for the 67 mg/mL PDO solution and an 18-gauge blunt needle for all other solutions and electrospun with optimized parameters (Table 9) [76]. Fibers were collected on a 20 x 750 x 5 mm grounded, stainless steel rectangular mandrel that was rotating 1250 rpm and translating 6.5 cm/s over 13 cm. Additional higher concentrations of chloroquine were incorporated into the electrospun biomaterials during optimization (See Appendix). For all experiments, 8 mm diameter discs of the electrospun biomaterials were cut using a biopsy punch (Cat. No. P825, Acuderm Inc., Fr. Lauderdale, FL, USA) and stored in a desiccator until use. Prior to cell culture, the biomaterials were irradiated with ultraviolet light at a wavelength of 365 nm using an 8 W lamp (Cat. No. EN280L, Spectroline, Westbury, NY, USA) at a working distance of 9.5 cm. The samples were disinfected for 10 minutes on each side in a sterile, laminar flow hood and kept disinfected until cell culture.

Table 9. Electrospun biomaterials were fabricated with optimized parameters.

	Polymer Concentration [mg/mL]	Chloroquine Concentration [mg/mL]	Flow Rate [mL/h]	Airgap Distance [cm]	Applied Voltage [+ kV]
Small Fibers	67	0	0.25	13	14
	70	0.07	0.5	12	13
Large Fibers	138	0	4.0	28	25
	138	0.07	3.2	28	25

Biomaterial Characterization

The biomaterials were imaged with a scanning electron microscope, and SEMs were analyzed in FibraQuant 1.3 software (nanoTemplate Technologies, LLC) to quantify fiber diameter as previously described [76]. Briefly, 150 semi-automated random measurements per SEM were taken to determine the average and corresponding standard deviation for fiber diameter.

Chloroquine Elution from Biomaterials

The elution of chloroquine from the biomaterials was quantified over the first 24 hours using a microplate reader to measure absorbance as described [319]. The biomaterials (n = 4) were placed in a 96-well cell culture plate, and 150 µL of 1x HBSS (calcium, magnesium, and phenol red free, Cat. No. 14175095, Thermo Fisher Scientific, Waltham, MA, USA) were added to each well. After incubating at 37°C for 30 minutes, 1 hour, 3 hours, 6 hours, and 24 hours, the supernatant was removed and refreshed with 150 µL of HBSS. The absorbance of the collected supernatant was read on a SpectraMax i3x Multi-Mode Microplate Reader at 330 nm, and the chloroquine concentration was interpolated from a standard dilution ranging from 333 µg/mL to 0 µg/mL in HBSS (See Appendix

Supplementary Figure 1). In addition to concentration, the average percent release and standard deviation were calculated for each biomaterial.

Isolation and Culture of Primary Human Neutrophils

Heparinized, whole blood from healthy donors was obtained by venipuncture from Tennessee Blood Services. Since purchased or donated samples are not traceable back to the donor, it does not qualify as human subjects research as determined by the University of Memphis Institutional Review Board on November 22, 2016. Neutrophils were then isolated as previously described using Isolymph density separation [31, 76, 259]. After isolation, neutrophils were resuspended in HBSS with 10 mM HEPES and 0.2% autologous serum at a concentration of 1 million neutrophils/mL. The disinfected biomaterials (n = 3) were placed in a 96-well plate, and 40 µL of the cell culture media were added to each well to hydrate the biomaterials. Negative and positive TCP wells (n = 3) received 30 µL of the cell culture media prior to cell seeding. Subsequently, 100 µL of cell culture media containing 100,000 neutrophils were added to each well followed by 10 µL of heparin (Cat. No. H3393, Sigma Aldrich, St. Louis, MO, USA) at a final concentration of 10 U/mL heparin. Heparin was added to dissociate NET-associated MPO as previously described [50, 88]. The negative vehicle and positive controls added to TCP wells were 0.15% DMSO in 10 µL of HBSS and 100 nM PMA (Cat. No. P8139, Sigma Aldrich, St. Louis, MO, USA) in 10 µL of HBSS, respectively. The neutrophils were cultured at 37°C and 5% CO_2 for 3 and 6 hours. Following incubation, the samples were placed on ice for 10 minutes to inhibit neutrophil stimulation prior to processing. Three experiments were performed with unique donors (male, between 18 and 40 years of age), and the results were pooled for analysis.

Quantification of NETs and Secreted Signals

Supernatants were collected and assayed using a ProcartaPlex multiplex immunomagnetic assay (Cat. No. PPX, Thermo Fisher Scientific, Waltham, MA, USA) on a MAGPIX® microplate reader (Luminex Corporation, Austin, TX, USA). The assayed analytes included angiopoietin, fibroblast growth factor 2, GM-CSF, HGF, IL-1β, interleukin 1 receptor antagonist, interleukin 6, IL-8, interleukin 10, interleukin 22, monocyte chemoattractant protein 1, MMP-9, MPO, TNF-α, and VEGF-A. To quantify percent NET release, the concentration of MPO was normalized to the concentration of MPO in the positive control at 6 hours [50, 88].

Fluorescent Microscopy

Samples were fixed with 10% buffered formalin (Cat. No. SF1004, Thermo Fisher Scientific, Waltham, MA, USA) and stained with 5 µM SYTOX orange (Cat. No. S34861, Thermo Fisher Scientific, Waltham, MA, USA) and NucBlue™ Fixed Cell ReadyProbes™ Reagent (DAPI, Cat. No. R37606, Thermo Fisher Scientific, Waltham, MA, USA) as described [88]. Briefly, samples were sequentially incubated with each stain for 5 minutes at room temperature. Three washes with 1x PBS for 5 minutes each were performed between each step. Cells and NETs were visualized on an Olympus BX43 fluorescent microscope.

Statistical Analysis

Statistical significance between fiber diameters was tested with a Kruskal Wallis and Dunn's multiple comparisons test. All other statistical significance was tested with an ANOVA and Holm-Sidak's multiple comparisons test. Statistical analyses were

performed in Prism version 8.4.3 (GraphPad Software, San Diego, CA, USA) at a significance level of 0.05. Data are reported as mean ± standard deviation.

Results

Electrospun PDO Rapidly Elutes Chloroquine

PDO was electrospun to create biomaterials with small fibers and large fibers (Figure 36A). Based on our previous work, the small and large fiber biomaterials in this study represent materials that trigger two distinct neutrophil NET responses and two distinct potentials for tissue regeneration [31, 76]. In order to make comparisons independent of fiber size, the polymer concentration was adjusted for the small and large fiber biomaterials so that the addition of chloroquine did not alter the resulting fibers (Figure 36B). Any differences in the neutrophil inflammatory response can therefore be attributed to chloroquine elution. Both the small and large fiber biomaterials rapidly eluted chloroquine with near 100% elution within the first hour and no detectable increase after 3 hours (Figure 36C). The elution equated to a concentration of 11.8 ± 1.33 μM and 12.2 ± 1.63 μM chloroquine for the small and large fiber biomaterials, respectively (Figure 36D). This elution was optimized by changing chloroquine incorporation during biomaterial fabrication to achieve an eluted concentration near those previously reported in the literature [317, 320]. Additional biomaterials were also fabricated to elute higher concentrations of chloroquine (See Appendix Supplementary Figure 2).

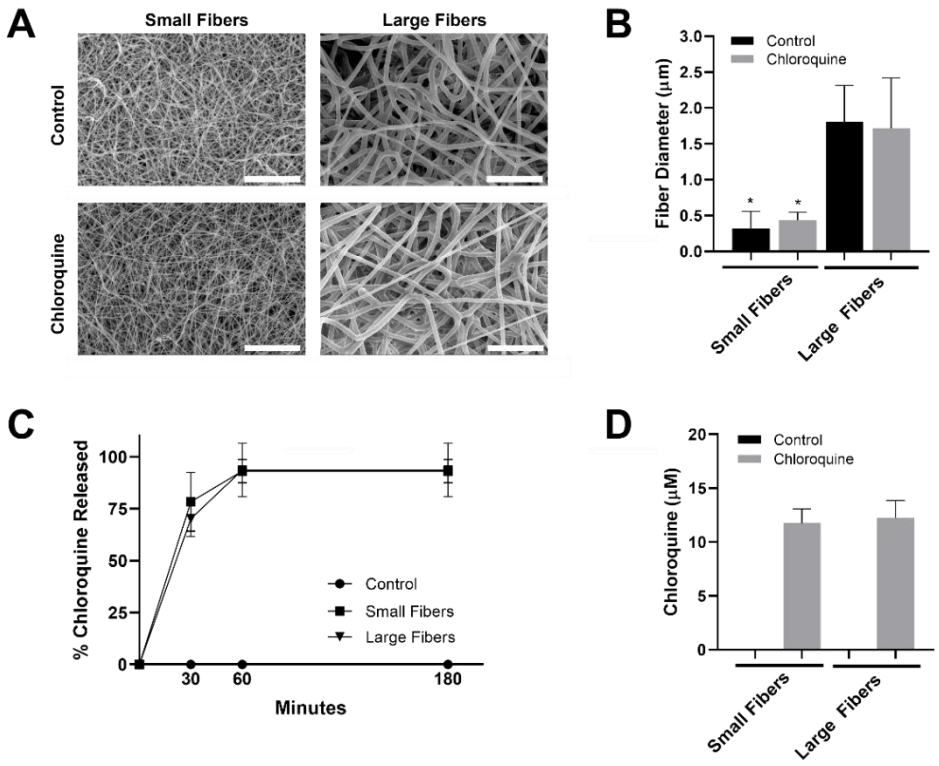

Figure 36. Chloroquine incorporation into electrospun biomaterials results in uniform fibers that rapidly elute the additive. (A) Representative SEMs of the control and chloroquine-loaded biomaterials. Micrographs were acquired at 1000x magnification and scale bars are 30 µm. (B) Fiber diameters of the electrospun biomaterials. Measurements (n = 150) were taken in FibraQuant 1.3 software. (C) Percent chloroquine released from the biomaterials and (D) eluted chloroquine concentration at 3 hours. There was no increase in concentration after 3 hours. See Supplementary Figure 1 for the standard curve used to interpolate concentration (n = 4) from absorbance. Graphs show mean ± standard deviation. * $p < 0.0001$ was determined using a Kruskal Wallis and Dunn's multiple comparisons test.

Chloroquine Elution Inhibits NET Release on Small Fibers

Neutrophils were isolated from the whole blood of healthy donors and seeded on electrospun biomaterials with or without chloroquine to trigger biomaterial-induced NET release. As anticipated, neutrophils had an increased propensity to form NETs on the small fibers compared to the large fibers at 3 hours (Figure 37A). More importantly, the elution of chloroquine from the small fiber biomaterials significantly reduced NET release to the level of the large fibers at 3 hours while having no effect upon elution from

the large fibers (Figure 37B). By 6 hours, the difference between small and large fibers was less pronounced, and increased NET release was observed on both chloroquine-eluting biomaterials, suggesting a temporal, therapeutic window for inhibiting acute NET release (Figure 37B).

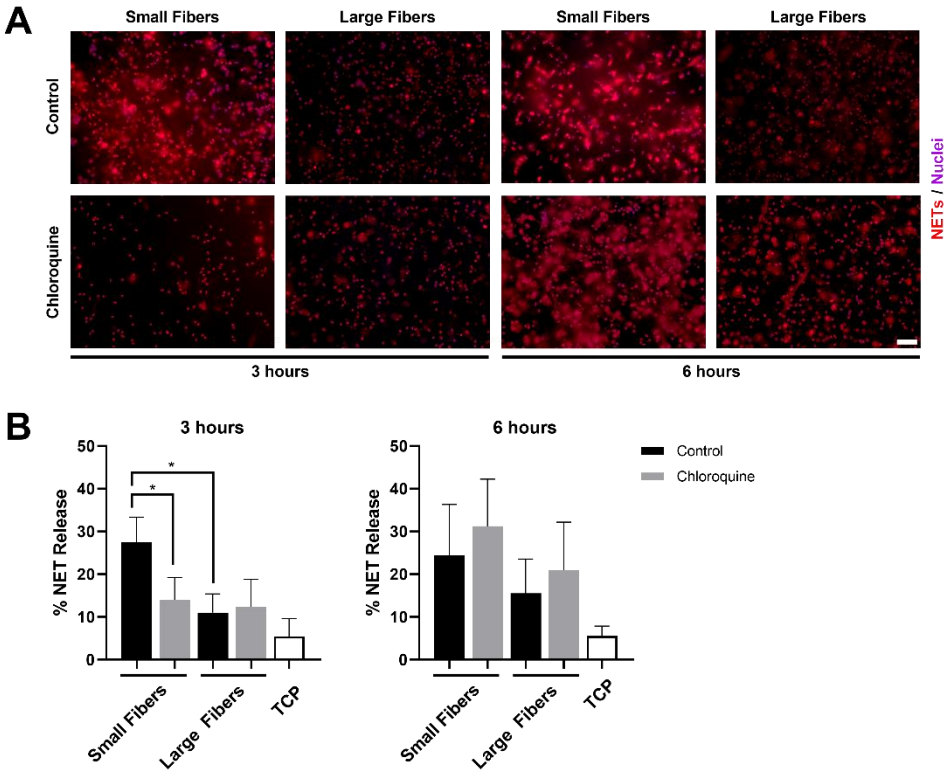

Figure 37. Chloroquine elution inhibits NET release on small fibers but has no effect on large fibers. (A) Fluorescent micrographs of neutrophils on the electrospun biomaterials at 3 and 6 hours after seeding. Staining of NETs (red) and nuclei (purple) reveals that chloroquine elution from the small fibers attenuates NET formation at the early time point, but not at the late time point. Conversely, chloroquine elution from the large fibers does not modulate NET release. Scale bar is 50 μm. (B) Percent NET release at 3 (left) and 6 (right) hours as quantified by the ELISA for NET-disassociated MPO. The quantification of percent NET release (n = 3) indicates that chloroquine elution from the small fibers reduces NET release to the level of the large fibers at 3 hours with no effect at 6 hours. The data represent the mean ± standard deviation of three independent experiments with unique donors. * $p < 0.0001$ was determined using an ANOVA and Holm-Sidak's multiple comparisons test.

Chloroquine Elution Decreases Inflammatory Signal Secretion

Given the documented anti-inflammatory effects, we also evaluated if chloroquine elution would modulate the inflammatory response through the secretion of soluble signals using a multiplexed immunomagnetic assay. Of the assayed inflammatory analytes, only IL-8 and MMP-9 were detected in the supernatant (Figure 38). IL-8 is the archetypal neutrophil chemoattractant secreted by damaged cells as well as neutrophils during an acute inflammatory response. At both 3 and 6 hours, IL-8 secretion was significantly greater on the small fiber biomaterials compared to the large fibers (Figure 38A). Since the small fibers appear to up-regulate NET release in a pro-inflammatory response, it is not surprising that IL-8 secretion mimicked the trends in NET release. However, despite observing a temporal inhibition of acute NET release at 3 hours only, the elution of chloroquine from both small and large fibers continued to significantly suppress IL-8 secretion at 6 hours. These data suggest there is independent regulation of NET release and IL-8 synthesis and secretion in the context of biomaterial-induced activation, which may be important for reducing aberrant neutrophil recruitment during the tissue repair program [321-323]. Similar to IL-8, MMP-9 secretion was significantly greater on the small fiber biomaterials compared to the large fibers with chloroquine elution suppressing secretion at 3 hours (Figure 38B). However, unlike IL-8, MMP-9 secretion was near equivalent on all biomaterials by 6 hours, suggesting a temporal modulation of MMP-9. As a promiscuous endopeptidase, elevated MMP-9 is correlated with tissue degradation and chronic inflammation, so its acute suppression by chloroquine may prevent triggering a continuum of matrix destruction during the initial inflammatory response [304-306].

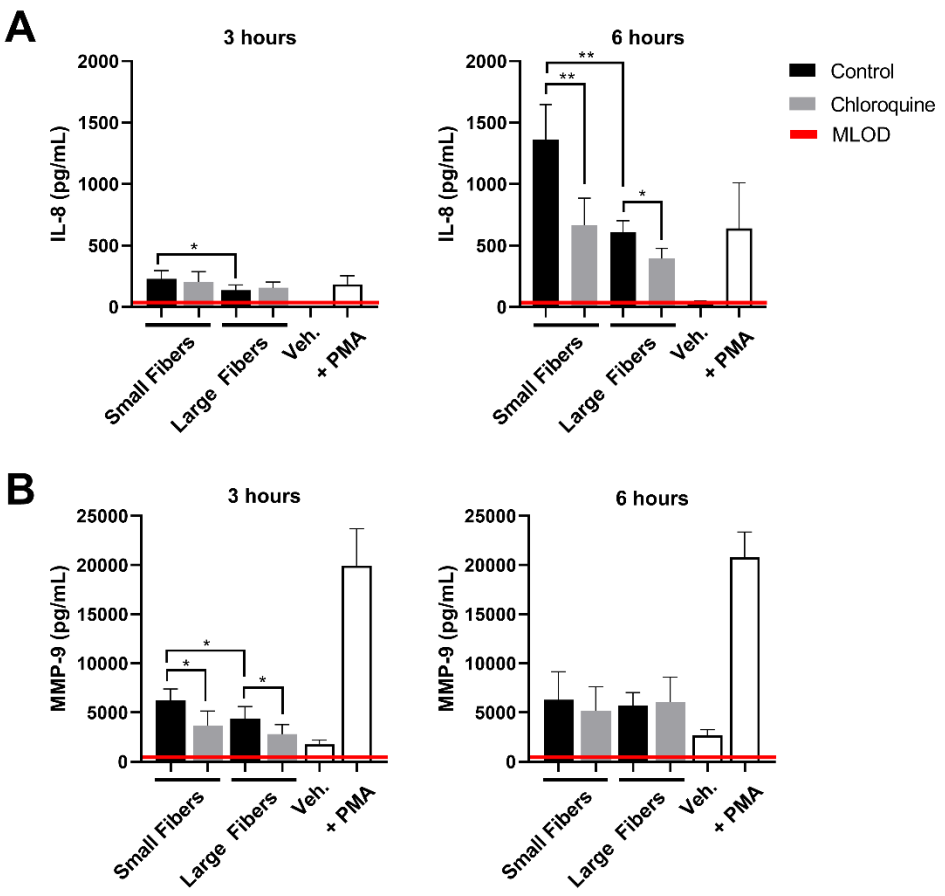

Figure 38. Chloroquine-eluting biomaterials suppress inflammatory IL-8 and MMP-9 secretion from neutrophils. (A) IL-8 and (B) MMP-9 secretion at 3 (left) and 6 (right) hours after neutrophil seeding. Chloroquine elution down-regulated IL-8 secretion at both time points whereas it only attenuates the acute secretion of MMP-9. The data (n = 3) represent the mean ± standard deviation of three independent experiments with unique donors. * $p < 0.05$ and ** $p < 0.0001$ were determined using an ANOVA and Holm-Sidak's multiple comparisons test.

Chloroquine Elution Increases Regenerative Signal Secretion

Although well characterized for its anti-inflammatory effects, chloroquine is not well studied for its potential regenerative effects. Therefore, we also evaluated if chloroquine elution would regulate the secretion of regenerative signals from biomaterial-interacting neutrophils. While several regenerative and anti-inflammatory analytes were assayed, only HGF, VEGF-A, and IL-22 were detected (Figure 39). The secretion of

HGF (Figure 39A) and VEGF-A (Figure 39B) followed very similar trends at 3 hours with both having significantly greater secretion on large fibers compared to small fibers, which is the inverse of NET release. Additionally, the elution of chloroquine from the small fibers increased the secretion of HGF and VEGF-A to the level of the large fibers. By 6 hours, the trends remained the same with an overall increase in the magnitude of secretion. Since they are classic angiogenic signals [181, 309, 310, 324, 325], these data indicate that chloroquine elution may help establish a more regenerative microenvironment around a biomaterial. Likewise, IL-22 secretion followed the same trends as HGF and VEGF-A, but its secretion was not detectable until 6 hours, suggesting an absence of readily available stores [326]. Nonetheless, as a proliferative and pro-angiogenic signal [326, 327], the increased IL-22 secretion observed in response to chloroquine elution from the small fibers further suggests that chloroquine modulates the neutrophil phenotype towards healing and regeneration.

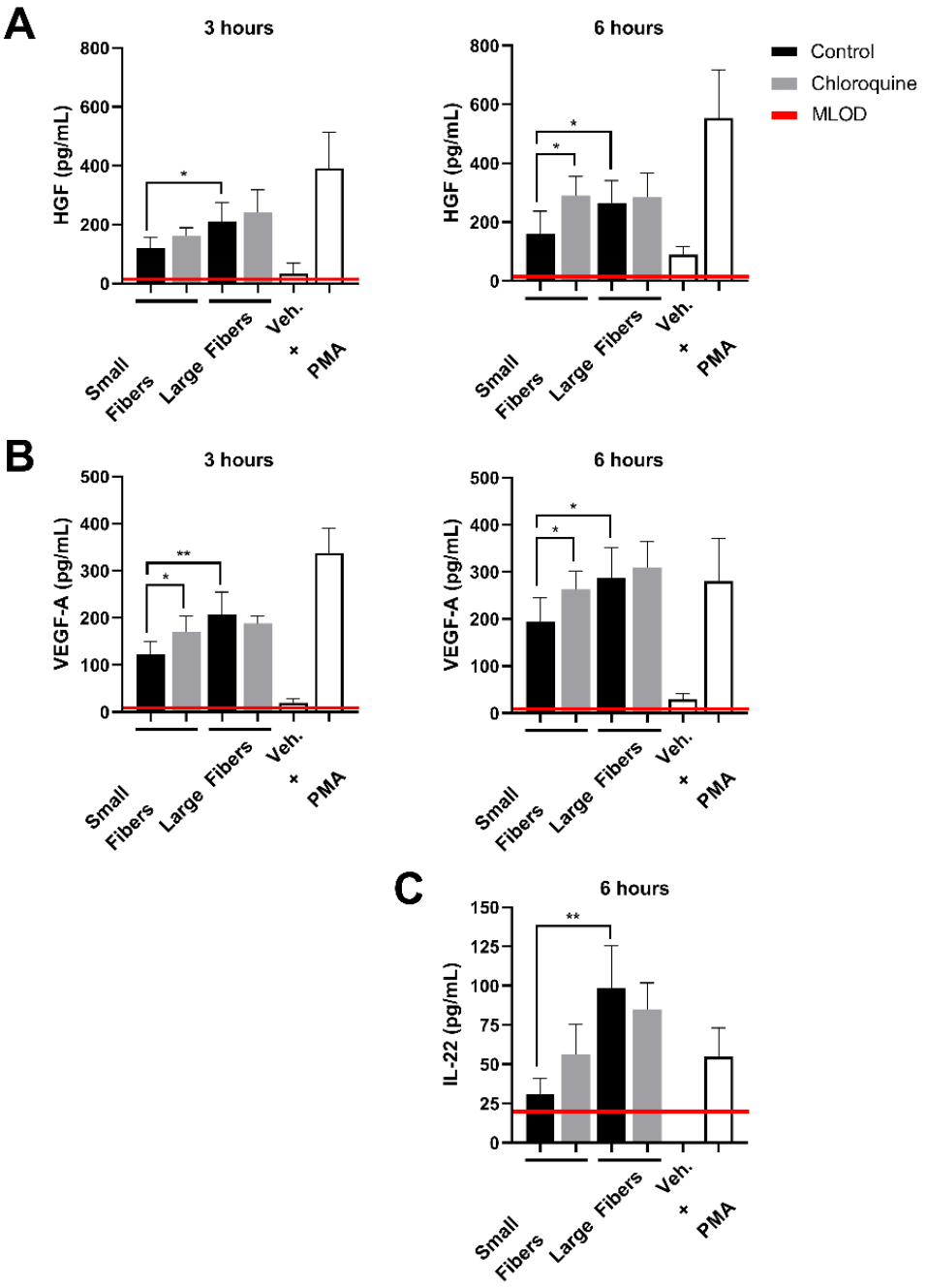

Figure 39. Chloroquine-eluting biomaterials increase regenerative HGF, VEGF-A, and IL-22 secretion from neutrophils. (A) HGF and (B) VEGF-A were up-regulated with chloroquine elution at 3 (left) and 6 (right) hours after seeding whereas (C) IL-22 was only detectable and up-regulated at 6 hours after seeding. The data (n = 3) represent the mean ± standard deviation of three independent experiments with unique donors. * $p < 0.05$ and ** $p < 0.0001$ were determined using an ANOVA and Holm-Sidak's multiple comparisons test.

Discussion

Electrospun biomaterials are excellent candidates for guided *in situ* tissue regeneration applications because they have a biomimetic structure that can also function as a drug delivery system to modulate acute inflammation [2, 5]. In recent years, neutrophils have gained attention as an important part of the acute inflammatory response to a biomaterial and the initiation of the tissue repair program [17, 31, 88, 175]. Neutrophil recruitment, the release of NETs, and the secretion of soluble mediators can have diametrically opposed effects, leading to the resolution of inflammation and healing or chronic inflammation and fibrosis [17]. Indeed, seminal work in neutrophil biology has highlighted the phenotypic plasticity of neutrophils and their ability to regulate the tissue environment [176, 181, 328]. Given the emphasis on endogenous cells for *in situ* tissue regeneration, regulation of the neutrophil response during acute inflammation is of utmost importance for cell integration and regeneration.

In this work, we developed electrospun PDO biomaterials that elute chloroquine to regulate biomaterial-induced neutrophil activation. Chloroquine is an inexpensive drug historically used to treat malaria that has more recently garnered attention for its immunomodulatory and anti-thrombotic effects [313-315, 329]. As a weak base that concentrates in acidic vesicles, it is classified as an inhibitor of lysosomes, lysosomal degradation, and endosomal TLR signaling as well as an inhibitor of autophagy [139, 330, 331]. Recently, several groups have shown that chloroquine can be used to inhibit NET release [126, 127, 317, 318, 320]. Since it is implicated in tissue fibrosis and thrombosis, NET formation is an appealing pharmacological target, especially in the context of biomaterial-induced NET release [100, 162, 303, 332, 333]. Our group has shown that neutrophils have an increased

propensity to form NETs on the surface of small fiber electrospun biomaterials, leading to fibrotic encapsulation, whereas large fiber biomaterials down-regulate NET release and guide tissue integration [31]. Jhunjhunwala *et al.* observed similar outcomes with implanted microcapsules that up-regulated NET release [21], thus indicating the need to engineer biomaterials that attenuate NET formation during the acute inflammatory response.

In these experiments, we incorporated chloroquine into the electrospun biomaterials to modulate NET release. At a dose 99.9% lower than the daily oral dose for malaria prophylaxis [334, 335], we found that chloroquine eluted from small fiber biomaterials down-regulated NET release to the level of the large fiber biomaterials while chloroquine elution from large fibers had no effect on NET release at the early time point. These findings are quite interesting given that both materials eluted the same concentration of drug with near identical release profiles. We observed a similar effect upon incorporating Cl-amidine into the electrospun biomaterials, which inhibits the enzyme PAD4 that is involved in NET formation [63, 76]. In both cases, these data suggest several mechanisms may be governing the release of NETs on electrospun biomaterials. Additionally, by the later time point, increased NET release was observed on both chloroquine-eluting biomaterials, suggesting a temporal, therapeutic window for inhibiting acute NET release. Since the half-life of chloroquine is estimated to be 13 to 55 days, the observed increase in NET formation at 6 hours again suggests that other regulatory mechanisms are involved in biomaterial-induced NET release [329, 334]. Last, biomaterials that eluted higher concentrations of chloroquine (See Appendix Supplementary Figure 2) were developed to determine the therapeutic range of NET

inhibition by chloroquine. Our data (See Appendix Supplementary Figure 3) indicate that increasing the chloroquine concentration did not inhibit biomaterial-induced NET release and may have resulted in cytotoxic effects as previously reported [336].

Although we and others have shown that chloroquine can inhibit NET release, one group has found that a concentration of chloroquine similar to ours did not inhibit NET formation [126, 127, 317, 318, 320]. When chloroquine was shown to be effective at blocking NET release, neutrophils were stimulated with platelet activating factor, LPS, or our electrospun biomaterials [317, 318]. When chloroquine was shown to be ineffective, neutrophils were primed with GM-CSF and stimulated with C5a, which initiates distinctly different, vital NET release, or the release of mitochondrial NETs [72, 320]. These data indicate that the therapeutic efficacy of chloroquine for inhibiting NET formation is stimuli dependent and that there may be some overlap in the signaling pathways for biomaterial-induced NET release and other reported triggers of NET release [86, 89, 254]. Further work is needed to determine the specific signaling pathway involved in biomaterial-induced NET release, but our current data suggests involvement of surface-adsorbed IgG [114].

In addition to inhibiting NETs, chloroquine has been reported to have immunomodulatory effects by altering the secretion of pro-inflammatory mediators. IL-1β, IL-8, MMP-9, and TGF-β have all been shown to decrease with chloroquine treatment to attenuate inflammation [337-340]. Likewise, in this work, we found that IL-8 and MMP-9 secretion were suppressed on the chloroquine-eluting biomaterials. IL-8 secretion is significantly up-regulated in neutrophils several hours after stimulation before returning to baseline levels, after which monocytes become the major source of

IL-8 *in vivo* [322]. Although neutrophils are necessary for tissue healing [176, 178, 295], these data suggest that suppression of IL-8 by chloroquine at both early and later time points may down-regulate acute inflammation by reducing pernicious neutrophil chemotaxis [341]. Similar to IL-8, MMP-9 is robustly secreted from neutrophils during acute inflammation and functions to degrade the ECM for enhanced cell motility [182, 342]. Consequently, MMP-9 can drive both tissue destruction through excessive ECM degradation and the rapid induction of angiogenesis [49, 296, 304, 306, 343, 344]. While angiogenesis is paramount for tissue regeneration, elevated levels of MMP-9 could perpetuate inflammation and cyclic matrix destruction, so its suppression by chloroquine may approximate levels more conducive to regeneration, although this remains to be determined.

In conjunction with pro-inflammatory signals, we also evaluated the potential impact of chloroquine elution on regenerative signals. To our knowledge, no one has yet to explore this aspect of chloroquine's anti-inflammatory effects. We found that both HGF and VEGF-A secretion were increased with chloroquine elution from the biomaterials. HGF is a pro-angiogenic growth factor that promotes regeneration and homeostasis while inhibiting chronic inflammation and fibrosis in various tissues [310, 324, 325, 345]. Similarly, VEGF-A is the canonical angiogenic signal secreted by neutrophils that has also been shown to recruit a pro-angiogenic subset of neutrophils [181, 309, 311, 346]. IL-22 closely followed the trends for HGF and VEGF-A, but was only detectable at the later time point, likely because of the time needed to up-regulate synthesis and secretion [347]. IL-22 has been shown to be both protective and inflammatory depending on the disease and model [326, 348, 349]. However, it was more recently found to support angiogenesis in the tumor microenvironment by inducing endothelial cell proliferation, survival, and

chemotaxis [327]. Together, the increased secretion of HGF, VEGF-A, and IL-22 on chloroquine-eluting biomaterials suggests a previously unrecognized aspect of chloroquine's immunomodulatory effects.

Conclusion

Taken together, our novel incorporation of chloroquine into electrospun biomaterials illustrates the potential therapeutic benefit of this drug for biomaterial-guided, *in situ* tissue regeneration applications. Although we are the first to repurpose it as an electrospun template additive for tissue engineering applications, chloroquine has been incorporated into a coating for urine catheters to reduce sterile inflammation by reducing neutrophil necrosis and IL-8 secretion [350]. Likewise, our data indicate that local delivery through electrospun PDO biomaterials may down regulate acute neutrophil-driven inflammation while simultaneously up-regulating their regenerative phenotype. The mechanisms underlying chloroquine's regulation of NET formation and signal secretion as well as its *in vivo* efficacy are the subject of further investigations. Additional future work includes evaluation of these biomaterials with platelets and platelet-neutrophil interactions to begin elucidating if chloroquine's anti-thrombotic properties are correlated with its inhibition of NET formation [126, 351]. In conclusion, we have shown that our chloroquine-eluting biomaterials regulate acute neutrophil-driven inflammatory responses *in vitro* by down-regulating NET release and inflammatory signals while up-regulating regenerative signals. These responses may have synergistic effects that are advantageous for biomaterial-guided *in situ* tissue regeneration.

CHAPTER 8

CONCLUSION

The goal of biomaterial-guided *in situ* tissue regeneration is to design biomaterials that harness the body's endogenous, regenerative processes to drive functional tissue repair at sites of tissue loss, injury, or disease. Because of their versatility, cost-effectiveness, and relatively simple fabrication, electrospun biomaterials have great potential for the realization of *in situ* tissue regeneration. The key steps that must occur for success are resolution of acute inflammation, rapid cell migration into the biomaterial, integration with the surrounding ECM, robust angiogenesis, and eventually neotissue formation. Therefore, the success of *in situ* tissue regeneration is largely dependent on the efficiency of the first step, resolution of acute neutrophil-driven inflammation.

In this work, we evaluated NET release in response to electrospun biomaterials in an effort to address a significant gap in the literature and elucidate how the release of NETs may be regulated to improve biomaterial-guided *in situ* tissue regeneration. In Chapter 3, we found that NETs are differentially released on electrospun biomaterials based on the polymer composition and electrospun fiber size of the biomaterial with the most dramatic differences in NET release observed on small and large fiber PDO. Moreover, we showed that the increased propensity to release NETs on electrospun PDO with small fibers inhibited tissue integration *in vivo* and nucleated fibrosis, demonstrating for the first time a negative physiological impact of NETs on electrospun biomaterials. In Chapters 4 and 5, we delved into the mechanisms of regulation on electrospun PDO with small and large fibers and demonstrated that the SAVR regulates the adsorption of IgG, which then drives NET release through outside-in signaling via FcγRIIIb. Finally,

Chapters 6 and 7 illustrated that electrospun biomaterial-induced NET release can be inhibited with the incorporation and release of drugs from the biomaterials, improving tissue integration and promoting a regenerative neutrophil phenotype. Taken together, the results of this dissertation suggest that neutrophils and their release of NETs are significant in the preconditioning of an electrospun biomaterial and an increased understanding of the neutrophil response may improve the design of immunomodulatory biomaterials for *in situ* tissue regeneration.

CHAPTER 9

FUTURE WORK

Although it sheds light on the role of neutrophils and NETs in preconditioning biomaterials for *in situ* tissue regeneration, this dissertation raises a number of important questions for future research. One group of questions is related directly to the work in Chapters 3-7, continuing the investigation of NETs on electrospun biomaterials. Another group of questions is tangentially related and inspired by this work, focusing on the neutrophil's actions as a pro-healing cell when it is not releasing NETs. In addition, this work was largely conducted without emphasis on a specific application and discussed in a broad context of *in situ* tissue regeneration. While applicable to many electrospun biomaterial-guided tissue regeneration applications, the findings and implications of this work are especially important for blood-contacting biomaterials such as small diameter vascular grafts. Therefore, this chapter will emphasize vascular tissue engineering. I will describe ideas for future work that will build upon the findings of this dissertation and additionally bring attention to studying the neutrophil as a pro-healing cell capable of driving angiogenesis.

Continuing Research on NETs

Chapter 3

In Chapter 3, we showed that the collagen electrospun biomaterials significantly attenuated NET release compared to the PDO biomaterials, regardless of the electrospun fiber size. Although this was not further investigated in the dissertation, it is an important finding because it suggests that natural polymers attenuate NET release independent of the biomaterial's design features, which could provide more flexibility in design criteria.

Given the assortment of natural polymers, it would be beneficial to study the ability of others to attenuate electrospun-biomaterial induced NET release. However, electrospun biomaterials fabricated from natural polymers do not provide sufficient mechanical properties for vascular tissue engineering, and a synthetic component is needed for increased mechanical integrity. In Chapter 3, we also found that PC biomaterials induced a similar level of NET release compared to the pure PDO biomaterials. Although this suggests the attenuation of NETs is lost in a blend, it may be that increasing the collagen component beyond 10% rescues the effect. Therefore, I propose that investigating various blends of natural polymers with PDO at a variety of ratios could generate important data for regulating NET release on a mechanically sound vascular graft, independent of electrospun fiber size.

Additionally, Chapter 3 also illustrated that abundant NETs promote fibrotic encapsulation of an electrospun biomaterial in a subcutaneous pocket, but the mechanism was not resolved. In order to better understand how NETs are linked to fibrosis on a biomaterial, and additionally thrombosis, co-culture experiments are necessary. Given the importance of macrophage polarization [352], neutrophil and macrophage co-cultures or serial seeding on electrospun biomaterials would be interesting to assess phenotype modulation of both populations. Similarly, platelet-neutrophil crosstalk is significant in the response to small diameter vascular grafts and contributes to thrombosis [48]. Evaluating neutrophils and platelets in a co-culture system would give insight into the first multicellular interactions that occur before macrophages arrive. Later in the tissue repair program, endothelial cells migrate onto vascular grafts to regenerate the intima, so studying the endothelial cell response to NET-conditioned electrospun biomaterials may

increase our understanding of problems associated with impaired neointimal regeneration. Together, such experiments could establish functional links between NETs, fibrosis, and thrombosis in the context of electrospun biomaterials and enhance the design of small diameter vascular grafts.

Chapter 4 and 5

Chapter 4 and 5 began to unravel how the electrospun biomaterials modulate NET release, illustrating that SAVR-dependent adsorption of IgG initiates outside-in signaling for NET release through FcγRIIIb. Because we found that IgG adsorption on PDO is a stimulator for NET formation, several questions can be asked about how to alter this signaling, focusing on IgG. First, it may be possible to pre-coat the biomaterials with a desired protein to inhibit or delay IgG adsorption long enough to avoid the induction of NETs. Determining what a desirable protein is that has an affinity for the biomaterial surface would require multiple preliminary experiments to ensure (1) the protein does not also trigger NETs and (2) the protein is not readily replaced by IgG during competitive adsorption/desorption [242, 294]. Second, it may be possible to alter the biomaterial's surface chemistry to regulate the adsorption of IgG. This could be accomplished with acid or plasma treatments through fairly straightforward procedures [215, 353]. Third, it is possible that incorporating a natural polymer, as previously discussed, alters protein adsorption in a favorable manner to reduce NET release. Such experiments would improve our understanding of protein adsorption on electrospun PDO and how it regulates NET formation.

In addition, a focus on FcγRIIIb and its signaling pathway could be beneficial for regulating electrospun biomaterial-induced NET release. This would first require a

thorough investigation of the full signaling pathway from the receptor to the release of the NET. Then, relevant pharmacological inhibitors could be incorporated into the biomaterial for local delivery to modulate NET release. Likewise, signal transmission can be blocked at the level of the receptor with neutralizing antibodies. Incorporation of neutralizing antibodies to FcγRIIIb may be costly and would require optimization to ensure they retain their biological activity after electrospinning, which is also necessary for drug incorporation. Together, a more detailed understanding of how biomaterial design regulates and modulates NET release would improve the design of vascular biomaterials that avoid the adverse effects of NETs.

Chapter 6 and 7

In Chapter 6 and 7, we found that local delivery of two drugs with different functionalities, Cl-amidine and chloroquine, were able to reduce biomaterial-induced NET release. For both drugs, neither was able to completely abrogate NET formation. Therefore, it would be interesting to continue exploring the incorporation of inhibitors, and potential combinations of inhibitors, into electrospun biomaterials to see if a more efficacious inhibitor or combination exists. Those with anti-inflammatory and anti-thrombotic properties would be most beneficial for small diameter vascular grafts. A combination would likely provide the greatest benefits since multiple stimuli and signaling pathways exist for triggering NET release [136], and our data indicate surface adsorbed IgG does not appear to be the sole regulator on electrospun PDO. Moreover, one extremely important unanswered question is the level of NETs needed for functional tissue regeneration. It is possible that complete inhibition of NETs does more harm than good, similar to the need for a ratio of M1 and M2 macrophages [354]. Therefore,

experiments assessing the dose-response impact of NETs on tissue regeneration would help determine the desired level of regulation. These proposed experiments would improve our understanding of regulatory mechanisms.

All Chapters

The experiments described in this dissertation were largely conducted *in vitro* with primary human neutrophils, and several of the findings were extended to acute subcutaneous implant models in rats to validate their physiological significance. While important for this work, it is necessary to build on it with longer *in vivo* models to assess the long-term impact of NET regulation on *in situ* tissue regeneration over multiple weeks while the biomaterial is resorbed. Moreover, after characterization as a subcutaneous implant, it is important to progress towards tissue specific models and work in a small diameter vascular graft format. Related to this, the rat is a good animal model for assessing the acute neutrophil inflammatory response in a subcutaneous implant, but the rat is not appropriate for small diameter vascular grafts because it cannot accommodate diameters and lengths on the human scale for peripheral limb applications, such as femoral-tibial and femoropopliteal bypasses. For these studies, a larger animal model should be carefully selected for the appropriate sizing with blood composition in mind. In particular, it is highly important that the animal's blood composition is similar to humans because this dictates protein adsorption, the proportion of acutely interacting cells, and thus the tissue repair program. Finally, it would be interesting to collect clinical samples of failed small diameter vascular grafts and look for the presence of NETs to strengthen our data with clinical evidence, as others have done in NET-related

pathologies [126, 355]. Together, such experiments would greatly expound upon this dissertation.

Studying Neutrophils as Pro-Healing Cells

After focusing extensively on the neutrophil's effects while dying and releasing a NET, it was only logical to begin postulating what the neutrophil is doing when it is living and not releasing a NET in the context of biomaterial-guided *in situ* tissue regeneration. Recently, several benchmark publications in tumor biology recently indicated that neutrophils are responsible for driving tumor-associated angiogenesis through their secretion of MMP-9. First, Ardi *et al*. identified that MMP-9 is uniquely released from neutrophils TIMP-free, resulting in rapid activation *in vitro* and *in vivo* to induce angiogenesis [49, 296]. Subsequently, Deryugina *et al*. highlighted the role of neutrophils in tumor-induced angiogenesis by showing that TANs secrete 40- to 50-fold more MMP-9 within 2 hours compared to macrophages cultured over 48 hours and also found that neutrophil-derived MMP-9 was needed for pericyte recruitment and vascular stability [182]. It is believed that neutrophil-derived MMP-9 is an extremely potent inducer of angiogenesis because it is released TIMP-free and because it has diverse enzymatic activity [356], degrading the ECM and freeing cells for migration and proliferation. Ultimately, these paradigm-shifting data in tumor biology provide inspiration to explore the role of neutrophils and their pro-angiogenic delivery of MMP-9 in *in situ* biomaterial-guided tissue regeneration.

In fact, neutrophils are involved in physiological angiogenesis and tissue growth and development in multiple tissues and organs [357]. During endometrial development, neutrophils are the most abundant during the early growth of the decidua, decrease during

menstruation, and are not present during tissue stability [358]. In a model of hindlimb ischemia, wildtype mice treated with GM-CSF facilitate revascularization and tissue regeneration through enhanced recruitment of neutrophils compared to untreated controls [359]. These examples demonstrate that there are endogenous mechanisms to induce neovascularization and overcome the ischemic load in developing tissue, driven by the neutrophil.

Several levels of regulation could be targeted to engage neutrophils and their MMP-9 in biomaterial-guided tissue regeneration (Figure 40). The secretion of MMP-9 could be controlled at the intracellular level through MMP-9 synthesis and degranulation, at the extracellular level through the inhibition or activation of MMP-9 in the ECM, and at the level of cell recruitment. Each level could be targeted by engineering the properties of the biomaterial to elicit the appropriate immunomodulatory response. No matter the level of regulation, the overriding effect of the biomaterial should be to engage the neutrophils as drivers of functional tissue regeneration.

The first level of regulation is the intracellular level where MMP-9 could be controlled at the level of synthesis and degranulation (Figure 40A). MMP-9 synthesis is regulated at the level of transcription primarily by ERK1/2 in the mitogen-activated protein kinase pathway [360, 361]. Activation of the pathway induces MMP-9 gene expression and could be used as a therapeutic target to regulate MMP-9 secretion. In addition, integrin and TLR interactions can induce neutrophil degranulation and provide a second intracellular point of intervention. Mature neutrophils circulate with proMMP-9 packaged into secretory vesicles for rapid release [362]. Thus, engaging integrins (e.g. L-selectin and Mac-1) and TLRs (e.g. TLR2 and TLR4) could be used to regulate MMP-9

secretion [363-365]. Various cytokines and chemokines binding to their receptors can also modulate neutrophil degranulation and further participate in autocrine and paracrine neutrophil

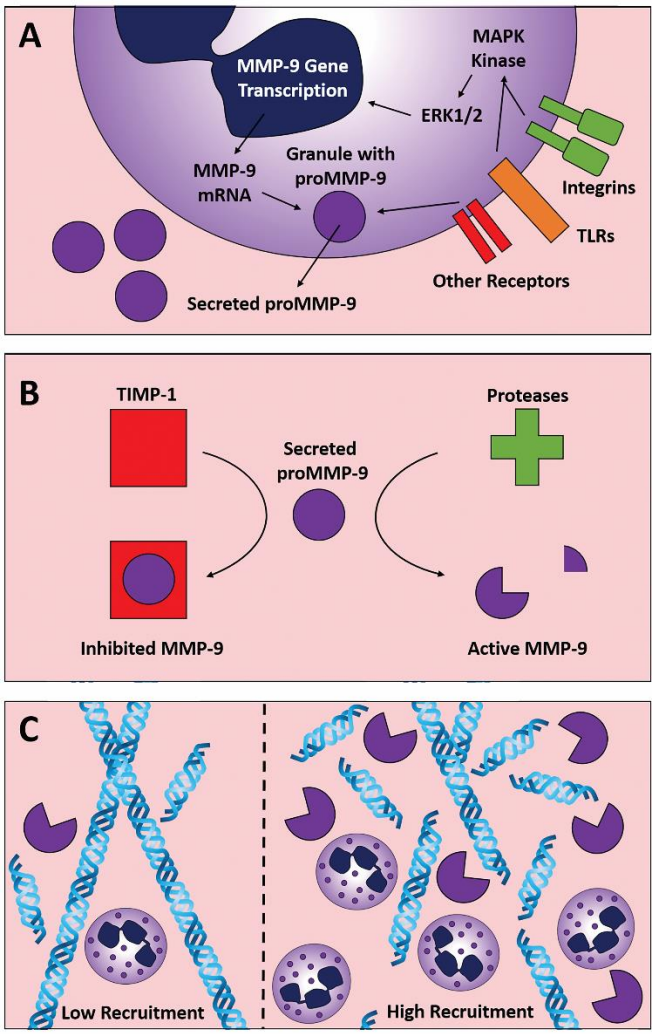

Figure 40. Potential levels of regulation to engage neutrophil MMP9 in matrix reprogramming. (A) Cellular targets include intracellular signaling pathways and ligation of integrins, TLRs, and other receptors. (B) Regulation could also include the availability of activators and inhibitors. (C) Finally, the secretion of MMP9 could be regulated at the level of neutrophil recruitment to enhance ECM degradation and sprouting angiogenesis.

feedback loops. As an example, neutralizing TNF-α suppresses MMP-9 secretion in a model of central nervous system tuberculosis [360]. These data all suggest that MMP-9

secretion could be regulated at the intracellular level, through transcription or outside-in signaling, to increase the potential for biomaterial-guided angiogenesis.

Another level of MMP-9 regulation that could be targeted through biomaterial design involves the activation or inhibition of MMP-9 after secretion into the microenvironment (Figure 40B). MMP-9 is initially secreted as a zymogen that requires activation [296]. The availability of activators therefore affects the enzymatic potential of MMP-9. Multiple proteases are known to active proMMP-9, including cathepsin K, MMP-2, MMP-3, and plasmin, which explains the rapid activation upon secretion [296, 366-368]. In addition, MMP-9 can be inhibited by TIMP before or after activation. Even without neutrophils producing it, TIMP could be present in the microenvironment as it is constitutively expressed in many tissues [369]. Thus, devising a strategy to ensure efficient MMP-9 activation in the local microenvironment while minimizing or delaying inhibition may increase the potential for angiogenesis and regeneration.

The last regulatory level that could be targeted to engage neutrophils in biomaterial-guided tissue regeneration is neutrophil recruitment (Figure 40C). The knockout of neutrophils is known to impair angiogenesis and tissue regeneration [178, 295, 359]. Therefore, their recruitment to sites of inflammation is essential to wound healing, partly due to their delivery of growth factors and chemokines that promote the resolution of inflammation. Increasing the recruitment of a pro-angiogenic subset of neutrophils through VEGF-A secretion may be particularly beneficial for biomaterial-guided angiogenesis [311, 370]. Nonetheless, regulating angiogenesis at the level of recruitment may present additional challenges as the sustained recruitment of neutrophils and degradation of the ECM play a central role in chronic inflammation and poor wound healing [304, 306,

[343]. Due to multiple levels of regulation, several points of intervention exist for engineers to regulate neutrophil MMP-9 secretion to initiate angiogenesis and tissue regeneration.

Conclusion

In situ tissue regeneration has the potential to revolutionize the field of tissue engineering through the design of immunomodulatory biomaterials that harness the pro-angiogenic potential of neutrophils to repair and regenerate. These studies lead to the idea that the key for successful tissue regeneration lies in the swift resolution of neutrophil-driven inflammation and progression in the tissue repair program. Because the importance of neutrophils in tissue repair has only been recognized in recent years, there are many unanswered questions for the development of immunomodulatory biomaterials that regulate the neutrophil response, release of NETs, and resolution of inflammation for functional tissue regeneration. The current literature suggests the readily available neutrophils are of critical importance to wound healing beyond the release of NETs. Given that biomaterials are immediately bombarded by the body's highly orchestrated innate immune response upon implantation, we should utilize what physiology has provided as endogenous drivers of angiogenesis. Studying the abundant, circulating neutrophils and the use of the body as the ideal bioreactor to vigorously drive *in situ* biomaterial-guided tissue regeneration will generate a new knowledge base to propel the field of tissue engineering into the next generation of biomaterials.

REFERENCES

1. Li, Q, Ma, L, and Gao, C. Biomaterials for in situ tissue regeneration: Development and perspectives. J Mater Chem 2015;3:8921-8938.

2. Kelleher, CM, and Vacanti, JP. Engineering extracellular matrix through nanotechnology. J R Soc Interface 2010;7:S717-S729.

3. Ramakrishna, S, Fujihara, K, Teo, WE, Lim, TC, and Ma, Z. Introduction to electrospinning and nanofibers: World Scientific Publishing Company, Incorporated; 2005.

4. Lannutti, J, Reneker, D, Ma, T, Tomasko, D, and Farson, D. Electrospinning for tissue engineering scaffolds. J Mater Chem 2007;27:504-509.

5. Minden-Birkenmaier, B, Selders, G, Fetz, A, Gehrmann, C, and Bowlin, G. Electrospun systems for drug delivery. Electrospun materials for tissue engineering and biomedical applications: Elsevier; 2017. pp. 117-145.

6. Mescher, AL, and Neff, AW. Regenerative capacity and the developing immune system. Regenerative medicine i: Springer; 2005. pp. 39-66.

7. Karin, M, and Clevers, H. Reparative inflammation takes charge of tissue regeneration. Nature 2016;529:307.

8. Anderson, JM, Rodriguez, A, and Chang, DT. Foreign body reaction to biomaterials. Semin Immunol 2008;20:86-100.

9. Pittman, K, and Kubes, P. Damage-associated molecular patterns control neutrophil recruitment. J Innate Immun 2013;5:315-323.

10. Russo, RC, Garcia, CC, Teixeira, MM, and Amaral, FA. The CXCL8/IL-8 chemokine family and its receptors in inflammatory diseases. Expert Rev Clin Immunol 2014;10:593-619.

11. Afonso, PV, Janka-Junttila, M, Lee, YJ, et al. LTB4 is a signal-relay molecule during neutrophil chemotaxis. Dev Cell 2012;22:1079-1091.

12. Lämmermann, T, Afonso, PV, Angermann, BR, et al. Neutrophil swarms require LTB4 and integrins at sites of cell death in vivo. Nature 2013;498:371-375.

13. Hoover, RL, Karnovsky, MJ, Austen, KF, Corey, E, and Lewis, RA. Leukotriene B4 action on endothelium mediates augmented neutrophil/endothelial adhesion. PNAS 1984;81:2191-2193.

14. Hynes, RO. The extracellular matrix: Not just pretty fibrils. Science 2009;326:1216-1219.

15. Horbett, T. The role of adsorbed proteins in tissue response to biomaterials. Biomater Sci 2004;2:237-246.

16. Tang, L, Thevenot, P, and Hu, W. Surface chemistry influences implant biocompatibility. Curr Top Med Chem 2008;8:270-280.

17. Selders, GS, Fetz, AE, Radic, MZ, and Bowlin, GL. An overview of the role of neutrophils in innate immunity, inflammation and host-biomaterial integration. Regen Biomat 2017;4:55-68.

18. Theilgaard-Mönch, K, Knudsen, S, Follin, P, and Borregaard, N. The transcriptional activation program of human neutrophils in skin lesions supports their important role in wound healing. J Immunol 2004;172:7684-7693.

19. Taneja, R, Parodo, J, Jia, SH, et al. Delayed neutrophil apoptosis in sepsis is associated with maintenance of mitochondrial transmembrane potential and reduced caspase-9 activity. Crit Care Med 2004;32:1460-1469.

20. Chitnis, D, Dickerson, C, Munster, AM, and Winchurch, RA. Inhibition of apoptosis in polymorphonuclear neutrophils from burn patients. J Leuko Biol 1996;59:835-839.

21. Jhunjhunwala, S, Aresta-DaSilva, S, Tang, K, et al. Neutrophil responses to sterile implant materials. PLoS One 2015;10:e0137550.

22. Scannell, M, Flanagan, MB, destefani, A, et al. Annexin-1 and peptide derivatives are released by apoptotic cells and stimulate phagocytosis of apoptotic neutrophils by macrophages. J Immunol 2007;178:4595-4605.

23. de Oliveira, S, Rosowski, EE, and Huttenlocher, A. Neutrophil migration in infection and wound repair: Going forward in reverse. Nature Rev Immunol 2016;16:378-391.

24. Jun, JI, Kim, KH, and Lau, L. The matricellular protein CCN1 mediates neutrophil efferocytosis in cutaneous wound healing. Nature Comm 2015;6:1-14.

25. Greenlee-Wacker, MC. Clearance of apoptotic neutrophils and resolution of inflammation. J Immunol Rev 2016;273:357-370.

26. Anderson, JM. Biological responses to materials. Annu Rev Mater Res 2001;31:81-110.

27. Brinkmann, V, Reichard, U, Goosmann, C, et al. Neutrophil extracellular traps kill bacteria. Science 2004;303:1532-1535.

28. Huang, H, Tohme, S, Al-Khafaji, AB, et al. Damage-associated molecular pattern–activated neutrophil extracellular trap exacerbates sterile inflammatory liver injury. Hepatology 2015;62:600-614.

29. Stakos, DA, Kambas, K, Konstantinidis, T, et al. Expression of functional tissue factor by neutrophil extracellular traps in culprit artery of acute myocardial infarction. Eur Heart J 2015;36:1405-1414.

30. Elliott, MJ, De Coppi, P, Speggiorin, S, et al. Stem-cell-based, tissue engineered tracheal replacement in a child: A 2-year follow-up study. Lancet 2012;380:994-1000.

31. Fetz, AE, Neeli, I, Rodriguez, IA, Radic, MZ, and Bowlin, GL. Electrospun template architecture and composition regulate neutrophil NETosis in vitro and in vivo. Tissue Engin Part A 2017;19:1054-1063.

32. Urban, CF, Ermert, D, Schmid, M, et al. Neutrophil extracellular traps contain calprotectin, a cytosolic protein complex involved in host defense against candida albicans. PLoS Pathog 2009;5:e1000639.

33. Bruschi, M, Petretto, A, Santucci, L, et al. Neutrophil extracellular traps protein composition is specific for patients with lupus nephritis and includes methyl-oxidized αenolase (methionine sulfoxide 93). Sci Rep 2019;9:1-13.

34. Khandpur, R, Carmona-Rivera, C, Vivekanandan-Giri, A, et al. NETs are a source of citrullinated autoantigens and stimulate inflammatory responses in rheumatoid arthritis. Sci Transl Med 2013;5:178ra140-178ra140.

35. Chatfield, SM, Grebe, K, Whitehead, LW, et al. Monosodium urate crystals generate nuclease-resistant neutrophil extracellular traps via a distinct molecular pathway. J Immunol 2018;200:1802-1816.

36. Chapman, EA, Lyon, M, Simpson, D, et al. Caught in a trap? Proteomic analysis of neutrophil extracellular traps in rheumatoid arthritis and systemic lupus erythematosus. Front Immunol 2019;10:423.

37. Yu, Y, Kwon, K, Tsitrin, T, et al. Characterization of early-phase neutrophil extracellular traps in urinary tract infections. PLoS pathogens 2017;13:e1006151.

38. O'Donoghue, AJ, Jin, Y, Knudsen, GM, et al. Global substrate profiling of proteases in human neutrophil extracellular traps reveals consensus motif predominantly contributed by elastase. PLoS One 2013;8:e75141.

39. Ahrens, S, Zelenay, S, Sancho, D, et al. F-actin is an evolutionarily conserved damage-associated molecular pattern recognized by DNGR-1, a receptor for dead cells. Immunity 2012;36:635-645.

40. Lazarides, E, and Lindberg, U. Actin is the naturally occurring inhibitor of deoxyribonuclease I. PNAS 1974;71:4742-4746.

41. Dinsdale, R, Hazeldine, J, Al Tarrah, K, et al. Dysregulation of the actin scavenging system and inhibition of dnase activity following severe thermal injury. Br J Surg 2019;107:391-401.

42. Bang, H, Egerer, K, Gauliard, A, et al. Mutation and citrullination modifies vimentin to a novel autoantigen for rheumatoid arthritis. Arthritis Rheum 2007;56:2503-2511.

43. Podor, TJ, Singh, D, Chindemi, P, et al. Vimentin exposed on activated platelets and platelet microparticles localizes vitronectin and plasminogen activator inhibitor complexes on their surface. J Biol Chem 2002;277:7529-7539.

44. Colburn, ZT, and Jones, JC. Complexes of α6β4 integrin and vimentin act as signaling hubs to regulate epithelial cell migration. J Cell Sci 2018;131:jcs214593.

45. Vogl, T, Tenbrock, K, Ludwig, S, et al. Mrp8 and mrp14 are endogenous activators of toll-like receptor 4, promoting lethal, endotoxin-induced shock. Nat Med 2007;13:1042-1049.

46. Ryckman, C, Vandal, K, Rouleau, P, Talbot, M, and Tessier, PA. Proinflammatory activities of S100: Proteins S100A8, S100A9, and S100A8/A9 induce neutrophil chemotaxis and adhesion. J Immunol 2003;170:3233-3242.

47. Wilson, TJ, Nannuru, KC, and Singh, RK. Cathepsin G–mediated activation of pro–matrix metalloproteinase 9 at the tumor-bone interface promotes transforming growth factor-β signaling and bone destruction. Mol Cancer Res 2009;7:1224-1233.

48. Elaskalani, O, Razak, NBA, and Metharom, P. Neutrophil extracellular traps induce aggregation of washed human platelets independently of extracellular DNA and histones. Cell Comm Signal 2018;16:1-15.

49. Ardi, VC, Kupriyanova, TA, Deryugina, EI, and Quigley, JP. Human neutrophils uniquely release TIMP-free MMP-9 to provide a potent catalytic stimulator of angiogenesis. PNSA 2007;104:20262-20267.

50. Parker, H, Albrett, AM, Kettle, AJ, and Winterbourn, CC. Myeloperoxidase associated with neutrophil extracellular traps is active and mediates bacterial killing in the presence of hydrogen peroxide. J Leuko Biol 2012;91:369-376.

51. Cruz, DBd, Helms, J, Aquino, LR, et al. DNA-bound elastase of neutrophil extracellular traps degrades plasminogen, reduces plasmin formation, and decreases fibrinolysis: Proof of concept in septic shock plasma. FASEB 2019;33:14270-14280.

52. Chua, F, and Laurent, GJ. Neutrophil elastase: Mediator of extracellular matrix destruction and accumulation. Proc Am Thorac Soc 2006;3:424-427.

53. Ferry, G, Lonchampt, M, Pennel, L, et al. Activation of MMP-9 by neutrophil elastase in an in vivo model of acute lung injury. FEBS Lett 1997;402:111-115.

54. Tschesche, H, Zölzer, V, Triebel, S, and Bartsch, S. The human neutrophil lipocalin supports the allosteric activation of matrix metalloproteinases. Eur J Biochem 2001;268:1918-1928.

55. Allam, R, Kumar, SV, Darisipudi, MN, and Anders, HJ. Extracellular histones in tissue injury and inflammation. J Mol Med 2014;92:465-472.

56. Frangou, E, Chrysanthopoulou, A, Mitsios, A, et al. Redd1/autophagy pathway promotes thromboinflammation and fibrosis in human systemic lupus erythematosus (SLE) through NETs decorated with tissue factor (TF) and interleukin-17a (IL-17a). Ann Rheum Dis 2019;78:238-248.

57. Kambas, K, Chrysanthopoulou, A, Vassilopoulos, D, et al. Tissue factor expression in neutrophil extracellular traps and neutrophil derived microparticles in antineutrophil cytoplasmic antibody associated vasculitis may promote thromboinflammation and the thrombophilic state associated with the disease. Ann Rheum Dis 2014;73:1854-1863.

58. Janciauskiene, S, Tumpara, S, Wiese, M, et al. Alpha1-antitrypsin binds hemin and prevents oxidative activation of human neutrophils: Putative pathophysiological significance. J Leuko Biol 2017;102:1127-1141.

59. Mor-Vaknin, N, Punturieri, A, Sitwala, K, and Markovitz, DM. Vimentin is secreted by activated macrophages. Nat Cell Biol 2003;5:59-63.

60. Donato, R, R cannon, B, Sorci, G, et al. Functions of S100 proteins. Curr Mol Med 2013;13:24-57.

61. Schiopu, A, and Cotoi, OS. S100A8 and A100A9: DAMPs at the crossroads between innate immunity, traditional risk factors, and cardiovascular disease. Mediators Inflamm 2013;2013:828354.

62. Wu, Y, Li, Y, Zhang, C, et al. S100A8/A9 released by CD11b+ GR1+ neutrophils activates cardiac fibroblasts to initiate angiotensin II–induced cardiac inflammation and injury. Hypertension 2014;63:1241-1250.

63. Leshner, M, Wang, S, Lewis, C, et al. PAD4 mediated histone hypercitrullination induces heterochromatin decondensation and chromatin unfolding to form neutrophil extracellular trap-like structures. Front Immunol 2012;3:307.

64. Dwivedi, N, Upadhyay, J, Neeli, I, et al. Felty's syndrome autoantibodies bind to deiminated histones and neutrophil extracellular chromatin traps. Arthritis Rheum 2012;64:982-992.

65. Nicholls, SJ, and Hazen, SL. Myeloperoxidase and cardiovascular disease. Arterioscler Throm Vasc Biol 2005;25:1102-1111.

66. Yan, L, Borregaard, N, Kjeldsen, L, and Moses, MA. The high molecular weight urinary matrix metalloproteinase (MMP) activity is a complex of gelatinase b/MMP-9 and neutrophil gelatinase-associated lipocalin (NGAL) modulation of MMP-9 activity by NGAL. J Biol Chem 2001;276:37258-37265.

67. Saffarzadeh, M, Cabrera-Fuentes, HA, Veit, F, et al. Characterization of rapid neutrophil extracellular trap formation and its cooperation with phagocytosis in human neutrophils. Discoveries 2014;2:e19.

68. Gorgulho, CM, Romagnoli, GG, Bharthi, R, and Lotze, MT. Johnny on the spot-chronic inflammation is driven by HMGB1. Front Immunol 2019;10:1561.

69. Garcia-Romo, GS, Caielli, S, Vega, B, et al. NETting neutrophils are major inducers of type I IFN production in pediatric systemic lupus erythematosus. Sci Transl Med 2011;3:73ra20-73ra20.

70. Mitroulis, I, Kambas, K, Chrysanthopoulou, A, et al. Neutrophil extracellular trap formation is associated with IL-1β and autophagy-related signaling in gout. PLoS One 2011;6:e29318.

71. Kambas, K, Mitroulis, I, Apostolidou, E, et al. Autophagy mediates the delivery of thrombogenic tissue factor to neutrophil extracellular traps in human sepsis. PLoS One 2012;7:e45427.

72. Yousefi, S, Mihalache, C, Kozlowski, E, Schmid, I, and Simon, HU. Viable neutrophils release mitochondrial DNA to form neutrophil extracellular traps. Cell Death Differ 2009;16:1438-1444.

73. McIlroy, DJ, Jarnicki, AG, Au, GG, et al. Mitochondrial DNA neutrophil extracellular traps are formed after trauma and subsequent surgery. J Crit Care 2014;29: e1131-1133.

74. Yousefi, S, Gold, JA, Andina, N, et al. Catapult-like release of mitochondrial DNA by eosinophils contributes to antibacterial defense. Nat Med 2008;14:949-953.

75. Boeltz, S, Amini, P, Anders, HJ, et al. To NET or not to NET: Current opinions and state of the science regarding the formation of neutrophil extracellular traps. Cell Death and Differentiation 2019;1.

76. Fetz, AE, Neeli, I, Buddington, KK, et al. Localized delivery of cl-amidine from electrospun polydioxanone templates to regulate acute neutrophil NETosis: A preliminary evaluation of the PAD4 inhibitor for tissue engineering. Front Pharmacol 2018;9:289.

77. Van Der Linden, M, Westerlaken, GH, Van Der Vlist, M, Van Montfrans, J, and Meyaard, L. Differential signalling and kinetics of neutrophil extracellular trap release revealed by quantitative live imaging. Sci Rep 2017;7:1-11.

78. Neubert, E, Meyer, D, Rocca, F, et al. Chromatin swelling drives neutrophil extracellular trap release. Nature communications 2018;9:1-13.

79. McDonald, B, Davis, RP, Kim, S-J, et al. Platelets and neutrophil extracellular traps collaborate to promote intravascular coagulation during sepsis in mice. Blood 2017;blood-2016-2009-741298.

80. Abaricia, JO, Shah, AH, Musselman, RM, and Olivares-Navarrete, R. Hydrophilic titanium surfaces reduce neutrophil inflammatory response and NETosis. Biomater Sci 2020;8:2289-2299.

81. Fuchs, TA, Abed, U, Goosmann, C, et al. Novel cell death program leads to neutrophil extracellular traps. J Cell Biol 2007;176:231-241.

82. Papayannopoulos, V, Metzler, KD, Hakkim, A, and Zychlinsky, A. Neutrophil elastase and myeloperoxidase regulate the formation of neutrophil extracellular traps. J Cell Biol 2010;191:677-691.

83. Lapponi, MJ, Carestia, A, Landoni, VI, et al. Regulation of neutrophil extracellular trap formation by anti-inflammatory drugs. J Pharm Exp Ther 2013;345:430-437.

84. Hoppenbrouwers, T, Autar, AS, Sultan, AR, et al. In vitro induction of NETosis: Comprehensive live imaging comparison and systematic review. PLoS One 2017;12:e0176472.

85. Fuchs, TA, Brill, A, Duerschmied, D, et al. Extracellular DNA traps promote thrombosis. PNAS 2010;107:15880-15885.

86. Farley, K, Stolley, JM, Zhao, P, Cooley, J, and Remold-O'Donnell, E. A SerpinB1 regulatory mechanism is essential for restricting neutrophil extracellular trap generation. J Immunol 2012;189:4574-4581.

87. de Bont, CM, Koopman, WJ, Boelens, WC, and Pruijn, GJ. Stimulus-dependent chromatin dynamics, citrullination, calcium signalling and ROS production during NET formation. Biochimic Biophys Acta Mol Cell Res 2018;1865:1621-1629.

88. Minden-Birkenmaier, BA, Smith, RA, Radic, MZ, van der Merwe, M, and Bowlin, GL. Manuka honey reduces NETosis on an electrospun template within a therapeutic window. Polymers 2020;12:1430.

89. Khan, MA, Farahvash, A, Douda, DN, et al. Jnk activation turns on LPS-and gram-negative bacteria-induced nadph oxidase-dependent suicidal NETosis. Sci Rep 2017;7:1-16.

90. Keshari, RS, Jyoti, A, Dubey, M, et al. Cytokines induced neutrophil extracellular traps formation: Implication for the inflammatory disease condition. PLoS One 2012;7:e48111.

91. Tatsiy, O, and McDonald, PP. Physiological stimuli induce PAD4-dependent, ROS-independent NETosis, with early and late events controlled by discrete signaling pathways. Front Immunol 2018;9:2036.

92. Gupta, AK, Giaglis, S, Hasler, P, and Hahn, S. Efficient neutrophil extracellular trap induction requires mobilization of both intracellular and extracellular calcium pools and is modulated by cyclosporine A. PLoS One 2014;9:e97088.

93. Etulain, J, Martinod, K, Wong, SL, et al. P-selectin promotes neutrophil extracellular trap formation in mice. Blood 2015;126:242-246.

94. Maugeri, N, Brambilla, M, Camera, M, et al. Human polymorphonuclear leukocytes produce and express functional tissue factor upon stimulation. J Thromb Haemost 2006;4:1323-1330.

95. Carestia, A, Kaufman, T, Rivadeneyra, L, et al. Mediators and molecular pathways involved in the regulation of neutrophil extracellular trap formation mediated by activated platelets. J Leuko Biol 2016;99:153-162.

96. Cools-Lartigue, J, Spicer, J, McDonald, B, et al. Neutrophil extracellular traps sequester circulating tumor cells and promote metastasis. J Clinic Invest 2013;123:3446-3458.

97. Okeke, EB, Louttit, C, Fry, C, et al. Inhibition of neutrophil elastase prevents neutrophil extracellular trap formation and rescues mice from endotoxic shock. Biomaterials 2020;238:119836.

98. Narasaraju, T, Yang, E, Samy, RP, et al. Excessive neutrophils and neutrophil extracellular traps contribute to acute lung injury of influenza pneumonitis. Am J Pathol 2011;179:199-210.

99. Antonelou, M, Michaëlsson, E, Evans, RD, et al. Therapeutic myeloperoxidase inhibition attenuates neutrophil activation, anca-mediated endothelial damage, and crescentic GN. J Am Soc Nephrol 2020;31:350-364.

100. Demers, M, Krause, DS, Schatzberg, D, et al. Cancers predispose neutrophils to release extracellular DNA traps that contribute to cancer-associated thrombosis. PNAS 2012;109:13076-13081.

101. Tadie, JM, Bae, HB, Jiang, S, et al. HMGB1 promotes neutrophil extracellular trap formation through interactions with toll-like receptor 4. Am J Physiol-Lung C 2013;304:L342-L349.

102. Pieterse, E, Rother, N, Yanginlar, C, Hilbrands, LB, and van der Vlag, J. Neutrophils discriminate between lipopolysaccharides of different bacterial sources and selectively release neutrophil extracellular traps. Front Immunol 2016;7:484.

103. Raetz, CR, and Whitfield, C. Lipopolysaccharide endotoxins. Annu Rev Biochem 2002;71:635-700.

104. Clark, SR, Ma, AC, Tavener, SA, et al. Platelet TLR4 activates neutrophil extracellular traps to ensnare bacteria in septic blood. Nat Med 2007;13:463-469.

105. Remijsen, Q, Berghe, TV, Wirawan, E, et al. Neutrophil extracellular trap cell death requires both autophagy and superoxide generation. Cell Res 2011;21:290.

106. Müller, S, Behnen, M, Bieber, K, et al. Dimethylfumarate impairs neutrophil functions. J Invest Dermatol 2016;136:117-126.

107. Sil, P, Wicklum, H, Surell, C, and Rada, B. Macrophage-derived IL-1β enhances monosodium urate crystal-triggered NET formation. Inflammation Research 2017;66:227-237.

108. Brinkmann, V, Goosmann, C, Kuhn, LI, and Zychlinsky, A. Automatic quantification of in vitro NET formation. Front Immunol 2012;3:413.

109. Gupta, AK, Joshi, MB, Philippova, M, et al. Activated endothelial cells induce neutrophil extracellular traps and are susceptible to NETosis-mediated cell death. FEBS Lett 2010;584:3193-3197.

110. Mizurini, DM, Aslan, JS, Gomes, T, et al. Salivary thromboxane A2-binding proteins from triatomine vectors of chagas disease inhibit platelet-mediated neutrophil extracellular traps (NETs) formation and arterial thrombosis. PLoS Negl Trop Dis 2015;9:e0003869.

111. Alsousou, J, Ali, A, Willett, K, and Harrison, P. The role of platelet-rich plasma in tissue regeneration. Platelets 2013;24:173-182.

112. Muñoz, LE, Bilyy, R, Biermann, MH, et al. Nanoparticles size-dependently initiate self-limiting NETosis-driven inflammation. PNSA 2016;113:E5856-E5865.

113. Sperling, C, Fischer, M, Maitz, MF, and Werner, C. Neutrophil extracellular trap formation upon exposure of hydrophobic materials to human whole blood causes thrombogenic reactions. Biomater Sci 2017;5:1998-2008.

114. Fetz, AE, Fantaziu, CA, Smith, RA, Radic, MZ, and Bowlin, GL. Surface area to volume ratio of electrospun polydioxanone templates regulates the adsorption of soluble proteins from human serum. Bioeng 2019;6:78.

115. Du, M, Yang, W, Schmull, S, Gu, J, and Xue, S. Inhibition of peptidyl arginine deiminase-4 protects against myocardial infarction induced cardiac dysfunction. Int Immunopharmacol 2020;78:106055.

116. Knight, JS, Zhao, W, Luo, W, et al. Peptidylarginine deiminase inhibition is immunomodulatory and vasculoprotective in murine lupus. J Clin Invest 2013;123:2981-2993.

117. Chumanevich, AA, Causey, CP, Knuckley, BA, et al. Suppression of colitis in mice by cl-amidine: A novel peptidylarginine deiminase inhibitor. Am J PHysiol-Gastr L 2011;300:G929-G938.

118. Willis, VC, Gizinski, AM, Banda, NK, et al. N-alpha-benzoyl-n5-(2-chloro-1-iminoethyl)-l-ornithine amide, a protein arginine deiminase inhibitor, reduces the severity of murine collagen-induced arthritis. J Immunol 2011;186:4396-4404.

119. Lewis, HD, Liddle, J, Coote, JE, et al. Inhibition of PAD4 activity is sufficient to disrupt mouse and human NET formation. Nat Chem Biol 2015;11:189-191.

120. Hosseinzadeh, A, Messer, PK, and Urban, CF. Stable redox-cycling nitroxide tempol inhibits NET formation. Front Immunol 2012;3:391.

121. Magaña-Guerrero, FS, Domínguez-López, A, Martínez-Aboytes, P, Buentello-Volante, B, and Garfias, Y. Human amniotic membrane mesenchymal stem cells inhibit neutrophil extracellular traps through TSG-6. Sci Rep 2017;7:1-15.

122. Yang, SC, Chen, PJ, Chang, S-H, et al. Luteolin attenuates neutrophilic oxidative stress and inflammatory arthritis by inhibiting Raf1 activity. Biochem Pharmacol 2018;154:384-396.

123. Zeng, J, Xu, H, Fan, Pz, et al. Kaempferol blocks neutrophil extracellular traps formation and reduces tumour metastasis by inhibiting ROS-PAD4 pathway. J Cell Mol Med 2020;24:7590-7599.

124. Zabieglo, K, Majewski, P, Majchrzak-Gorecka, M, et al. The inhibitory effect of secretory leukocyte protease inhibitor (SLPI) on formation of neutrophil extracellular traps. J Leuko Biol 2015;98:99-106.

125. Furumoto, Y, Smith, CK, Blanco, L, et al. Tofacitinib ameliorates murine lupus and its associated vascular dysfunction. Arthritis Rheumatol 2017;69:148-160.

126. Boone, BA, Murthy, P, Miller-Ocuin, J, et al. Chloroquine reduces hypercoagulability in pancreatic cancer through inhibition of neutrophil extracellular traps. BMC Cancer 2018;18:678.

127. Murthy, P, Singhi, AD, Ross, MA, et al. Enhanced neutrophil extracellular trap (NET) formation in acute pancreatitis contributes to disease severity and is reduced by chloroquine. Front Immunol 2019;10:28.

128. Neeli, I, Khan, SN, and Radic, M. Histone deimination as a response to inflammatory stimuli in neutrophils. J Immunol 2008;180:1895-1902.

129. Behnen, M, Leschczyk, C, Möller, S, et al. Immobilized immune complexes induce neutrophil extracellular trap release by human neutrophil granulocytes via FcγRIIIb and Mac-1. J Immunol 2014;1400478.

130. Chen, K, Nishi, H, Travers, R, et al. Endocytosis of soluble immune complexes leads to their clearance by FcγRIIIb but induces neutrophil extracellular traps via RcγRIIa in vivo. Blood 2012;4421-4431.

131. Totani, L, Amore, C, Di Santo, A, et al. Roflumilast inhibits leukocyte–platelet interactions and prevents the prothrombotic functions of polymorphonuclear leukocytes and monocytes. J Thromb Haemost 2016;14:191-204.

132. Wang, Y, Li, M, Stadler, S, et al. Histone hypercitrullination mediates chromatin decondensation and neutrophil extracellular trap formation. J Cell Biol 2009;184:205-213.

133. Li, P, Li, M, Lindberg, MR, et al. PAD4 is essential for antibacterial innate immunity mediated by neutrophil extracellular traps. J Exp Med 2010;207:1853-1862.

134. Martinod, K, Demers, M, Fuchs, TA, et al. Neutrophil histone modification by peptidylarginine deiminase 4 is critical for deep vein thrombosis in mice. PNAS 2013;110:8674-8679.

135. Perdomo, J, Leung, HH, Ahmadi, Z, et al. Neutrophil activation and NETosis are the major drivers of thrombosis in heparin-induced thrombocytopenia. Nature 2019;10:1-14.

136. Kenny, EF, Herzig, A, Krüger, R, et al. Diverse stimuli engage different neutrophil extracellular trap pathways. Immunol Cell Biol 2017;6:e24437.

137. Hosseinzadeh, A, Thompson, PR, Segal, BH, and Urban, CF. Nicotine induces neutrophil extracellular traps. J Leuko Biol 2016;100:1105-1112.

138. Björnsdottir, H, Welin, A, Michaëlsson, E, et al. Neutrophil NET formation is regulated from the inside by myeloperoxidase-processed reactive oxygen species. Free Radic Biol Med 2015;89:1024-1035.

139. Mauthe, M, Orhon, I, Rocchi, C, et al. Chloroquine inhibits autophagic flux by decreasing autophagosome-lysosome fusion. Autophagy 2018;14:1435-1455.

140. Neeli, I, Dwivedi, N, Khan, S, and Radic, M. Regulation of extracellular chromatin release from neutrophils. J Innate Immun 2009;1:194-201.

141. Branzk, N, Lubojemska, A, Hardison, SE, et al. Neutrophils sense microbe size and selectively release neutrophil extracellular traps in response to large pathogens. Nat Immunol 2014;15:1017-1025.

142. Jenne, CN, Wong, CH, Zemp, FJ, et al. Neutrophils recruited to sites of infection protect from virus challenge by releasing neutrophil extracellular traps. Cell Host Microbe 2013;13:169-180.

143. Schauer, C, Janko, C, Munoz, LE, et al. Aggregated neutrophil extracellular traps limit inflammation by degrading cytokines and chemokines. Nat Med 2014;20:511.

144. Hahn, J, Schauer, C, Czegley, C, et al. Aggregated neutrophil extracellular traps resolve inflammation by proteolysis of cytokines and chemokines and protection from antiproteases. FASEB 2019;33:1401-1414.

145. Dvorak, HF. Tumors: Wounds that do not heal. NEJM 1986;315:1650-1659.

146. Ratajczak, MZ, Bujko, K, Mack, A, Kucia, M, and Ratajczak, J. Cancer from the perspective of stem cells and misappropriated tissue regeneration mechanisms. Leukemia 2018;32:2519-2526.

147. Takesue, S, Ohuchida, K, Shinkawa, T, et al. Neutrophil extracellular traps promote liver micrometastasis in pancreatic ductal adenocarcinoma via the activation of cancer-associated fibroblasts. Int J Oncol 2020;56:596-605.

148. Yang, L, Liu, Q, Zhang, X, et al. DNA of neutrophil extracellular traps promotes cancer metastasis via CCDC25. Nature 2020;1-6.

149. Park, J, Wysocki, RW, Amoozgar, Z, et al. Cancer cells induce metastasis-supporting neutrophil extracellular DNA traps. Sci Transl Med 2016;8:361ra138-361ra138.

150. Lee, W, Ko, SY, Mohamed, MS, et al. Neutrophils facilitate ovarian cancer premetastatic niche formation in the omentum. J Exp Med 2019;216:176-194.

151. Rayes, RF, Mouhanna, JG, Nicolau, I, et al. Primary tumors induce neutrophil extracellular traps with targetable metastasis-promoting effects. JCI insight 2019;4:e128008.

152. Xing, F, Saidou, J, and Watabe, K. Cancer associated fibroblasts (CAFs) in tumor microenvironment. Front Biosci 2010;15:166.

153. Miller-Ocuin, JL, Liang, X, Boone, BA, et al. DNA released from neutrophil extracellular traps (nets) activates pancreatic stellate cells and enhances pancreatic tumor growth. Oncoimmunology 2019;8:e1605822.

154. Erpenbeck, L, and Schön, M. Neutrophil extracellular traps: Protagonists of cancer progression? Oncogene 2017;36:2483-2490.

155. Tohme, S, Yazdani, HO, Al-Khafaji, AB, et al. Neutrophil extracellular traps promote the development and progression of liver metastases after surgical stress. Cancer Res 2016;76:1367-1380.

156. Yu, M, Li, T, Li, B, et al. Phosphatidylserine-exposing blood cells, microparticles and neutrophil extracellular traps increase procoagulant activity in patients with pancreatic cancer. Thromb Res 2020;188:5-16.

157. Mauracher, LM, Posch, F, Martinod, K, et al. Citrullinated histone H3, a biomarker of neutrophil extracellular trap formation, predicts the risk of venous thromboembolism in cancer patients. J Thromb Haemost 2018;16:508-518.

158. Cherpokova, D, Jouvene, CC, Libreros, S, et al. Resolvin D4 attenuates the severity of pathological thrombosis in mice. Blood 2019;134:1458-1468.

159. Nakazawa, D, Desai, J, Steiger, S, et al. Activated platelets induce Mlkl-driven neutrophil necroptosis and release of neutrophil extracellular traps in venous thrombosis. Cell death discovery 2018;4:1-11.

160. Sorvillo, N, Mizurini, DM, Coxon, C, et al. Plasma peptidylarginine deiminase IV promotes VWf-platelet string formation and accelerates thrombosis after vessel injury. Circulation research 2019;125:507-519.

161. Meegan, JE, Beard Jr, RS, Yang, X, et al. Neutrophil extracellular traps contribute to endothelial barrier dysfunction during sepsis. FASEB 2017;31:679.671-679.671.

162. Chrysanthopoulou, A, Mitroulis, I, Apostolidou, E, et al. Neutrophil extracellular traps promote differentiation and function of fibroblasts. J Pathol 2014;233:294-307.

163. Martinod, K, Witsch, T, Erpenbeck, L, et al. Peptidylarginine deiminase 4 promotes age-related organ fibrosis. 2017;214:439-458.

164. Didier, K, Giusti, D, Le Jan, S, et al. Neutrophil extracellular traps generation relates with early stage and vascular complications in systemic sclerosis. Clin Med 2020;9:2136.

165. Jin, Z, Sun, J, Song, Z, et al. Neutrophil extracellular traps promote scar formation in post-epidural fibrosis. NPJ Regen Med 2020;5:1-9.

166. Dalbeth, N, Pool, B, Gamble, GD, et al. Cellular characterization of the gouty tophus: A quantitative analysis. Arthritis Rheum 2010;62:1549-1556.

167. Jiménez-Alcázar, M, Rangaswamy, C, Panda, R, et al. Host DNases prevent vascular occlusion by neutrophil extracellular traps. Science 2017;358:1202-1206.

168. Aitken, M. Clinical trials of recombinant human DNase in cystic fibrosis patients. Monaldi Arch Chest Dis 1993;48:653-656.

169. Kang, L, Yu, H, Yang, X, et al. Neutrophil extracellular traps released by neutrophils impair revascularization and vascular remodeling after stroke. Nature Comm 2020;11:1-15.

170. Vaibhav, K, Braun, M, Alverson, K, et al. Neutrophil extracellular traps exacerbate neurological deficits after traumatic brain injury. Science Advan 2020;6:eaax8847.

171. Farrera, C, and Fadeel, B. Macrophage clearance of neutrophil extracellular traps is a silent process. J Immunol 2013;191:2647-2656.

172. Elliott, MR, Koster, KM, and Murphy, PS. Efferocytosis signaling in the regulation of macrophage inflammatory responses. J Immunol 2017;198:1387-1394.

173. Liu, D, Yang, P, Gao, M, et al. Nlrp3 activation induced by neutrophil extracellular traps sustains inflammatory response in the diabetic wound. Clin Sci 2019;133:565-582.

174. Phillipson, M, and Kubes, P. The healing power of neutrophils. Trends Immunol 2019;7:635-647.

175. Fetz, AE, Radic, MZ, and Bowlin, GL. Neutrophils in biomaterial-guided tissue regeneration: Matrix reprogramming for angiogenesis. Tissue Engin Part B 2020.

176. Horckmans, M, Ring, L, Duchene, J, et al. Neutrophils orchestrate post-myocardial infarction healing by polarizing macrophages towards a reparative phenotype. Eur Heart J 2016;38:187-197.

177. Blázquez-Prieto, J, López-Alonso, I, Amado-Rodríguez, L, et al. Impaired lung repair during neutropenia can be reverted by matrix metalloproteinase-9. Thorax 2018;73:321-330.

178. Stirling, DP, Liu, S, Kubes, P, and Yong, VW. Depletion of LY6G/Gr-1 leukocytes after spinal cord injury in mice alters wound healing and worsens neurological outcome. J Neurosci 2009;29:753-764.

179. Kovtun, A, Bergdolt, S, Wiegner, R, et al. The crucial role of neutrophil granulocytes in bone fracture healing. Eur Cell Mater 2016;32:152-162.

180. Peiseler, M, and Kubes, P. More friend than foe: The emerging role of neutrophils in tissue repair. J Clin Invest 2019;129:2629-2639.

181. Fridlender, ZG, Sun, J, Kim, S, et al. Polarization of tumor-associated neutrophil phenotype by TGF-β:"N1" versus "N2" TAN. Cancer Cell 2009;16:183-194.

182. Deryugina, EI, Zajac, E, Juncker-Jensen, A, et al. Tissue-infiltrating neutrophils constitute the major in vivo source of angiogenesis-inducing MMP-9 in the tumor microenvironment. Neoplasia 2014;16:771-788.

183. Itagaki, K, Kaczmarek, E, Lee, YT, et al. Mitochondrial DNA released by trauma induces neutrophil extracellular traps. PLoS One 2015;10:e0120549.

184. Ollivier, V, Roques, C, Receveur, N, et al. Bioreactivity of stent material: Activation of platelets, coagulation, leukocytes and endothelial cell dysfunction in vitro. Platelets 2017;28:529-539.

185. Korabecna, M, Opatrna, S, Wirth, J, et al. Cell-free plasma DNA during peritoneal dialysis and hemodialysis and in patients with chronic kidney disease. Ann NY Acad Sci 2008;1137:296-301.

186. Won, J-E, Lee, YS, Park, J-H, et al. Hierarchical microchanneled scaffolds modulate multiple tissue-regenerative processes of immune-responses, angiogenesis, and stem cell homing. Biomaterials 2020;227:119548.

187. Korabecna, M, and Tesar, V. NETosis provides the link between activation of neutrophils on hemodialysis membrane and comorbidities in dialyzed patients. Inflammation Research 2017;66:369-378.

188. Vitkov, L, Krautgartner, WD, Obermayer, A, et al. The initial inflammatory response to bioactive implants is characterized by NETosis. PLoS One 2015;10:e0121359.

189. Puleo, DA, and Bizios, R. Biological interactions on materials surfaces: Understanding and controlling protein, cell, and tissue responses: Springer Science & Business Media; 2009.

190. Radic, MZ, and Bowlin, GL. Innate immunity response to tissue engineering templates: The determinant. Journal of Tissue Science & Engineering 2014;5:1.

191. Williams, DF. The biomaterials conundrum in tissue engineering. Tissue Engineering Part A 2014;20:1129-1131.

192. Jaillon, S, Galdiero, MR, Del Prete, D, et al. Neutrophils in innate and adaptive immunity. Semin Immunopathol 2013;35:377-394.

193. Kolaczkowska, E, and Kubes, P. Neutrophil recruitment and function in health and inflammation. Nature Rev Immunol 2013;13:159-175.

194. Kumar, V, and Sharma, A. Neutrophils: Cinderella of innate immune system. Int Immunopharmacol 2010;10:1325-1334.

195. Soehnlein, O, Weber, C, and Lindbom, L. Neutrophil granule proteins tune monocytic cell function. Trends Immunol 2009;30:538-546.

196. Soehnlein, O, Zernecke, A, Eriksson, EE, et al. Neutrophil secretion products pave the way for inflammatory monocytes. Blood 2008;112:1461-1471.

197. Tamassia, N, Cassatella, MA, and Bazzoni, F. Fast and accurate quantitative analysis of cytokine gene expression in human neutrophils. Neutrophil methods and protocols: Springer; 2014. pp. 451-467.

198. Wheeler, MA, Smith, SD, García-Cardeña, G, et al. Bacterial infection induces nitric oxide synthase in human neutrophils. J Clin Invest 1997;99:110-116.

199. Vandenabeele, P, Galluzzi, L, Berghe, TV, and Kroemer, G. Molecular mechanisms of necroptosis: An ordered cellular explosion. Nature Rev Mol Cell Biol 2010;11:700-714.

200. Warnatsch, A, Ioannou, M, Wang, Q, and Papayannopoulos, V. Neutrophil extracellular traps license macrophages for cytokine production in atherosclerosis. Science 2015;349:316-320.

201. Rajan, N, Habermehl, J, Coté, MF, Doillon, CJ, and Mantovani, D. Preparation of ready-to-use, storable and reconstituted type I collagen from rat tail tendon for tissue engineering applications. Nat Protoc 2006;1:2753.

202. Sergeant, S, Waite, KA, Heravi, J, and McPhail, LC. Phosphatidic acid regulates tyrosine phosphorylating activity in human neutrophils enhancement of FGR activity. J Biol Chem 2001;276:4737-4746.

203. Wang, D, Pabst, KM, Aida, Y, and Pabst, MJ. Lipopolysaccharide-inactivating activity of neutrophils is due to lactoferrin. J Leuko Biol 1995;57:865-874.

204. Barnes, CP, Pemble IV, CW, Brand, DD, Simpson, DG, and Bowlin, GL. Cross-linking electrospun type II collagen tissue engineering scaffolds with carbodiimide in ethanol. Tissue Eng 2007;13:1593-1605.

205. Yoganarasimha, S, Trahan, WR, Best, AM, et al. Peracetic acid: A practical agent for sterilizing heat-labile polymeric tissue-engineering scaffolds. Tissue Eng Part C 2014;20:714-723.

206. Remijsen, Q, Kuijpers, T, Wirawan, E, et al. Dying for a cause: NETosis, mechanisms behind an antimicrobial cell death modality. Cell Death Differ 2011;18:581-588.

207. Brinkmann, V, Laube, B, Abu Abed, U, Goosmann, C, and Zychlinsky, A. Neutrophil extracellular traps: How to generate and visualize them. J Vis Exp 2010;36:1724.

208. Mantovani, A, Cassatella, MA, Costantini, C, and Jaillon, S. Neutrophils in the activation and regulation of innate and adaptive immunity. Nat Rev Immunol 2011;11:519-531.

209. Spillmann, C, Osorio, D, and Waugh, R. Integrin activation by divalent ions affects neutrophil homotypic adhesion. Ann Biomed Eng 2002;30:1002-1011.

210. Garg, K, Ryan, JJ, and Bowlin, GL. Modulation of mast cell adhesion, proliferation, and cytokine secretion on electrospun bioresorbable vascular grafts. J Biomed Mater Res Part A 2011;97:405-413.

211. Boland, ED, Coleman, BD, Barnes, CP, et al. Electrospinning polydioxanone for biomedical applications. Acta Biomater 2005;1:115-123.

212. Matthews, JA, Wnek, GE, Simpson, DG, and Bowlin, GL. Electrospinning of collagen nanofibers. Biomacromolecules 2002;3:232-238.

213. Chiu, JB, Liu, C, Hsiao, BS, Chu, B, and Hadjiargyrou, M. Functionalization of poly (L-lactide) nanofibrous scaffolds with bioactive collagen molecules. J Biomed Mater Res Part A 2007;83:1117-1127.

214. Sun, XY, Nobles, LR, Borner, HG, and Spontak, RJ. Field-driven surface segregation of biofunctional species on electrospun PMMA/PEO microfibers. Macromol Rapid Commun 2008;29:1455-1460.

215. Boland, ED, Telemeco, TA, Simpson, DG, Wnek, GE, and Bowlin, GL. Utilizing acid pretreatment and electrospinning to improve biocompatibility of poly(glycolic acid) for tissue engineering. J Biomed Mater Res Part B 2004;71:144-152.

216. Wong, SL, Demers, M, Martinod, K, et al. Diabetes primes neutrophils to undergo NETosis, which impairs wound healing. Nat Med 2015;21:815-819.

217. Hakkim, A, Fürnrohr, BG, Amann, K, et al. Impairment of neutrophil extracellular trap degradation is associated with lupus nephritis. PNAS 2010;107:9813-9818.

218. Czaikoski, PG, Mota, JMSC, Nascimento, DC, et al. Neutrophil extracellular traps induce organ damage during experimental and clinical sepsis. PLoS One 2016;11:e0148142.

219. Cheng, OZ, and Palaniyar, N. NET balancing: A problem in inflammatory lung diseases. Front Immunol 2013;4:1.

220. Martinod, K, and Wagner, DD. Thrombosis: Tangled up in NETs. Blood 2014;123:2768-2776.

221. Yipp, BG, and Kubes, P. NETosis: How vital is it? Blood 2013;122:2784-2794.

222. Raftery, MJ, Lalwani, P, Krautkrämer, E, et al. B2 integrin mediates hantavirus-induced release of neutrophil extracellular traps. J Exp Med 2014;211:1485-1497.

223. Kaplan, MJ, and Radic, M. Neutrophil extracellular traps: Double-edged swords of innate immunity. J Immunol 2012;189:2689-2695.

224. Garg, K, Pullen, NA, Oskeritzian, CA, Ryan, JJ, and Bowlin, GL. Macrophage functional polarization (M1/M2) in response to varying fiber and pore dimensions of electrospun scaffolds. Biomaterials 2013;34:4439-4451.

225. Vroman, L, and Adams, AL. Findings with the recording ellipsometer suggesting rapid exchange of specific plasma proteins at liquid/solid interfaces. Surface Science 1969;16:438-446.

226. Kessenbrock, K, Krumbholz, M, Schönermarck, U, et al. NETting neutrophils in autoimmune small-vessel vasculitis. Nat Med 2009;15:623-625.

227. Riehl, DR, Roewe, J, Klebow, S, et al. Neutrophil extracellular traps drive bleomycin-induced lung fibrosis by regulating TGFβ1-dependent interactions of platelets and macrophages. FASEB 2016;30:50.51-50.51.

228. Busher, JT. Serum albumin and globulin. Clinical Methods 1990;3:101.

229. Hansen, MS. Fibronectin and coagulation factor XIII increases blood platelet adhesion to fibrin. Thromb Res 1984;34:551-556.

230. Janeway Jr, CA, Travers, P, Walport, M, and Shlomchik, MJ. The complement system and innate immunity. 2001;5.

231. Sontheimer, RD, Racila, E, and Racila, DM. C1Q: Its functions within the innate and adaptive immune responses and its role in lupus autoimmunity. J Invest Dermatol 2005;125:14-23.

232. Sahu, A, and Lambris, JD. Structure and biology of complement protein C3, a connecting link between innate and acquired immunity. Immunol Rev 2001;180:35-48.

233. Hendey, B, Klee, CB, and Maxfield, FR. Inhibition of neutrophil chemokinesis on vitronectin by inhibitors of calcineurin. Science 1992;258:296-299.

234. Tsuruta, Y, Park, Y-J, Siegal, GP, Liu, G, and Abraham, E. Involvement of vitronectin in lipopolysaccaride-induced acute lung injury. J Immunol 2007;179:7079-7086.

235. Bae, HB, Zmijewski, JW, Deshane, JS, et al. Vitronectin inhibits neutrophil apoptosis through activation of integrin-associated signaling pathways. Am J Respir Cell Mol Biol 2012;46:790-796.

236. Fahey, JL, and McKelvey, E. Quantitative determination of serum immunoglobulins in antibody-agar plates. J Immunol 1965;94:84-90.

237. Koblinski, JE, Wu, M, Demeler, B, Jacob, K, and Kleinman, HK. Matrix cell adhesion activation by non-adhesion proteins. J Cell Sci 2005;118:2965-2974.

238. Nathan, C, Xie, Q, Halbwachs-Mecarelli, L, and Jin, WW. Albumin inhibits neutrophil spreading and hydrogen peroxide release by blocking the shedding of CD43 (sialophorin, leukosialin). J Cell Biol 1993;122:243-256.

239. Neubert, E, Senger-Sander, SN, Manzke, VS, et al. Serum and serum albumin inhibit in vitro formation of neutrophil extracellular traps (NETs). Front Immunol 2019;10:12.

240. Gonzalez-Quintela, A, Alende, R, Gude, F, et al. Serum levels of immunoglobulins (IgG, IgA, IgM) in a general adult population and their relationship with alcohol consumption, smoking and common metabolic abnormalities. Clin Exp Immunol 2008;151:42-50.

241. Buijs, J, van den Berg, PA, James, WT, Norde, W, and Lyklema, J. Adsorption dynamics of IgG and its F(ab′) and Fc fragments studied by reflectometry. J Colloid Interface Sci 1996;178:594-605.

242. Arai, T, and Norde, W. The behavior of some model proteins at solid—liquid interfaces 2. Sequential and competitive adsorption. Colloid Surface 1990;51:17-28.

243. Vermeer, AW, Giacomelli, CE, and Norde, W. Adsorption of IgG onto hydrophobic Teflon. Differences between the Fab and Fc domains. Biochim Biophys Acta Gen Subj 2001;1526:61-69.

244. Selvaraj, P, Fifadara, N, Nagarajan, S, Cimino, A, and Wang, G. Functional regulation of human neutrophil Fc γ receptors. Immunol Res 2004;29:219-229.

245. Unkeless, JC, Shen, Z, Lin, C-W, and DeBeus, E. Function of human FcγRIIa and FcγRIIIb. Semin Immunol 1995;7:37-44.

246. Nagarajan, S, Venkiteswaran, K, Anderson, M, et al. Cell-specific, activation-dependent regulation of neutrophil CD32a ligand-binding function. Blood 2000;95:1069-1077.

247. Lood, C, Arve, S, Ledbetter, JA, and Elkon, KB. TLR8 activation shifts neutrophils from phagocytosis to NETosis through furin-dependent shedding of FcgRIIa. Am Assoc Immnol 2016;196:117.

248. Minden-Birkenmaier, BA, Cherukuri, K, Smith, RA, Radic, MZ, and Bowlin, GL. Manuka honey modulates the inflammatory behavior of a dHL-60 neutrophil model under the cytotoxic limit. Int J Biomater 2019;2019:6132581.

249. Minden-Birkenmaier, BA, Meadows, MB, Cherukuri, K, et al. The effect of manuka honey on dHL-60 cytokine, chemokine, and matrix-degrading enzyme release under inflammatory conditions. Med one 2019;4:e190005.

250. Piccard, H, Muschel, RJ, and Opdenakker, G. On the dual roles and polarized phenotypes of neutrophils in tumor development and progression. Crit Rev Oncol Hematol 2012;82:296-309.

251. Radic, M, and Marion, TN. Neutrophil extracellular chromatin traps connect innate immune response to autoimmunity. Semin Immunopathol 2013;35:465-480.

252. Albrengues, J, Shields, MA, Ng, D, et al. Neutrophil extracellular traps produced during inflammation awaken dormant cancer cells in mice. Science 2018;361:eaao4227.

253. Gray, RD, Lucas, CD, MacKellar, A, et al. Activation of conventional protein kinase c (PKC) is critical in the generation of human neutrophil extracellular traps. J Inflamm 2013;10:12.

254. Alemán, OR, Mora, N, Cortes-Vieyra, R, Uribe-Querol, E, and Rosales, C. Transforming growth factor-β-activated kinase 1 is required for human FcγRIIIb-induced neutrophil extracellular trap formation. Front Immunol 2016;7:277.

255. Short, KR, von Köckritz-Blickwede, M, Langereis, JD, et al. Antibodies mediate formation of neutrophil extracellular traps in the middle ear and facilitate secondary pneumococcal otitis media. J Infect 2014;82:364-370.

256. Guyre, PM, Campbell, AS, Kniffin, WD, and Fanger, MW. Monocytes and polymorphonuclear neutrophils of patients with streptococcal pharyngitis express increased numbers of type I IgG Fc receptors. J Clin Invest 1990;86:1892-1896.

257. Repp, R, Valerius, T, Sendler, A, et al. Neutrophils express the high affinity receptor for igg (Fc gamma RI, CD64) after in vivo application of recombinant human granulocyte colony-stimulating factor. Blood 1991;78:885-889.

258. Davis, BH. Improved diagnostic approaches to infection/sepsis detection. Expert Rev Mol Diagn 2005;5:193-207.

259. Neeli, I, and Radic, M. Opposition between pkc isoforms regulates histone deimination and neutrophil extracellular chromatin release. Front Immunol 2013;4:38.

260. Kudva, IT, Griffin, RW, Garren, JM, Calderwood, SB, and John, M. Identification of a protein subset of the anthrax spore immunome in humans immunized with the anthrax vaccine adsorbed preparation. Infect Immun 2005;73:5685-5696.

261. Aleyd, E, Al, M, Tuk, CW, van der Laken, CJ, and van Egmond, M. IgA complexes in plasma and synovial fluid of patients with rheumatoid arthritis induce neutrophil extracellular traps via FcαRI. J Immunol 2016;197:4552-4559.

262. Jönsson, F, Mancardi, DA, Kita, Y, et al. Mouse and human neutrophils induce anaphylaxis. J Clin Invest 2011;121:1484-1496.

263. Bergqvist, C, Safi, R, El Hasbani, G, et al. Neutrophil extracellular traps are present in immune-complex-mediated cutaneous small vessel vasculitis and correlate with the production of reactive oxygen species and the severity of vessel damage. Acta Derm Venereol 2019;100:adv00281.

264. Saffarzadeh, M, Cabrera-Fuentes, HA, Veit, F, et al. Characterization of rapid neutrophil extracellular trap formation and its cooperation with phagocytosis in human neutrophils. 2014;2:e19.

265. Kraaij, T, Tengström, FC, Kamerling, SW, et al. A novel method for high-throughput detection and quantification of neutrophil extracellular traps reveals ROS-independent NET release with immune complexes. Autoimmun Rev 2016;15:577-584.

266. Nimmerjahn, F, and Ravetch, JV. Fcγ receptors as regulators of immune responses. Nat Rev Immunol 2008;8:34-47.

267. Tosi, M, and Berger, M. Functional differences between the 40 kDa and 50 to 70 kDa IgG Fc receptors on human neutrophils revealed by elastase treatment and antireceptor antibodies. J Immunol 1988;141:2097-2103.

268. Selvaraj, P, Rosse, WF, Silber, R, and Springer, TA. The major Fc receptor in blood has a phosphatidylinositol anchor and is deficient in paroxysmal nocturnal haemoglobinuria. Nature 1988;333:565-567.

269. Alemán, OR, Mora, N, Cortes-Vieyra, R, Uribe-Querol, E, and Rosales, C. Differential use of human neutrophil Fcγ receptors for inducing neutrophil extracellular trap formation. J Immnol Res 2016;2016: 2908034.

270. Yu, L, Wang, L, and Chen, S. Endogenous toll-like receptor ligands and their biological significance. J Cell Molec Med 2010;14:2592-2603.

271. Battiston, K, Ouyang, B, Honarparvar, E, et al. Interaction of a block-co-polymeric biomaterial with immunoglobulin g modulates human monocytes towards a non-inflammatory phenotype. Acta Biomater 2015;24:35-43.

272. De La Cruz, C, Haimovich, B, and Greco, RS. Immobilized IgG and fibrinogen differentially affect the cytoskeletal organization and bactericidal function of adherent neutrophils. J Surg Res 1998;80:28-34.

273. Katz, DA, Haimovich, B, and Greco, RS. FcγRII, FcγRIII, and CD18 receptors mediate in part neutrophil activation on a plasma coated expanded polytetrafluoroethylene surface. Surgery 1995;118:154-161.

274. Hulander, M, Lundgren, A, Berglin, M, et al. Immune complement activation is attenuated by surface nanotopography. Int J Nanomedicine 2011;6:2653.

275. Hiraishi, K, Takeda, Y, Shiobara, N, et al. Studies on the mechanisms of leukocyte adhesion to cellulose acetate beads: An in vitro model to assess the efficacy of cellulose acetate carrier-based granulocyte and monocyte adsorptive apheresis. Ther Apher Dial 2003;7:334-340.

276. Nilsson, B, Ekdahl, KN, Mollnes, TE, and Lambris, JD. The role of complement in biomaterial-induced inflammation. Mol Immunol 2007;44:82-94.

277. Cowland, JB, and Borregaard, N. Granulopoiesis and granules of human neutrophils. Immunol Rev 2016;273:11-28.

278. Tak, T, Tesselaar, K, Pillay, J, Borghans, JA, and Koenderman, L. What's your age again? Determination of human neutrophil half-lives revisited. J Leuko Biol 2013;94:595-601.

279. Elks, PM, van Eeden, FJ, Dixon, G, et al. Activation of hypoxia-inducible factor-1α (HIF-1α) delays inflammation resolution by reducing neutrophil apoptosis and reverse migration in a zebrafish inflammation model. Blood 2011;118:712-722.

280. Wang, J, Hossain, M, Thanabalasuriar, A, et al. Visualizing the function and fate of neutrophils in sterile injury and repair. Science 2017;358:111-116.

281. Jones, HA, Schofield, JB, Krausz, T, Boobis, AR, and Haslett, C. Pulmonary fibrosis correlates with duration of tissue neutrophil activation. Am J Respir Crit Care Med 1998;158:620-628.

282. Rainer, PP, Hao, S, Vanhoutte, D, et al. Cardiomyocyte-specific transforming growth factor β suppression blocks neutrophil infiltration, augments multiple cytoprotective cascades, and reduces early mortality after myocardial infarction. Circ Res 2014;114:1246-1257.

283. Marino, F, Tozzi, M, Schembri, L, et al. Production of IL-8, VEGF and elastase by circulating and intraplaque neutrophils in patients with carotid atherosclerosis. PLoS One 2015;10:e0124565.

284. Luo, Y, Arita, K, Bhatia, M, et al. Inhibitors and inactivators of protein arginine deiminase 4: Functional and structural characterization. Biochemistry 2006;45:11727-11736.

285. Erceg-Hurn, DM, and Mirosevich, VM. Modern robust statistical methods: An easy way to maximize the accuracy and power of your research. Am Psychol 2008;63:591.

286. Xu, LW, Yang, FQ, and Qin, S. A parametric bootstrap approach for two-way anova in presence of possible interactions with unequal variances. J Multivar Anal 2013;115:172-180.

287. Lin, K, Chua, KN, Christopherson, GT, Lim, S, and Mao, H-Q. Reducing electrospun nanofiber diameter and variability using cationic amphiphiles. Polymer 2007;48:6384-6394.

288. Lebaron, P, Catala, P, and Parthuisot, N. Effectiveness of sytox green stain for bacterial viability assessment. Applied and Environmental Microbiology 1998;64:2697-2700.

289. Kusunoki, Y, Nakazawa, D, Shida, H, et al. Peptidylarginine deiminase inhibitor suppresses neutrophil extracellular trap formation and MPO-ANCA production. Front Immunol 2016;7:227.

290. Braster, Q, Silvestre Roig, C, Hartwig, H, et al. Inhibition of NET release fails to reduce adipose tissue inflammation in mice. PLoS One 2016;11:e0163922.

291. Delgado-Rizo, V, Martínez-Guzmán, MA, Iñiguez-Gutierrez, L, et al. Neutrophil extracellular traps and its implications in inflammation: An overview. Front Immunol 2017;8:81.

292. Pilsczek, FH, Salina, D, Poon, KK, et al. A novel mechanism of rapid nuclear neutrophil extracellular trap formation in response to staphylococcus aureus. J Immunol 2010;185:7413-7425.

293. Munks, MW, McKee, AS, MacLeod, MK, et al. Aluminum adjuvants elicit fibrin-dependent extracellular traps in vivo. Blood 2010;116:5191-5199.

294. Hirsh, SL, McKenzie, DR, Nosworthy, NJ, et al. The vroman effect: Competitive protein exchange with dynamic multilayer protein aggregates. Colloids Surf B 2013;103:395-404.

295. Lin, RZ, Lee, CN, Moreno-Luna, R, et al. Host non-inflammatory neutrophils mediate the engraftment of bioengineered vascular networks. Nat Biotechnol 2017;1:0081.

296. Ardi, VC, Van den Steen, PE, Opdenakker, G, et al. Neutrophil MMP-9 proenzyme, unencumbered by TIMP-1, undergoes efficient activation in vivo and catalytically induces angiogenesis via a basic fibroblast growth factor (FGF-2)/FGFR-2 pathway. J Biol Chem 2009;284:25854-25866.

297. Douda, DN, Khan, MA, Grasemann, H, and Palaniyar, N. Sk3 channel and mitochondrial ROS mediate NADPH oxidase-independent NETosis induced by calcium influx. PNAS 2015;112:2817-2822.

298. Mastronardi, FG, Wood, DD, Mei, J, et al. Increased citrullination of histone H3 in multiple sclerosis brain and animal models of demyelination: A role for tumor necrosis factor-induced peptidylarginine deiminase 4 translocation. J Neurosci 2006;26:11387-11396.

299. Sun, B, Dwivedi, N, Bechtel, TJ, et al. Citrullination of NF-kB p65 enhances its nuclear localization and TLR-induced expression of IL-1β and TNFα. Science immunology 2017;2:eaal3062.

300. Chen, GY, and Nuñez, G. Sterile inflammation: Sensing and reacting to damage. Nat Rev Immunol 2010;10:826-837.

301. Lacy, P. Mechanisms of degranulation in neutrophils. Allergy Asthma Clin Immunol 2006;2:98.

302. Gupta, AK, Hasler, P, Holzgreve, W, Gebhardt, S, and Hahn, S. Induction of neutrophil extracellular DNA lattices by placental microparticles and IL-8 and their presence in preeclampsia. Hum Immunol 2005;66:1146-1154.

303. Gregory, AD, Kliment, CR, Metz, HE, et al. Neutrophil elastase promotes myofibroblast differentiation in lung fibrosis. J Leuko Biol 2015;98:143-152.

304. Liu, Y, Min, D, Bolton, T, et al. Increased matrix metalloproteinase-9 predicts poor wound healing in diabetic foot ulcers. Diabetes Care 2009;32:117-119.

305. Nagaoka, I, and Hirota, S. Increased expression of matrix metalloproteinase-9 in neutrophils in glycogen-induced peritoneal inflammation of guinea pigs. Inflammation Research 2000;49:55-62.

306. Rayment, EA, Upton, Z, and Shooter, GK. Increased matrix metalloproteinase-9 (MMP-9) activity observed in chronic wound fluid is related to the clinical severity of the ulcer. Br J Dermatol 2008;158:951-961.

307. Harada, A, Sekido, N, Akahoshi, T, et al. Essential involvement of interleukin-8 (IL-8) in acute inflammation. J Leuko Biol 1994;56:559-564.

308. Martinez, FO, Sironi, M, Vecchi, A, et al. IL-8 induces a specific transcriptional profile in human neutrophils: Synergism with LPS for IL-1 production. Eur J Immunol 2004;34:2286-2292.

309. Taichman, NS, Young, S, Cruchley, AT, Taylor, P, and Paleolog, E. Human neutrophils secrete vascular endothelial growth factor. J Leuko Biol 1997;62:397-400.

310. McCourt, M, Wang, J, Sookhai, S, and Redmond, H. Activated human neutrophils release hepatocyte growth factor/scatter factor. Eur J Surg Oncol 2001;27:396-403.

311. Christoffersson, G, Vågesjö, E, Vandooren, J, et al. VEGF-A recruits a proangiogenic MMP-9-delivering neutrophil subset that induces angiogenesis in transplanted hypoxic tissue. Blood 2012;120:4653-4662.

312. Herath, TD, Larbi, A, Teoh, SH, James Kirkpatrick, C, and Goh, BT. Neutrophil-mediated enhancement of angiogenesis and osteogenesis in a novel triple cell co-culture model with endothelial cells and osteoblasts. J Tissue Eng Regen Med 2017;12: e1221-e1236.

313. Manic, G, Obrist, F, Kroemer, G, Vitale, I, and Galluzzi, L. Chloroquine and hydroxychloroquine for cancer therapy. Mol Cell Oncol 2014;1:e29911.

314. Wozniacka, A, Lesiak, A, Narbutt, J, McCauliffe, D, and Sysa-Jedrzejowska, A. Chloroquine treatment influences proinflammatory cytokine levels in systemic lupus erythematosus patients. Lupus 2006;15:268-275.

315. Schrezenmeier, E, and Dörner, T. Mechanisms of action of hydroxychloroquine and chloroquine: Implications for rheumatology. Nat Rev Rheumatol 2020;1-12.

316. Roldan, EQ, Biasiotto, G, Magro, P, and Zanella, I. The possible mechanisms of action of 4-aminoquinolines (chloroquine/hydroxychloroquine) against Sars-Cov-2 infection (COVID-19): A role for iron homeostasis? Pharmacol Res 2020;158:104904.

317. Smith, CK, Vivekanandan-Giri, A, Tang, C, et al. Neutrophil extracellular trap–derived enzymes oxidize high-density lipoprotein: An additional proatherogenic mechanism in systemic lupus erythematosus. Arthritis Rheum 2014;66:2532-2544.

318. Boone, BA, Orlichenko, L, Schapiro, NE, et al. The receptor for advanced glycation end products (RAGE) enhances autophagy and neutrophil extracellular traps in pancreatic cancer. Cancer Gene Ther 2015;22:326.

319. Lima, T, Feitosa, R, dos Santos-Silva, E, et al. Improving encapsulation of hydrophilic chloroquine diphosphate into biodegradable nanoparticles: A promising approach against herpes virus simplex-1 infection. Pharmaceutics 2018;10:255.

320. Germic, N, Stojkov, D, Oberson, K, Yousefi, S, and Simon, HU. Neither eosinophils nor neutrophils require ATG 5-dependent autophagy for extracellular DNA trap formation. Immunology 2017;152:517-525.

321. de Oliveira, S, Reyes-Aldasoro, CC, Candel, S, et al. CXCL8 (IL-8) mediates neutrophil recruitment and behavior in the zebrafish inflammatory response. J Immunol 2013;190:4349-4359.

322. Fujishima, S, Hoffman, AR, Vu, T, et al. Regulation of neutrophil interleukin 8 gene expression and protein secretion by LPS, TNF-α, and IL-1β. J Cell Physiol 1993;154:478-485.

323. Degroote, RL, Weigand, M, Hauck, SM, and Deeg, CA. IL8 and PMA trigger the regulation of different biological processes in granulocyte activation. Front Immunol 2020;10:3064.

324. Wislez, M, Rabbe, N, Marchal, J, et al. Hepatocyte growth factor production by neutrophils infiltrating bronchioloalveolar subtype pulmonary adenocarcinoma: Role in tumor progression and death. Cancer Res 2003;63:1405-1412.

325. He, M, Peng, A, Huang, XZ, et al. Peritumoral stromal neutrophils are essential for c-met-elicited metastasis in human hepatocellular carcinoma. Oncoimmunology 2016;5:e1219828.

326. Dyring-Andersen, B, Honoré, TV, Madelung, A, et al. IL-17a and IL-22 producing neutrophils in psoriatic skin. Br J Dermatol 2017;177:e321.

327. Protopsaltis, NJ, Liang, W, Nudleman, E, and Ferrara, N. Interleukin-22 promotes tumor angiogenesis. Angiogenesis 2019;22:311-323.

328. Buckley, CD, Ross, EA, McGettrick, HM, et al. Identification of a phenotypically and functionally distinct population of long-lived neutrophils in a model of reverse endothelial migration. J Leuko Biol 2006;79:303-311.

329. Moore, BR, Page-Sharp, M, Stoney, JR, et al. Pharmacokinetics, pharmacodynamics, and allometric scaling of chloroquine in a murine malaria model. Antimicrob Agents Chemother 2011;55:3899-3907.

330. Frustaci, A, Morgante, E, Antuzzi, D, Russo, MA, and Chimenti, C. Inhibition of cardiomyocyte lysosomal activity in hydroxychloroquine cardiomyopathy. Int J Cardiol 2012;157:117-119.

331. Sundelin, SP, and Terman, A. Different effects of chloroquine and hydroxychloroquine on lysosomal function in cultured retinal pigment epithelial cells. APMIS 2002;110:481-489.

332. Meng, H, Yalavarthi, S, Kanthi, Y, et al. In vivo role of neutrophil extracellular traps in antiphospholipid antibody–mediated venous thrombosis. Arthritis Rheum 2017;69:655-667.

333. Döring, Y, Soehnlein, O, and Weber, C. Neutrophil extracellular traps in atherosclerosis and atherothrombosis. Circ Res 2017;120:736-743.

334. Della Porta, A, Bornstein, K, Coye, A, et al. Acute chloroquine and hydroxychloroquine toxicity: A review for emergency clinicians. Am J Emerg Med 2020;38:2209-2217.

335. Solitro, AR, and MacKeigan, JP. Leaving the lysosome behind: Novel developments in autophagy inhibition. Future Med Chem 2016;8:73-86.

336. Pliyev, BK, and Menshikov, M. Differential effects of the autophagy inhibitors 3-methyladenine and chloroquine on spontaneous and TNF-α-induced neutrophil apoptosis. Apoptosis 2012;17:1050-1065.

337. Fujita, Y, Matsuoka, N, Temmoku, J, et al. Hydroxychloroquine inhibits IL-1β production from amyloid-stimulated human neutrophils. Arthritis Res Ther 2019;21:1-9.

338. Sharma, P, Yi, R, Nayak, AP, et al. Bitter taste receptor agonists mitigate features of allergic asthma in mice. Sci Rep 2017;7:1-14.

339. Zhang, Q, Itagaki, K, and Hauser, CJ. Mitochondrial DNA is released by shock and activates neutrophils via p38 MAP kinase. Shock 2010;34:55-59.

340. Delgado, MA, Poschet, JF, and Deretic, V. Nonclassical pathway of pseudomonas aeruginosa DNA-induced interleukin-8 secretion in cystic fibrosis airway epithelial cells. Infect Immun 2006;74:2975-2984.

341. Végran, F, Boidot, R, Michiels, C, Sonveaux, P, and Feron, O. Lactate influx through the endothelial cell monocarboxylate transporter mct1 supports an NF-κB/IL-8 pathway that drives tumor angiogenesis. Cancer Res 2011;71:2550-2560.

342. Lu, P, Takai, K, Weaver, VM, and Werb, Z. Extracellular matrix degradation and remodeling in development and disease. Cold Spring Harb Perspect Biol 2011;3:a005058.

343. Hsu, AT, Barrett, CD, DeBusk, MG, et al. Kinetics and role of plasma matrix metalloproteinase-9 expression in acute lung injury and the acute respiratory distress syndrome. Shock 2015;44:128-136.

344. Ladwig, GP, Robson, MC, Liu, R, et al. Ratios of activated matrix metalloproteinase-9 to tissue inhibitor of matrix metalloproteinase-1 in wound fluids are inversely correlated with healing of pressure ulcers. Wound Repair Regen 2002;10:26-37.

345. Matsumoto, K, Funakoshi, H, Takahashi, H, and Sakai, K. HGF–Met pathway in regeneration and drug discovery. Biomedicine 2014;2:275-300.

346. Christoffersson, G, Lomei, J, O'Callaghan, P, et al. Vascular sprouts induce local attraction of proangiogenic neutrophils. J Leuko Biol 2017;102:741-751.

347. Chen, F, Cao, A, Yao, S, et al. MTOR mediates IL-23 induction of neutrophil IL-17 and IL-22 production. J Immunol 2016;196:4390-4399.

348. Zindl, CL, Lai, JF, Lee, YK, et al. IL-22–producing neutrophils contribute to antimicrobial defense and restitution of colonic epithelial integrity during colitis. PNAS 2013;110:12768-12773.

349. Zenewicz, LA. IL-22: There is a gap in our knowledge. Immunohorizons 2018;2:198-207.

350. Puyo, CA, Earhart, A, Staten, N, et al. Mitochondrial DNA induces Foley catheter related bladder inflammation via toll-like receptor 9 activation. Sci Rep 2018;8:1-12.

351. Ouseph, MM, Huang, Y, Banerjee, M, et al. Autophagy is induced upon platelet activation and is essential for hemostasis and thrombosis. Blood 2015;126:1224-1233.

352. Dondossola, E, Holzapfel, BM, Alexander, S, et al. Examination of the foreign body response to biomaterials by nonlinear intravital microscopy. Nature Biomedical Engineering 2017;1:0007.

353. Techaikool, P, Daranarong, D, Kongsuk, J, et al. Effects of plasma treatment on biocompatibility of poly [(l-lactide)-co-(ϵ-caprolactone)] and poly [(l-lactide)-co-glycolide] electrospun nanofibrous membranes. Polym Int 2017;66:1640-1650.

354. Hesketh, M, Sahin, KB, West, ZE, and Murray, RZ. Macrophage phenotypes regulate scar formation and chronic wound healing. Int J Mol Sci 2017;18:1545.

355. Carmona-Rivera, C, Zhao, W, Yalavarthi, S, and Kaplan, MJ. Neutrophil extracellular traps induce endothelial dysfunction in systemic lupus erythematosus through the activation of matrix metalloproteinase-2. Ann Rheum Dis 2015;74:1417-1424.

356. Tazzyman, S, Lewis, CE, and Murdoch, C. Neutrophils: Key mediators of tumour angiogenesis. Int J Exp Pathol 2009;90:222-231.

357. Tecchio, C, and Cassatella, MA. Neutrophil-derived cytokines involved in physiological and pathological angiogenesis. Angiogenesis, lymphangiogenesis and clinical implications: Karger Publishers; 2014. pp. 123-137.

358. Salamonsen, LA, and Lathbury, LJ. Endometrial leukocytes and menstruation. Hum Reprod Update 2000;6:16-27.

359. Ohki, Y, Heissig, B, Sato, Y, et al. Granulocyte colony-stimulating factor promotes neovascularization by releasing vascular endothelial growth factor from neutrophils. FASEB 2005;19:2005-2007.

360. Ong, CW, Pabisiak, PJ, Brilha, S, et al. Complex regulation of neutrophil-derived mmp-9 secretion in central nervous system tuberculosis. J Neuroinflammation 2017;14:31.

361. Iyer, V, Pumiglia, K, and DiPersio, CM. A3β1 integrin regulates MMP-9 mRNA stability in immortalized keratinocytes: A novel mechanism of integrin-mediated MMP gene expression. J Cell Sci 2005;118:1185-1195.

362. MASURE, S, Proost, P, Van Damme, J, and Opdenakker, G. Purification and identification of 91-kDa neutrophil gelatinase: Release by the activating peptide interleukin-8. Eur J Biochem 1991;198:391-398.

363. Yan, SR, and Berton, G. Antibody-induced engagement of β2 integrins in human neutrophils causes a rapid redistribution of cytoskeletal proteins, Src-family tyrosine kinases, and p72syk that precedes de novo actin polymerization. J Leuko Biol 1998;64:401-408.

364. Page, K, Ledford, JR, Zhou, P, and Wills-Karp, M. A TLR2 agonist in german cockroach frass activates MMP-9 release and is protective against allergic inflammation in mice. J Immunol 2009;2009:0900838.

365. Tamassia, N, Le Moigne, V, Calzetti, F, et al. The Myd88-independent pathway is not mobilized in human neutrophils stimulated via TLR4. J Immunol 2007;178:7344-7356.

366. Ramos-DeSimone, N, Hahn-Dantona, E, Sipley, J, et al. Activation of matrix metalloproteinase-9 (MMP-9) via a converging plasmin/stromelysin-1 cascade enhances tumor cell invasion. J Biol Chem 1999;274:13066-13076.

367. Toth, M, Chvyrkova, I, Bernardo, MM, Hernandez-Barrantes, S, and Fridman, R. Pro-MMP-9 activation by the MT1-MMP/MMP-2 axis and MMP-3: Role of TIMP-2 and plasma membranes. Biochem Biophys Res Comm 2003;308:386-395.

368. Christensen, J, and Shastri, VP. Matrix-metalloproteinase-9 is cleaved and activated by cathepsin K. BMC Res Notes 2015;8:322.

369. Masciantonio, MG, Lee, CK, Arpino, V, Mehta, S, and Gill, SE. The balance between metalloproteinases and TIMPs: Critical regulator of microvascular endothelial cell function in health and disease. Prog Mol Biol Transl Sci: Elsevier; 2017. pp. 101-131.

370. Massena, S, Christoffersson, G, Vågesjö, E, et al. Identification and characterization of VEGF-A-responsive neutrophils expressing VEGFR1, CD49d and CXCR4 in mice and humans. Blood 2015;blood-2015-2003-631572.

APPENDIX

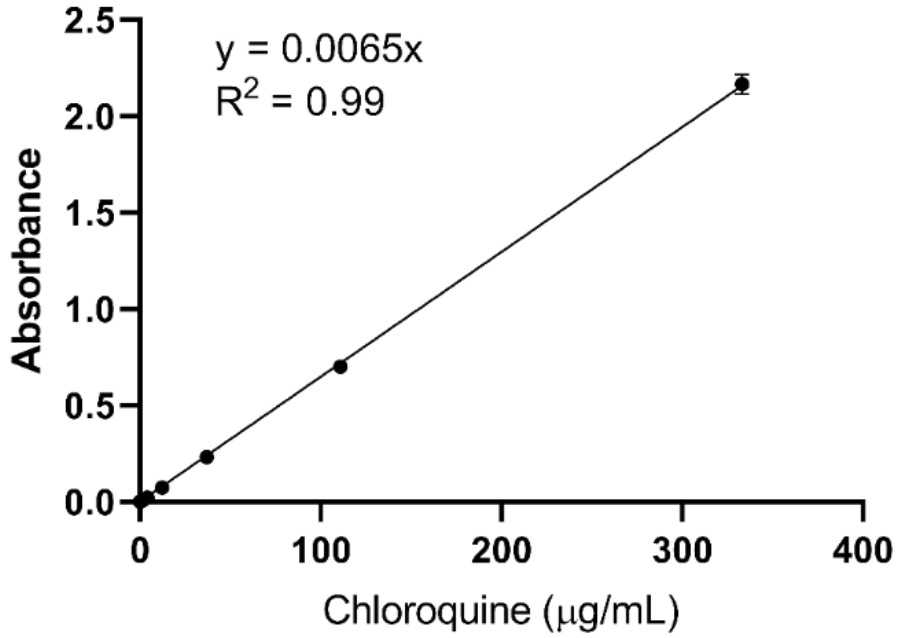

Supplementary Figure 1. Chloroquine concentration as determined by absorbance follows a linear trend. The standard dilution of chloroquine was prepared in HBSS and serially diluted by a factor of 3 from 333.3 µg/mL to 1.37 µg/mL. HBSS without chloroquine was included as a background control. Following, 150 µL of the standard dilution and HBSS background control (n = 2) were added to a 96-well plate and absorbance was measured. The resulting data were fit with a line of best fit ($y = 0.0065x$, $R^2 = 0.99$) to create the standard curve for interpolating unknown eluted chloroquine concentration.

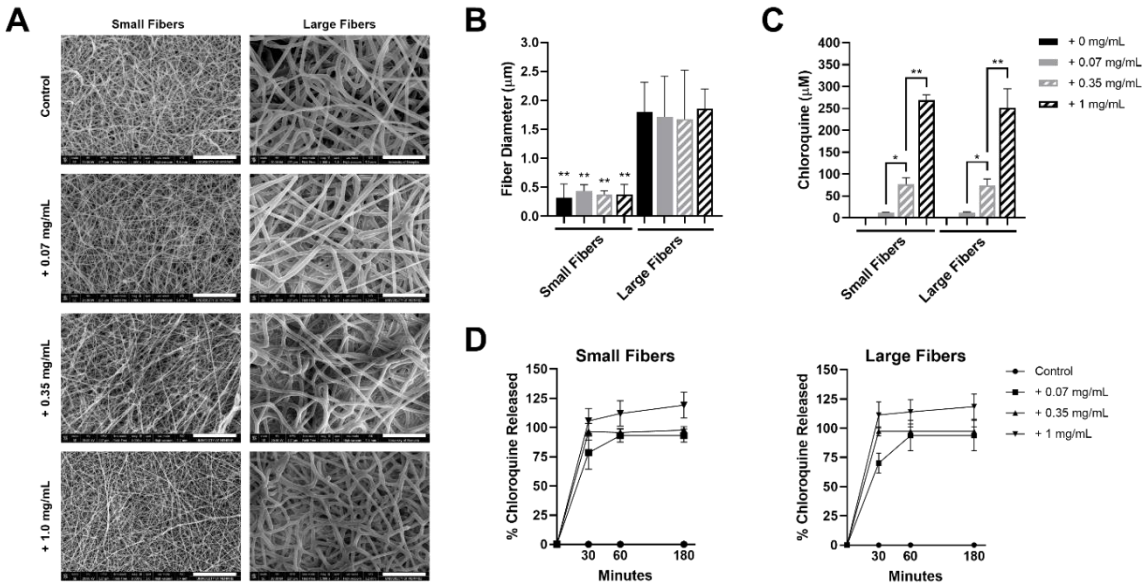

Supplementary Figure 2. Chloroquine incorporation into electrospun biomaterials results in uniform fibers that rapidly elute the additive. (A) Representative SEMs of the control and chloroquine-loaded biomaterials. Micrographs were acquired at 1000x magnification and scale bars are 30 μm. (B) Fiber diameters of the electrospun biomaterials. Measurements (n = 150) were taken in FibraQuant 1.3 software. (C) Concentration of eluted chloroquine at 3 hours and (D) percent chloroquine released from the small (left) and large (right) fibers at 3 hours. There was no increase in concentration after 3 hours. See Figure S1 for the standard curve used to interpolate concentration (n = 4) from absorbance. Graphs show mean ± standard deviation. * $p < 0.05$ and ** $p < 0.0001$ were determined using a Kruskal Wallis and Dunn's multiple comparisons test.

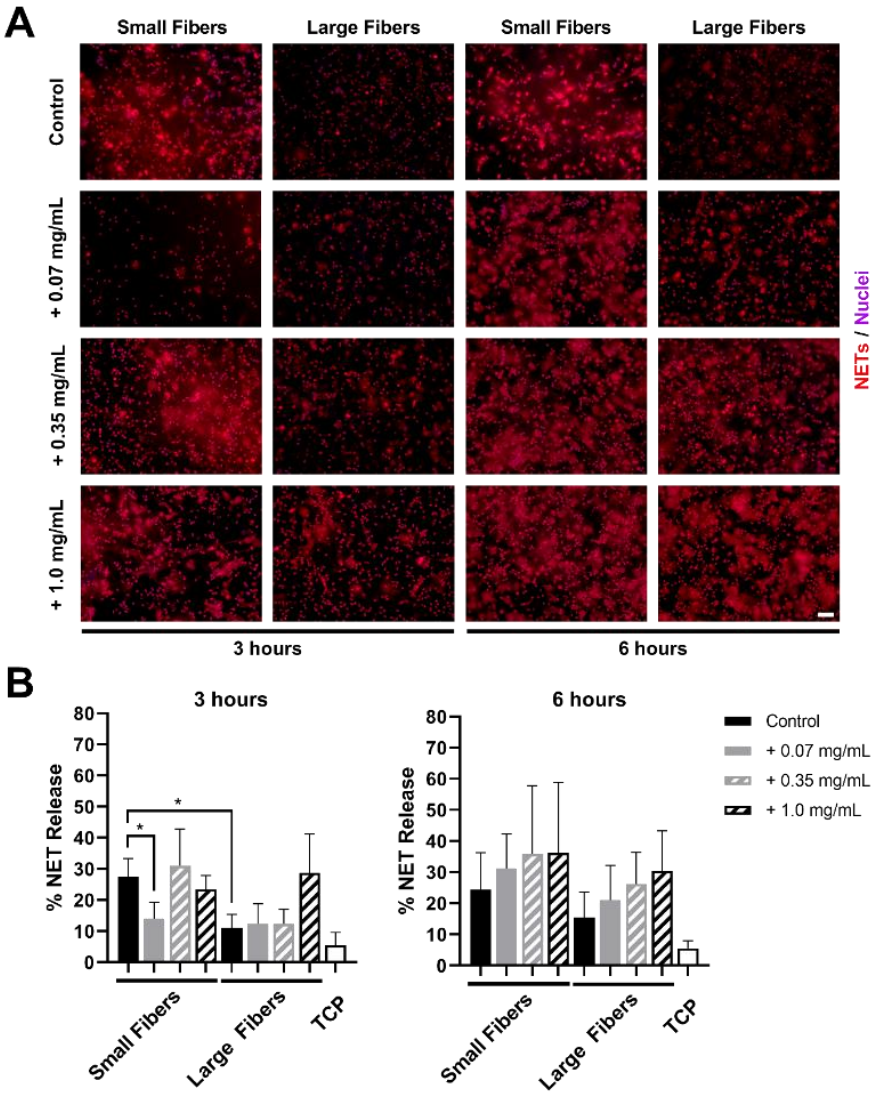

Supplementary Figure 3. Chloroquine elution inhibits NET release within a therapeutic window. (A) Fluorescent micrographs of neutrophils on the electrospun biomaterials at 3 and 6 hours after seeding. Staining of NETs (red) and nuclei (purple) reveals that chloroquine elution from the small fibers attenuates NET formation at the early time point at the lowest concentration, but not at the late time point. Conversely, chloroquine elution from the large fibers does not inhibit NET release at any concentration. Scale bar is 50 µm. (B) Percent NET release at 3 (left) and 6 (right) hours as quantified by the ELISA for NET-disassociated MPO. The quantification of percent NET release (n = 3) indicates that chloroquine elution from the small fibers reduces NET release to the level of the large fibers at 3 hours only at the lowest dose. At 6 hours, both small and large fibers eluting higher concentrations of chloroquine result in an apparent increase in NET release, suggesting a therapeutic window at the lowest chloroquine concentration and potential cytotoxic effects at higher concentrations. The data represent the mean ± standard deviation of three independent experiments with unique donors. * $p < 0.0001$ was determined using an ANOVA and Holm-Sidak's multiple comparisons test.